Supporting Information

An artificial molecular pump powered by light

Federico Nicoli,[‡,1,2,3] Chiara Taticchi,[‡,1,2] Stefano Corra,[1,2] Marina Tranfić Bakić,[1,2,4] Massimo Baroncini,[1,5] Serena Silvi,[1,6] Jessica Groppi,[1,7,*] and Alberto Credi[1,2,*]

[1] Center for Light Activated Nanostructures (CLAN), Alma Mater Studiorum – Università di Bologna and National Research Council of Italy (CNR), via Gobetti 101, 40129 Bologna, Italy

[2] Dipartimento di Chimica Industriale "Toso Montanari", Alma Mater Studiorum – Università di Bologna, via Gobetti 85, 40129 Bologna, Italy

[3] Present address: Institut de Science et d'Ingénierie Supramoléculaires (ISIS), University of Strasbourg & CNRS, UMR 7006 8 Allée Gaspard Monge, 67000 Strasbourg, France

[4] Present address: Faculty of Chemistry and Technology, University of Split, Ruđera Boškovića 35, 21000 Split, Croatia

[5] Dipartimento di Scienze e Tecnologie Agro-alimentari, Alma Mater Studiorum – Università di Bologna, viale Fanin 44-50, 40127 Bologna, Italy

[6] Dipartimento di Chimica "G. Ciamician", Alma Mater Studiorum – Università di Bologna, via Gobetti 85, 40129 Bologna, Italy

[7] Institute for Organic Synthesis and Photoreactivity (ISOF), National Research Council of Italy (CNR), via Gobetti 101, 40129 Bologna, Italy

‡ These authors contributed equally to this work

*Corresponding: alberto.credi@unibo.it, jessica.groppi@cnr.it

Table of Contents

1. Materials and methods

1.1. Materials

4-nitrosotoluene[1] and compounds **10**,[2] **11**[2] and **17**[3] were synthetized according to literature procedures. All reagents and chemicals were purchased from Merck, VWR or Fluorochem international and used as received unless otherwise stated. Flash column chromatography was performed using Merck Silica 40 (230-400 mesh size or 40-63 μm) as the stationary phase. Thin layer chromatography was performed on TLC Silica gel 60 F254 coated aluminum plates from Merck.

1.2. NMR Spectroscopy

NMR spectra were recorded on an Agilent DD2 spectrometer operating at 500 MHz. Chemical shifts are quoted in parts per million (ppm) relative to tetramethylsilane using the residual solvent peak as a reference standard and all coupling constants (J) are expressed in Hertz (Hz).

1.3. Mass Spectrometry

Mass spectrometry (LRMS and HRMS) measurements were performed either on a Waters Xevo G2-XS instrument equipped with an ESI source and a Q-TOF ion analyzer or a Waters Synapt GS2 instrument with MALDI source and Q-Tof ion analyzer.

1.4. NMR Photochemistry

Photochemical reactions were performed in air-equilibrated solutions at 298 K inside NMR tubes within the spectrometer probe-head, using a Prizmatix UHP-T-365-SR LED Illuminator (1.5 W, λ_{max}= 369 ± 15 nm, FWHM 15.56 nm) equipped with an FCASMA adaptor for optical fiber. The desired irradiation wavelength of 365±5 nm was selected using the appropriate hard coated OD 4.0 bandpass filter. Quartz optical fiber (core 1000 μm, 5 m) equipped with a SMA connector on one end was purchased from Thorlabs. The other end of the optical fiber was freed of the protective coatings, exposing 6 cm of the quartz core, and sanded in order to uniformly diffuse light in the solution. The exposed quartz fiber was submerged into the solution (V = 0.5 mL) within the NMR tube to be irradiated.

1.5. Least square fitting and numerical simulations

The fitting of the experimental data to the appropriate kinetic model was performed using Berkeley Madonna 10.[4]

1.6. UV-vis spectroscopy

Absorption spectra were recorded on Cary 300 (Varian - Agilent), lambda750 (Perkin Elmer) double beam spectrophotometers, and Cary 50 Bio single beam spectrophotometer. 1 cm pathlength quartz cuvettes (Hellma) were used. In the case of high absorption solutions, 1 mm or 2 mm pathlength cuvettes were used as well. Dedicated spectrophotometric cells endowed with two compartments separated by a quartz wall were employed for careful determination of the sum of the absorption spectra of the separated components (unmixed solutions) and the absorption spectrum obtained after the interaction between the two components (mixed solutions).

1.7. Time-resolved UV-vis spectroscopic measurements

Thermal back-isomerization kinetics were investigated by monitoring the absorbance changes over time in the dark. The obtained data were fitted according to a first order model. Fast reaction kinetic profiles (half-time below tens of seconds) were collected on air-equilibrated solutions at 298 K with an Applied Photophysics SX 18-MV equipment. Such stopped-flow spectrophotometer was equipped with a 1 cm pathlength cell and a driving ram for the mixing system at the N_2 pressure of 8.5 bar. Under these conditions, the time required to fill the cell is lower than 2 ms. A baseline correction was applied to the stopped-flow traces, to take into account the dependence of the instrument response on the pressure. In all the experiments, the cell block and drive syringes were thermostated by using a circulating constant-temperature bath maintained at the required temperature. The data obtained were fitted with software SPECFIT with a mixed order reaction (second order for threading, first order for dethreading), with the constrain that the ratio between the two constants should equal the thermodynamic constant obtained from NMR measurements.

1.8. UV-vis irradiation experiments

Irradiation experiments were performed on air equilibrated solutions, thoroughly stirred. A medium pressure Hg lamp (200 W) was used. The desired wavelength of irradiation was selected using an appropriate interference filter and the intensity of the incident light was regulated with a pinhole of opportune diameter. The incident photon flux of the irradiation lamp was measured by means of the ferrioxalate actinometer, according to the procedure reported for its "microversion".[5] The photoisomerization quantum yields Φ were determined from the disappearance or appearance of the $\pi\pi^*$ band of azobenzene unit by fitting of the global photokinetic using the software Berkeley Madonna.[4] The absorption spectra of the unknown *Z* isomers were extrapolated mathematically, according to the Fisher method.[6]

2. Synthetic procedures

2.1. Synthesis of compounds *E*-3 and 8

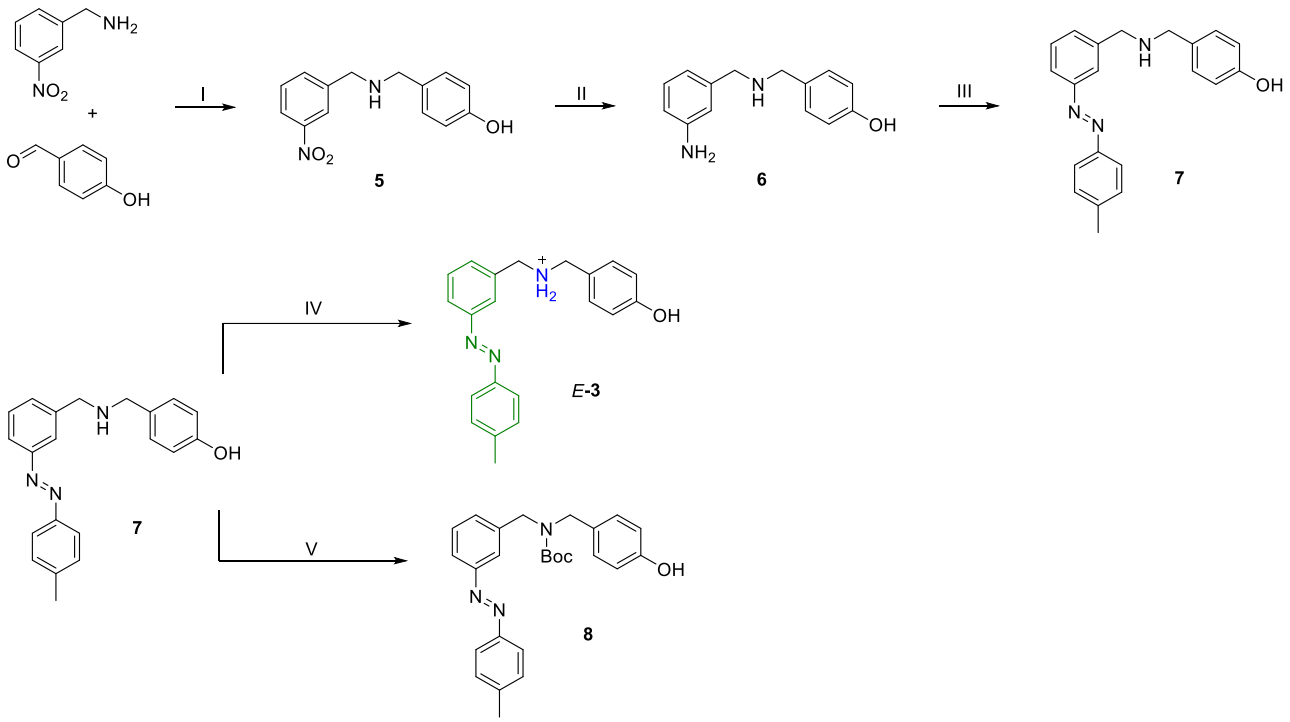

Scheme S1. I) a. toluene, rotavapor, b. $NaBH_4$, MeOH quant., II) H_2 Pd/C 10%, MeOH. Quant, III) 1-methyl-4-nitrosobenzene, CH_3CO_2H r.t. 75%, IV) a. HCl 37%, MeOH, b. NH_4PF_6 (sat), 68%, V) Boc_2O, THF r.t. 90%.

2.1.1. Synthesis of 5

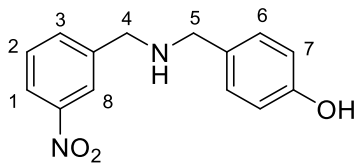

(3-nitrophenyl)methanamine (1.8 g,11.7 mmol) and 4-hydroxybenzaldehyde (1.44 g,11.7 mmol) were dissolved in toluene (100 ml). The mixture was stirred for 30 minutes, and the water formed during the condensation reaction was removed through azeotropic distillation. The resulting imine intermediate was isolated as a crystalline solid and dissolved in methanol (MeOH, 100 mL). $NaBH_4$ (1.55 g, 40.95 mmol) was added to the solution portionwise with stirring, completing the reduction to the corresponding secondary amine. The solvent was then removed under vacuum, and 100 mL of H_2O were added. The aqueous phases were extracted with ethyl acetate (AcOEt) (30 mL × 2), and the organic phase was washed with brine and finally dried over Na_2SO_4. The product was obtained in quantitative yield as a yellowish crystalline solid without further purification.

^{1}H NMR (500 MHz, $CDCl_3$, 298 K) δ 8.20 (s, 1H, H_8), 8.10 (d, J = 8.1 Hz, 1H, H_1), 7.68 (d, J = 7.6 Hz, 1H, H_3), 7.48 (t, J = 7.9 Hz, 1H, H_2), 7.14 (d, J = 8.2 Hz, 2H, H_6), 6.71 (d, J = 8.3 Hz, 2H, H_7), 3.90 (s, 2H, H_4), 3.87 (br, NH), 3.74 (s, 2H, H_5). **^{13}C NMR** (126 MHz, $CDCl_3$, 298 K) δ 155.4, 148.5, 142.0, 134.6, 131.0, 129.8, 129.5, 123.3, 122.4, 115.8, 52.7, 52.2.

2.1.2. Synthesis of 6

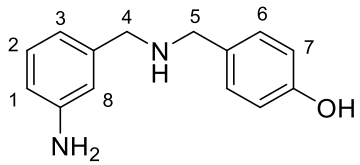

In a sealed double-neck round-bottom flask, compound **5** (1.2 g, 5.26 mmol) was dissolved in MeOH (50 mL) and exposed to H_2 gas (excess) in the presence of 10% Pd/C (100 mg). After two hours, the catalyst was filtered off under vacuum and the filtrate was collected. The solution was then concentrated under vacuum. The reagent was quantitatively converted into product **6**, a yellow oil, and no purification was necessary, resulting in a quantitative yield.**^{1}H NMR** (500 MHz, $CDCl_3$, 298 K) δ 7.10 (m, 3H, H_2+H_6), 6.70 (d, J = 7.6 Hz, 1H, H_3), 6.67 (m, 3H, H_7+H_8), 6.59 (d, J = 7.9 Hz, 1H, H_1), 3.71 (s, 2H, H_5), 3.69 (s, 2H, H_4). **^{13}C NMR** (126 MHz, $CDCl_3$, 298 K) δ 155.6, 146.6, 140.9, 131.1, 129.8, 129.6, 118.8, 115.7, 115.2, 114.2, 53.1, 52.6.

2.1.3. Synthesis of 7

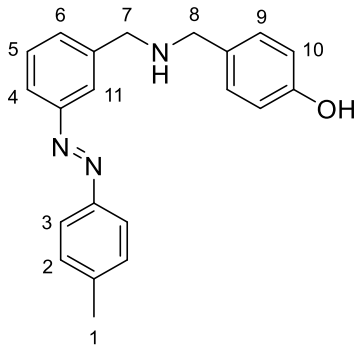

Compound **5** (0.97 g, 4.25 mmol) and 4-nitrosotoluene (1.3 g, 10.63 mmol) were dissolved in acetic acid (80 mL). The solution was stirred for 18 hours at room temperature. After this time, the solvent was removed under reduced pressure, and the crude mixture was dissolved in AcOEt. The organic phase was washed with $NaHCO_3$ (aq., sat.) and then with H_2O until the aqueous phases were neutralized. Finally, the organic phase was washed with brine and dried over Na_2SO_4. The product was purified *via* column chromatography on silica using *n*-Hex :AcOEt (1:1), followed by pure AcOEt as eluent. Product **7** was obtained as an orange crystalline solid in 75% yield.**^{1}H NMR** (500 MHz, $CDCl_3$, 298 K) δ 7.86 (s, 1H, H_{11}), 7.82 – 7.80 (m, 3H, H_3+H_5), 7.46 – 7.50 (m, 2H, H_4+H_6), 7.31 (d, J = 8.1 Hz, 2H, H_2), 7.14 (d, J = 8.4 Hz, 2H, H_9), 6.69 (d, J = 8.4 Hz, 2H, H_{10}), 3.91 (s, 2H, H_7), 3.78 (s br., 1H, -OH), 3.75 (s, 2H, H_8), 2.43 (s, 3H, H_1). **^{13}C NMR** (126 MHz, $CDCl_3$, 298 K) δ 155.5, 153.0, 150.9, 141.8, 140.9, 131.1, 130.8, 129.9, 129.8, 129.7, 123.0, 122.2, 122.15, 115.8, 52.9, 52.6, 21.6.

2.1.4. Synthesis of *E*-3

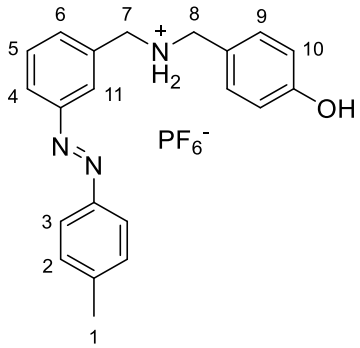

Compound **7** (50 mg, 0.1 mmol) was dissolved in the minimum amount of MeOH. Then, a few drops of HCl 37% were added until the precipitation of the chloride salt as a red solid. Subsequently, MeOH was added until the complete dissolution of the salt. A saturated solution of NH_4PF_6 (aq) was then added dropwise until the complete precipitation of the hexafluorophosphate salt. The solid was collected by vacuum filtration and washed with H_2O.The product was an orange solid obtained in 68% yield.**^{1}H NMR** (500 MHz, $(CD_3)_2SO$, 298 K) δ 9.69 (s, 1H, -OH), 9.10 (s, 2H, -NH_2), 8.02 (s, 1H, H_{11}), 7.94 (dt, *J* = 7.6 Hz, 1.8 Hz, 1H, H_4), 7.82 (d, *J* = 8.3 Hz, 2H, H_3), 7.71 – 7.60 (m, 2H, H_5+H_6), 7.43 (d, *J* = 7.8 Hz, 2H, H_2), 7.30 (d, *J* = 8.6 Hz, 2H, H_9), 6.81 (d, *J* = 8.6 Hz, 2H, H_{10}), 4.28 (s, 2H, H_7), 4.11 (s, 2H, H_8), 2.42 (s, 3H, H_1). **^{13}C NMR** (126 MHz, $(CD_3)_2SO$, 298 K) δ 158.1, 151.9, 150.0, 142.2, 133.4, 132.7, 131.7, 130.1, 129.8, 123.9, 123.0, 122.6, 121.7, 115.4, 50.1, 49.5, 21.0. **^{19}F NMR** (470 MHz, $(CD_3)_2SO$, 298 K) δ -70.17 (d, *J* = 711.2 Hz). **HRMS** (MALDI-TOF): m/z = 332.1765 (calcd 332.4189 for $C_{21}H_{22}N_3O^+$).

2.1.5. Synthesis of 8

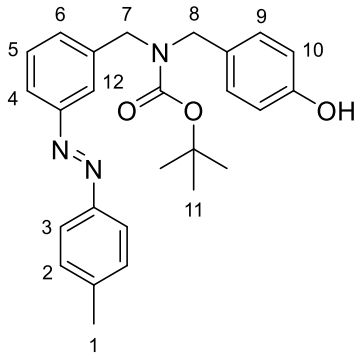

Compound **5** (1.0 g, 3.02 mmol) and di-tert-butyldicarbonate (0.659 g, 3.02 mmol) were dissolved in THF (60 mL) and stirred at room temperature. The reaction was monitored by TLC, eluent *n*-Hex:AcOEt (1:1). At the end of the reaction, the solvent was removed under reduced pressure and H_2O was added. The aqueous phases were extracted with AcOEt (30 mL × 4), and the organic phases were washed with brine and dried over Na_2SO_4. The crude was purified *via* column chromatography on silica, eluent *n*-Hex : AcOEt (4:1). The product was an orange solid obtained in 90% yield.**^{1}H NMR** (500 MHz, $CDCl_3$, 298 K) δ 7.86 – 7.79 (m, 3H, H_3+H_4), 7.75 (t, *J* = 2.0 Hz, 1H, H_{12}), 7.46 (t, *J* = 7.7 Hz, 1H, H_5), 7.32 (d, *J* = 8.2 Hz, 2H, H_2), 7.28 (br, 1H, H_6), 7.11 (br, 2H, H_9), 6.79 (d, *J* = 8.6 Hz, 2H, H_{10}), 4.60 – 4.16 (m, 4H, H_7+H_8), 2.44 (s, 3H, H_1), 1.52 (s, 9H, H_{11}). **^{13}C NMR** (126 MHz, $CDCl_3$, 298 K) δ 156.2, 155.2, 153.0, 150.8, 141.9, 130.2, 129.9, 129.7, 129.4, 123.0, 122.3, 121.8, 121.3, 115.6, 80.5, 49.2, 49.0, 28.6, 28.6, 21.7.

2.2. Synthesis of compounds 4 and 11

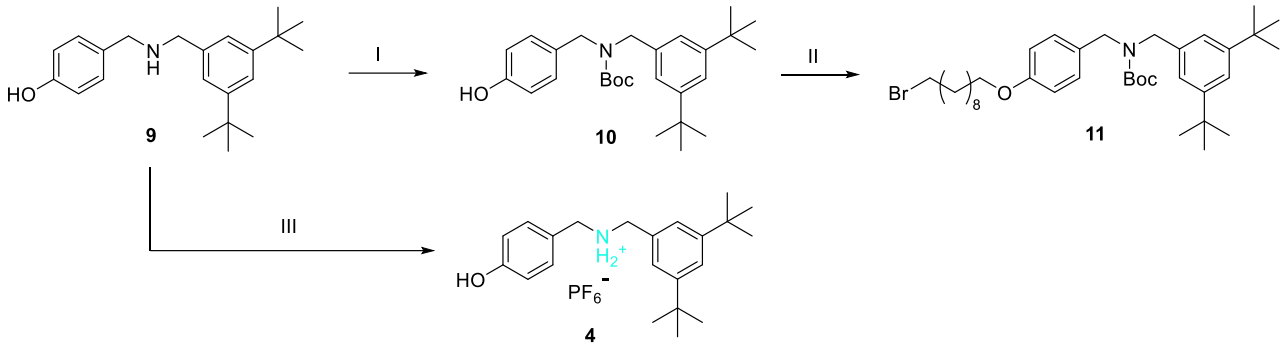

Scheme S2. I) Boc_2O, THF r.t. 87%,[2] II) 1,10-dibromodecane, K_2CO_3 CH_3CN (dry) 80°C. 56%. III) a. HCl 37%, CH_3CN, b. NH_4PF_6, acetone : H_2O, 72%.

2.2.1. Synthesis of 11

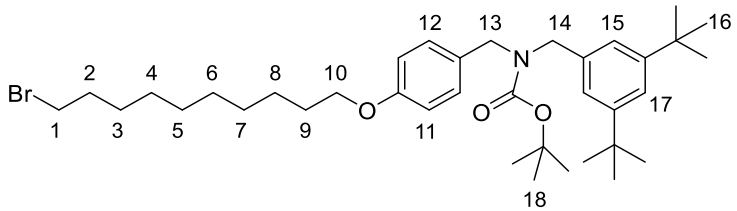

Compound **10 (**0.719 g, 1.68 mmol) of was dissolved in CH_3CN (20 mL), and K_2CO_3 (0.37 g, 2.67 mmol) was added. The mixture was left stirring at reflux temperature for 3 hours until it assumed a milky appearance. 10-dibromodecane (2.09 g, 6.9 mmol) of was added to the reaction mixture. The reaction was refluxed for 20 hours. The solvent was removed *in vacuo* and the crude was suspended in H_2O and extracted with Et_2O (3 × 50 mL). The organic layer was dried over Na_2SO_4. The product was isolated by chromatography over silica (eluent *n*-Hex : Et_2O, 9:1) to obtain a colorless oil in 56% yield. **^{1}H NMR** (500 MHz, $CDCl_3$, 298K) δ 7.31 (s, 1H, H_{17}), 7.19 – 6.98 (m, 4H, H_{12}+H_{15}), 6.84 (d, J = 8.6 Hz, 2H, H_{11}), 4.42 – 4.20 (m, 4H, H_{13}+H_{14}), 3.94 (t, J = 6.5 Hz, 2H, H_{10}), 3.41 (t, J = 6.8 Hz, 2H, H_1), 1.86 (p, J = 7.0 Hz, 2H, H_9), 1.78 (p, J = 6.7 Hz, 2H, H_2), 1.50 (s, 9H, H_{18}), 1.44 (m, 4H, H_3+H_8), 1.31 (m, 26H, H_4+H_5+H_6+H_7+H_{16}). **^{13}C NMR** (126 MHz, $CDCl_3$, 298 K) δ 158.5, 156.1, 150.9, 137.5, 129.6, 128.9, 122.0, 121.2, 114.6, 79.9, 68.1, 49.9, 48.6, 34.9, 34.1, 33.0, 31.6, 29.6, 29.5, 29.5, 29.4, 28.9, 28.6, 28.3, 26.2.

2.2.2. Synthesis of 4

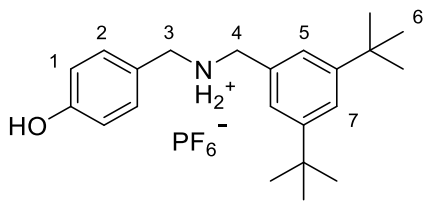

Compound **9** (120 mg, 0.4 mmol) was dissolved in the minimum amount of CH_3CN, then few drops of HCl 37% were added until the chloride salt precipitated. The resulting solid was washed with CH_3CN and then dissolved in a 1:1 mixture of acetone and H_2O. An excess of NH_4PF_6 was added to the solution and the mixture was stirred for 2 hours to ensure complete precipitation of the salt. The organic solvent was then removed by distillation under reduced pressure and the residue was extracted

with DCM. The organic layer was dried over Na_2SO_4 and the solvent was removed under reduced pressure. The product was a white solid obtained in 72% yield.**^{1}H NMR** (500 MHz, $(CD_3)_2SO$, 298 K) δ 9.69 (s, 1H, -O*H*), 8.85 (s, 2H, -NH_2^+-), 7.42 (s, 1H, H_7), 7.29 (m, 4H, H_2+H_5), 6.80 (d, J = 8.6 Hz, 2H, H_1), 4.09 (s, 2H, H_3), 4.05 (s, 2H, H_4) 1.29 (s, 18H, H_6). **^{13}C NMR** (126 MHz, $(CD_3)_2SO$, 298 K) δ 158.0, 150.8, 131.6, 123.8, 122.4, 115.4, 50.5, 50.2, 34.6, 31.2. **^{19}F NMR** (470 MHz, $(CD_3)_2SO$, 298 K) δ -70.17 (d, J = 711.5 Hz). **HRMS** (ESI): m/z = 326.2484 (calcd 326.2484 for $C_{22}H_{32}NO^+$).

2.3. Synthesis of compound *E*-1

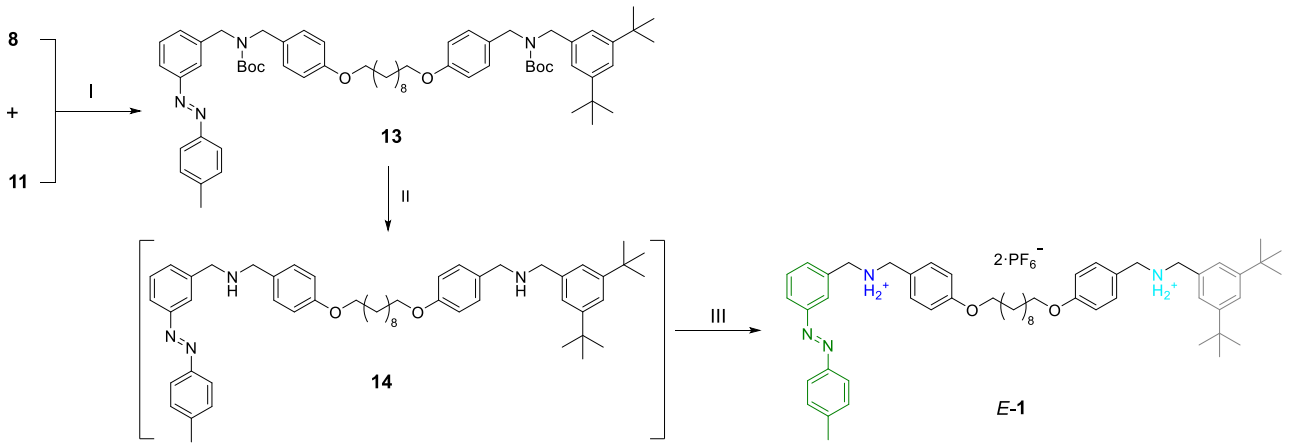

Scheme S3. I) K_2CO_3, CH_3CN 80°C. 84%, II) a. TFA, DCM b. $NaHCO_3$ Quant. III) MeOH, HCl 37%, NH_4PF_6 (sat), 69%.

2.3.1. Synthesis of 13

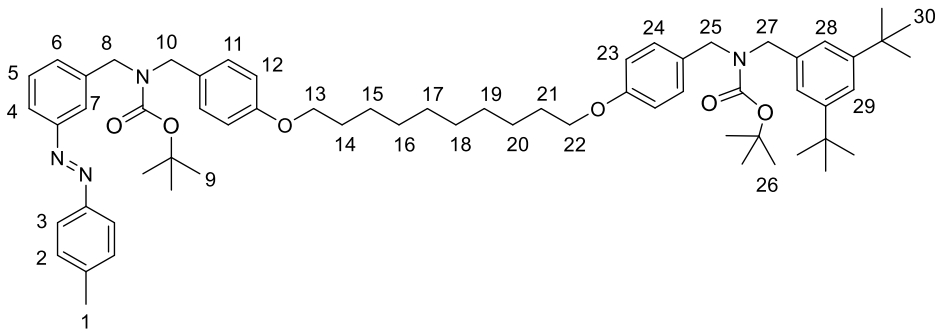

Compound **8** (0.250 g, 0.58 mmol) and compound **11** (0.589 g, 0.93 mmol) were dissolved in CH_3CN (40 mL), subsequently K_2CO_3 (0.200 g, 1.45 mmol) was added, and the mixture stirred at reflux for 24 hours. After the reaction was complete, the solvent was removed under vacuum, and the crude product was suspended in H_2O and extracted with AcOEt (3 × 60 mL). The organic layer was dried over Na_2SO_4 and the solvent was removed under vacuum. The product was isolated by chromatography using silica gel (eluent *n*-Hex : AcOEt, 9:1) to obtain a red foam in 84% yield.**^{1}H NMR** (500 MHz, $CDCl_3$, 298 K) δ 7.86 – 7.78 (m, 3H, H_3+H_4), 7.75 (s, 1H, H_7), 7.46 (t, J = 7.7 Hz, 1H, H_5), 7.36 – 7.27 (m, 4H, H_6+H_{29}+H_2), 7.25 – 6.99 (m, 6H, H_{11}+H_{24}+H_{28}), 6.94 – 6.79 (m, 4H, H_{12}+H_{23}), 4.55 – 4.21 (m, 8H, H_8+H_{10}+H_{25}+H_{27}), 3.94 (t, J = 6.5 Hz, 4H, H_{13}+H_{22}), 2.44 (s, 3H, H_1), 1.82 – 1.74 (m, 4H, H_{14}+H_{21}), 1.50 (m, 22H, H_9+H_{15}+H_{20}+H_{26}), 1.31 (m, 26H, H_{16}+H_{17}+H_{18}+H_{19}+H_{30}). **^{13}C NMR** (126 MHz, $CDCl_3$, 298 K) δ 158.6, 158.5, 158.5, 156.2, 153.1, 151.0, 150.9, 141.8, 139.6, 139.4, 137.5, 137.1, 130.2, 130.1, 129.9, 129.8, 129.6, 129.4, 129.0, 123.0,

122.4, 122.0, 121.7, 121.3, 121.2, 114.7, 114.6, 80.3, 79.9, 68.2, 68.2, 49.9, 49.5, 49.3, 48.9, 34.9, 31.6, 29.7, 29.6, 29.4, 28.6, 27.1, 27.0, 26.2, 21.7.

2.3.2. Synthesis of *E*-1

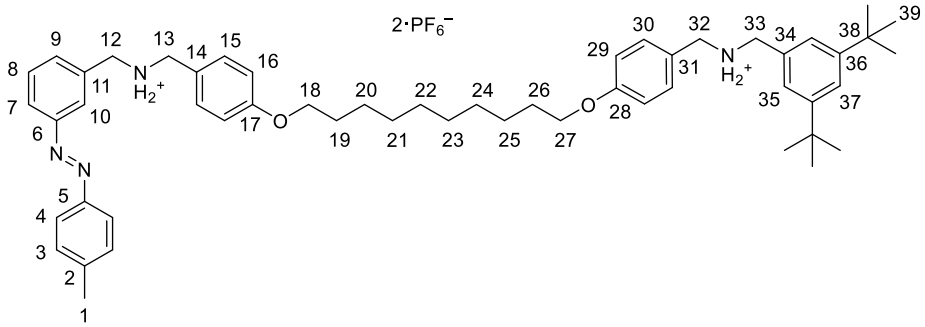

Compound **13** (0.150 g, 0.15 mmol) was dissolved in DCM (10 ml), subsequently trifluoroacetic acid (TFA) (1 mL,13.1 mmol) was added, the solution turned immediately dark red. The mixture was stirred at room temperature for 12 hours. At the end of the deprotection reaction, the solvent was removed under vacuum and the crude was dissolved in AcOEt (50 mL), the organic phase was washed with a saturated solution of $NaHCO_3$ (3 × 50 mL) and finally with brine. The organic layer was dried over Na_2SO_4 and the solvent was removed under reduced pressure. Product **14** was not isolated and the residue was directly employed for the next reaction. Compound **14** (0.1 g, 0.12 mmol) was dissolved in the minimum amount of MeOH, subsequently few drops of HCl 37% were added until precipitation of a red solid. A saturated solution of NH_4PF_6 (aq) was then added and the suspension was sonicated for 15 minutes. The resulting red solid was collected by vacuum filtration and washed with H_2O. The obtained solid compound was dissolved in DCM and Na_2SO_4 was added. The organic layer was filtered and concentrated in vacuo to yield a fine red powder in 69 % yield. **^{1}H NMR** (500 MHz, CD_2Cl_2/CD_3CN 3:7, 298 K) δ 7.97-7.95 (m, 2H, H_9, H_{10}), 7.83 (d, *J* = 8.6 Hz, 2H, H_4), 7.64 (t, *J*= 7.6 Hz, 1H, H_8), 7.59 (d, *J* = 7.7 Hz, 1H, H_7) 7.51 (t, *J*=1.7 Hz, 1H, H_{37}), 7.40-7.38 (m, 4H, H_{15}+H_{30}), 7.35 (d, *J*= 8.6 Hz, 2H, H_3), 7.27 (d, *J*=1.7 Hz, 2H, H_{35}), 7.18 (bs, -NH_2 I), 7.01 (bs, -NH_2 II), 6.96-6.93(m, 4H, H_{16}+H_{29}), 4.31 (s, 2H, H_{12}), 4.20 (s, 2H, H_{13}), 4.14 (s, 4H, H_{32}+H_{33}), 3.98 (t, *J*=6.6 Hz, 4H, H_{18}+H_{27}), 2.44 (s, 3H, H_1), 1.78-1.72 (m, 4H, H_{19}+H_{26}), 1.46-1.43 (m, 4H, H_{20}-H_{25}), 1.34 (bs, 8H, H_{21}+H_{22}+H_{23}+H_{24}), 1.32 (s, 18H, H_{39}). **^{13}C NMR** (126 MHz, CD_2Cl_2/CD_3CN 3:7, 298 K) δ 161.1 (28), 161.0 (17), 153.6 (6), 152.6 (36), 151.2 (5), 143.5 (2), 133.1 (7), 132.6 (3+15), 132.3 (11), 130.9 (8), 130.8 (30), 130.3 (34), 125.0 (35), 124.8 (9), 124.7 (10), 124.4 (37), 123.6 (4), 122.5 (31), 122.5 (14), 115.6 (16), 115.6 (29), 68.8 (18+27), 52.4 (32), 52.0 (13), 51.8 (33), 51.6 (12), 35.5 (38), 31.5 (39), 30.1 (22+23), 29.9 (21+24), 29.7 (19+26), 26.5 (20+25), 21.5 (1). **^{19}F NMR** (470 MHz, CD_2Cl_2/CD_3CN 3:7, 298 K) δ -72.93 (d, *J* = 707.2 Hz). **HRMS** (ESI): m/z = 944.5375 (calcd 944.5392 for $C_{53}H_{72}F_6N_4O_2P$).

2.4. Synthesis of crown ether 2

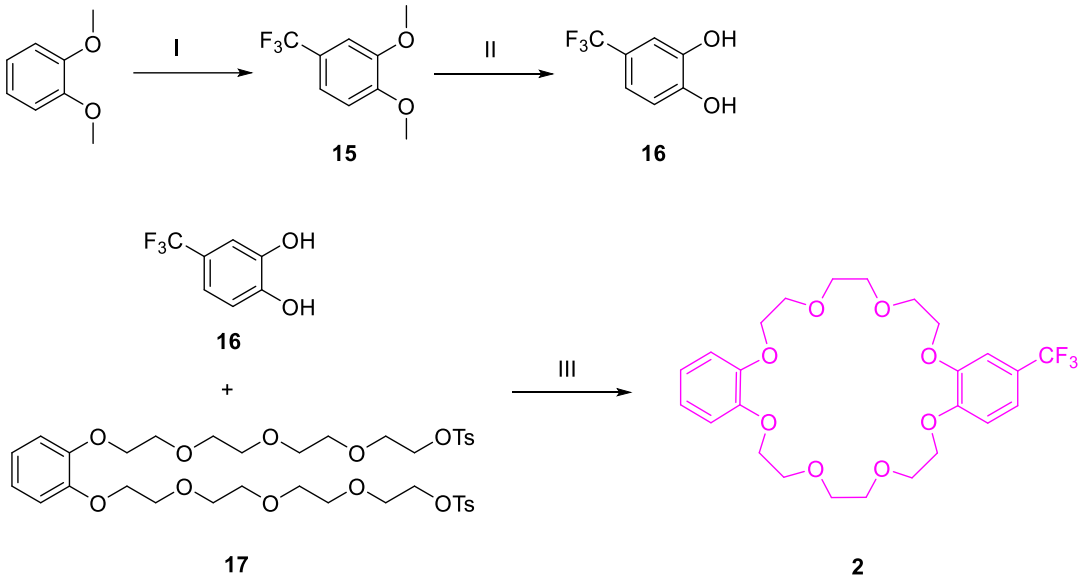

Scheme S4. I) CF_3SO_2Na tBuOOH, CH_3CN r.t. 12 h, 38% II) BBr_3, DCM, –15°C, 60% III) Cs_2CO_3, THF, 70°C, 48 h. 72%.

2.4.1. Synthesis of 15

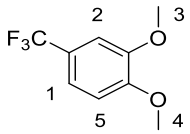

Veratrole (2 g, 14.3 mmol) and sodium triflinate ($NaCF_3SO_2$) (3,4 g, 21.8 mmol) were dissolved in CH_3CN (60 mL) in a Schlenk flask and stirred at 0 °C under nitrogen flux. Subsequently, *tert*-butyl hydroperoxide 70% in H_2O (6.4 mL) was slowly added to the flask with a syringe pump (Flow : 3mL/hour). The reaction was left to return to room temperature and stirred for 12 hours. After this time, the mixture was quenched with water and extracted with Et_2O (80 mL × 3 times), the organic phases were washed with water then with brine and finally dried over Na_2SO_4. The product was purified *via* column chromatography over silica, eluent CH_2Cl_2:cy-hex, 1:1. The product was a yellow oil obtained in 38% yield.
^{1}H NMR (500 MHz, $CDCl_3$, 298 K) δ 7.18 (d, J = 10.2 Hz, 1H, H_1), 7.05 (s, 1H, H_2), 6.87 (d, J = 10.2 Hz, 1H, H_5), 3.88 (s, 6H, H_3+H_4). **^{13}C NMR** (126 MHz, $CDCl_3$, 298 K) δ 151.9, 149.1, 124.4 (q, J = 271.2 Hz), 122.9 (q, J = 32.7 Hz), 118.4 (q, J = 4.2 Hz), 110.6, 108.1 (q, J = 3.5 Hz), 56.0, 56.0. **^{19}F NMR** (470 MHz, $CDCl_3$) δ -61.65 (s, 3F).

2.4.2. Synthesis of 16

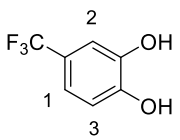

Compound **15** (1,14 g, 5,54 mmol) was dissolved in dry CH_2Cl_2 (100 mL). Boron tribromide (3,9 mL, 39 mmol) was slowly added to the solution maintained at -15 °C using a frigorific mixture bath

(20% w/w NH_4Cl in ice and H_2O). The reaction mixture was allowed to return to room temperature and stirred overnight. At the end of the reaction the mixture was quenched with water and extracted with AcOEt (50 mL × 3). The organic phase was washed with brine and dried over Na_2SO_4. The product was purified by column chromatography on silica (eluent *n*-Hex : AcOEt, 4:1). The product was a pale green oil obtained in 60% yield.
^{1}H NMR (500 MHz, $CDCl_3$, 298 K) δ 7.12 (s, 1H, H_2), 7.09 (d, J = 8.4 Hz, 1H, H_1), 6.93 (d, J = 8.3 Hz, 1H, H_3), 5.58 (br. 2H, -OH). **^{13}C NMR** (126 MHz, $CDCl_3$) δ 146.8, 143.7, 124.2 (q, J = 271.1 Hz), 123.4 (q, J = 33.0 Hz), 118.6 (q, J = 4.2 Hz), 115.3, 112.6 (q, J = 3.7 Hz). **^{19}F NMR** (470 MHz, $CDCl_3$) δ -61.66 (s, 3F).

2.4.3. Synthesis of 2

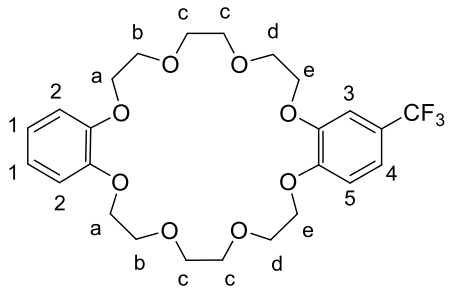

A solution of compound **16** (0.34 g, 1.9 mmol) and **17** (1.3 g, 1.5 mmol) in dry THF (50 mL) was added dropwise to a refluxing suspension of Cs_2CO_3 (3.1 g, 9.5 mmol) in dry THF (60 mL) under nitrogen. The reaction was stirred at reflux for 48 h, at the end of this time the solvent was removed under reduced pressure and the mixture was suspended in 100 mL of toluene. The organic phases were washed with water (100 mL × 3) and finally dried over Na_2SO_4. The product was purified by column chromatography over silica (eluent 3% MeOH in CH_2Cl_2) and subsequently recrystallized from boiling cyclohexane. The product was a white solid obtained in 72% yield. **^{1}H NMR** (500 MHz, CD_3CN, 298 K) δ 7.23 (d, J = 8.4 Hz, 1H, H_4), 7.18 (d, J = 2.0 Hz, 1H, H_3), 7.03 (d, J = 8.4 Hz, 1H, H_5), 6.95 – 6.86 (m, 4H, H_1+H_2), 4.18 – 4.13 (m, 4H, H_e), 4.11 – 4.07 (m, 4H, H_d), 3.84 – 3.77 (m, 8H, H_b+H_a), 3.69 (d, J = 1.8 Hz, 8H, H_c).**^{13}C NMR** (126 MHz, CD_3CN, 298 K) δ 152.6, 149.8, 149.8, 149.7, 125.6 (q, J = 270.4 Hz), 123.0 (q, J = 32.5 Hz), 122.2, 122.2, 119.4 (q, J = 4.3 Hz), 114.8, 114.8, 113.7, 111.1 (q, J = 3.6 Hz), 71.8, 71.7, 71.7, 70.6, 70.5, 70.3, 70.2, 70.1, 69.9, 69.7, 69.7. **^{19}F NMR** (470 MHz, CD_3CN) δ -61.93 (s, 3F). **HRMS** (ESI): m/z = 541.1947 [**2**+Na]$^+$ (calcd 541.1929 for $C_{25}H_{31}F_3O_8Na$).

3. NMR and MS characterization

3.1. NMR Characterization of the compounds

3.1.1. ^{1}H and ^{13}C NMR spectra of compound 5

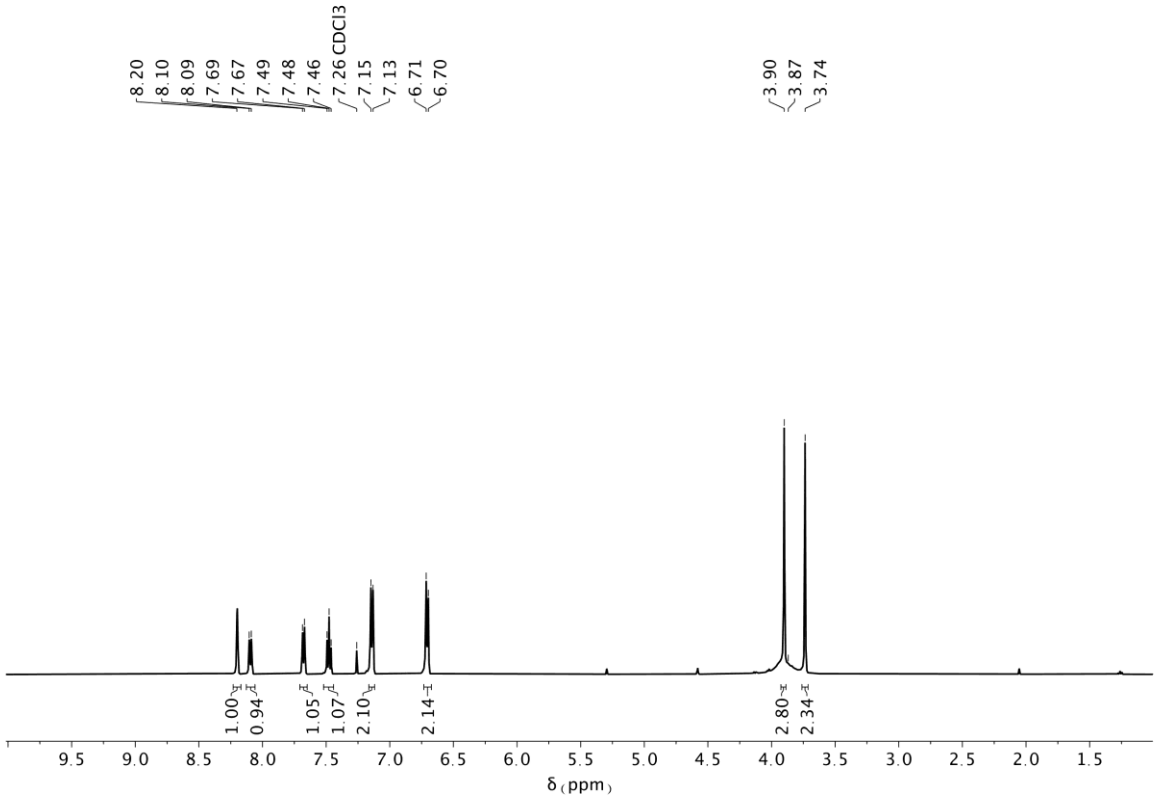

Figure S1. ^{1}H NMR spectrum of compound **5** ($CDCl_3$, 500 MHz, 298 K).

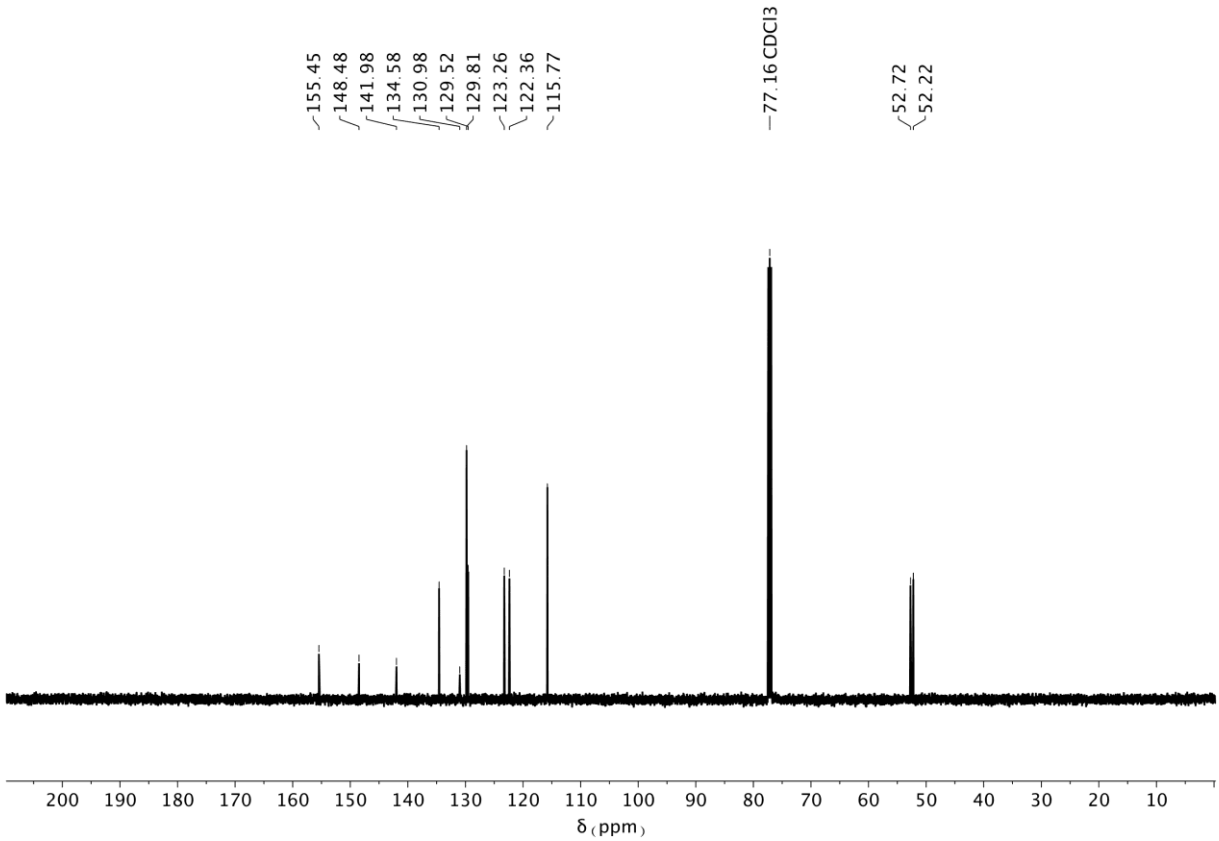

Figure S2. ^{13}C NMR spectrum of compound **5** ($CDCl_3$, 126 MHz, 298 K).

3.1.2. ^{1}H and ^{13}C NMR spectra of compound 6

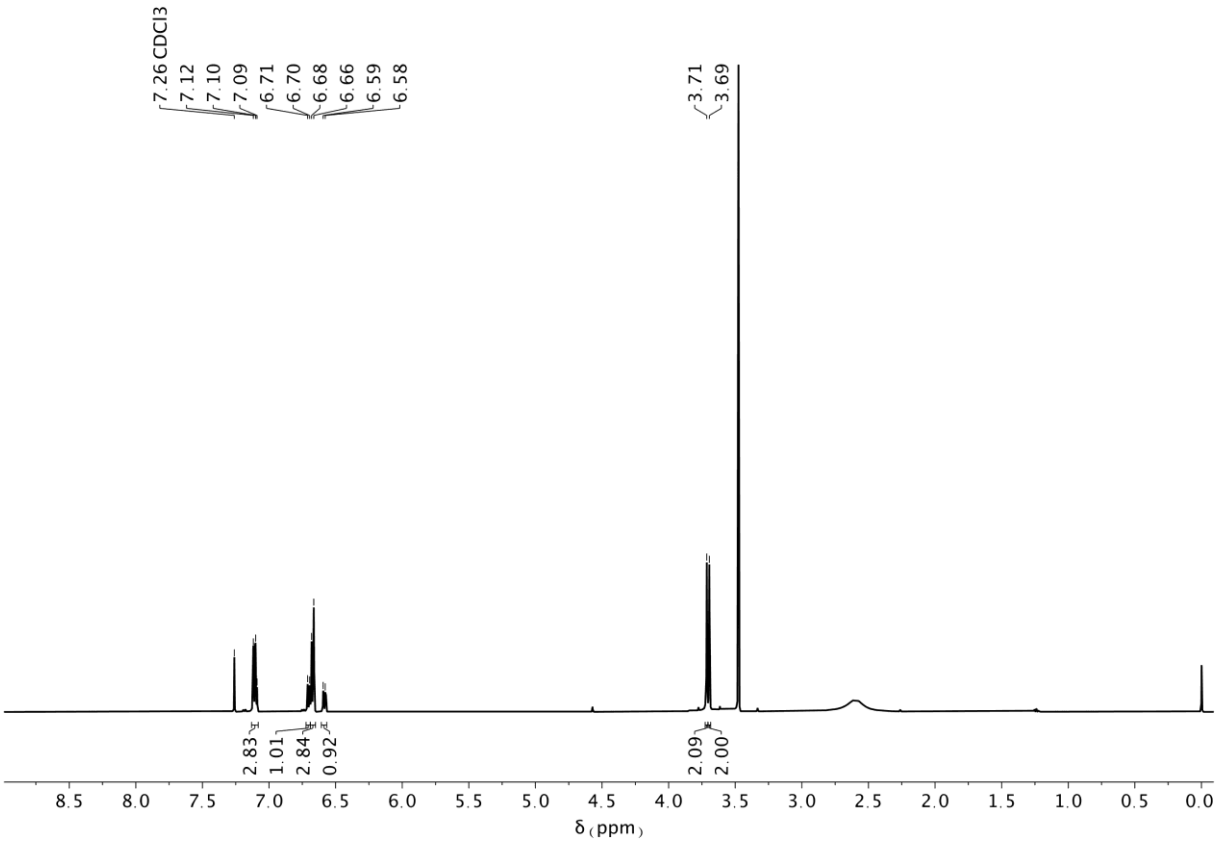

Figure S3. ^{1}H NMR spectrum of compound **6** ($CDCl_3$, 500 MHz, 298 K).

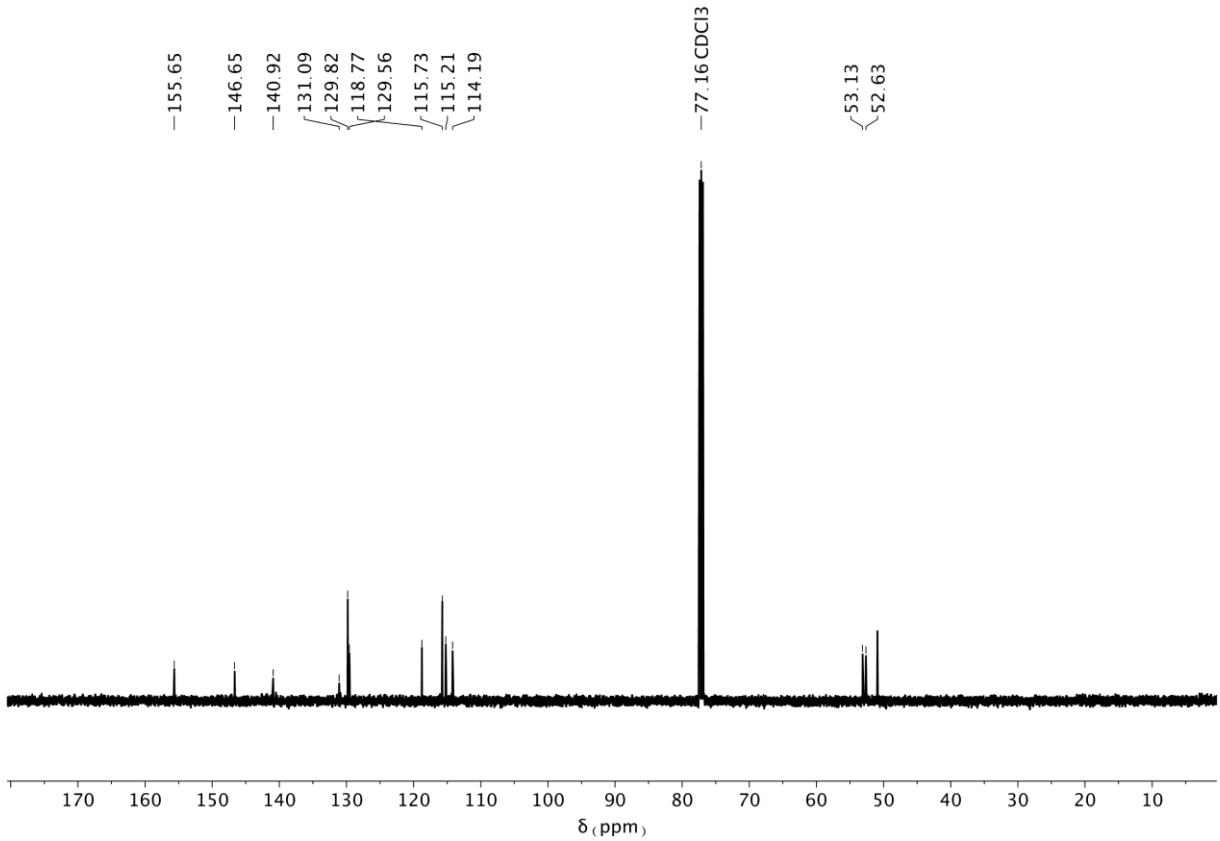

Figure S4. ^{13}C NMR spectrum of compound **6** ($CDCl_3$, 126 MHz, 298 K).

3.1.3. ^{1}H and ^{13}C NMR spectra of compound 7

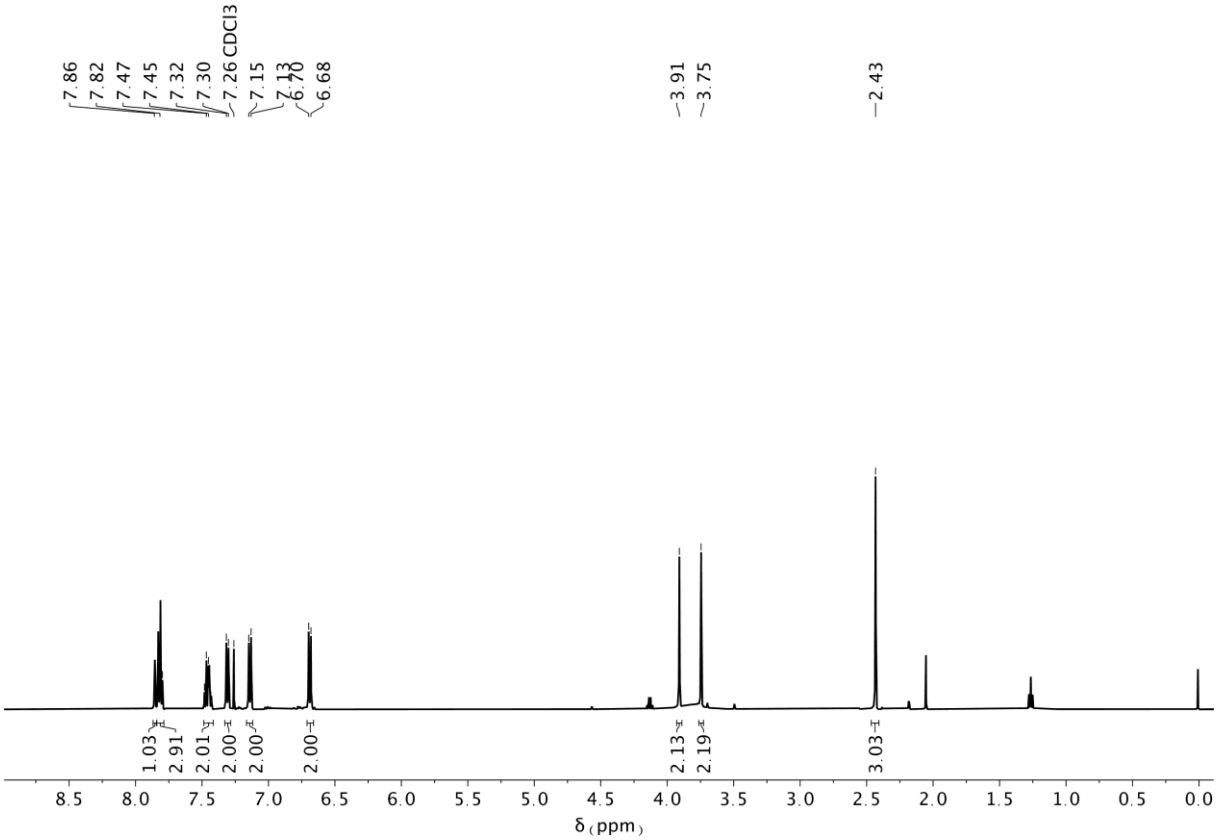

Figure S5. ^{1}H NMR spectrum of compound **7** ($CDCl_3$, 500 MHz, 298 K).

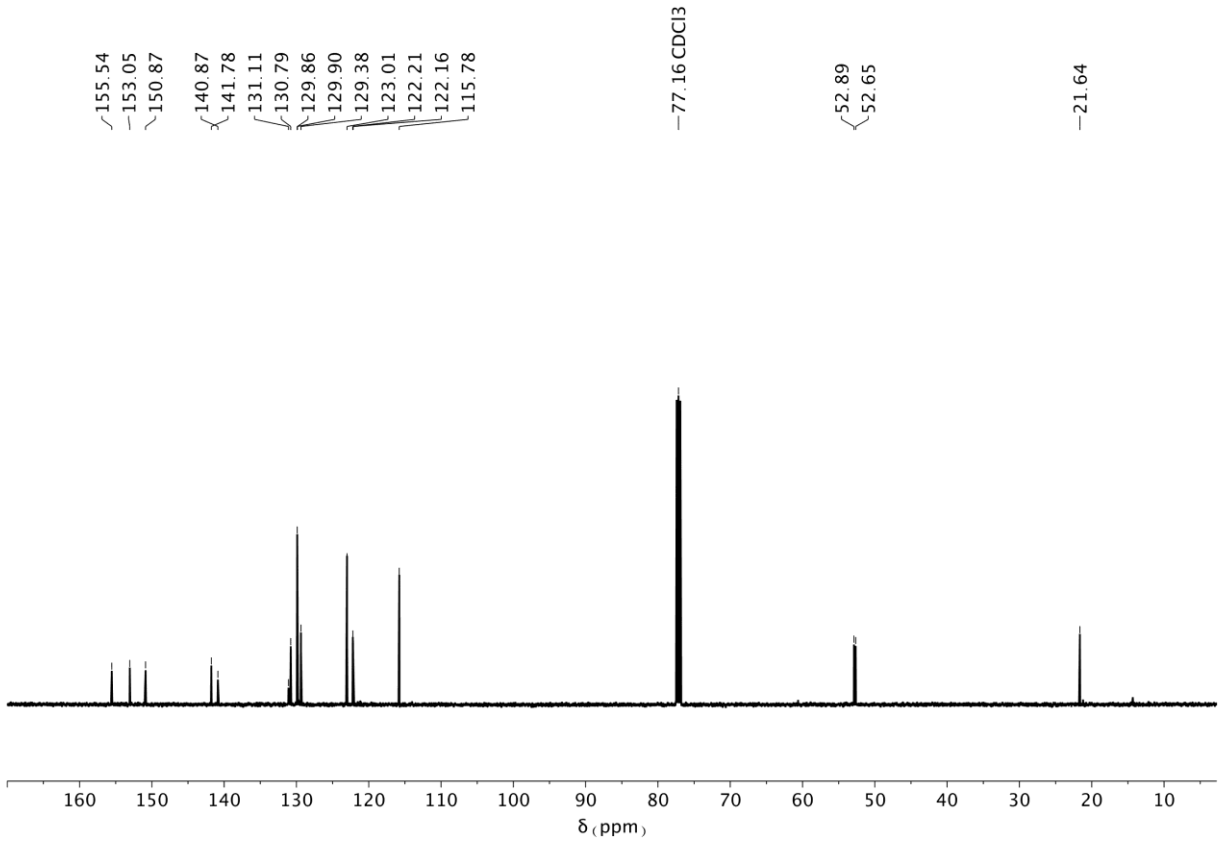

Figure S6. ^{13}C NMR spectrum of compound **7** ($CDCl_3$, 126 MHz, 298 K).

3.1.4. ^{1}H,^{13}C, ^{19}F NMR spectra of compound *E*-3

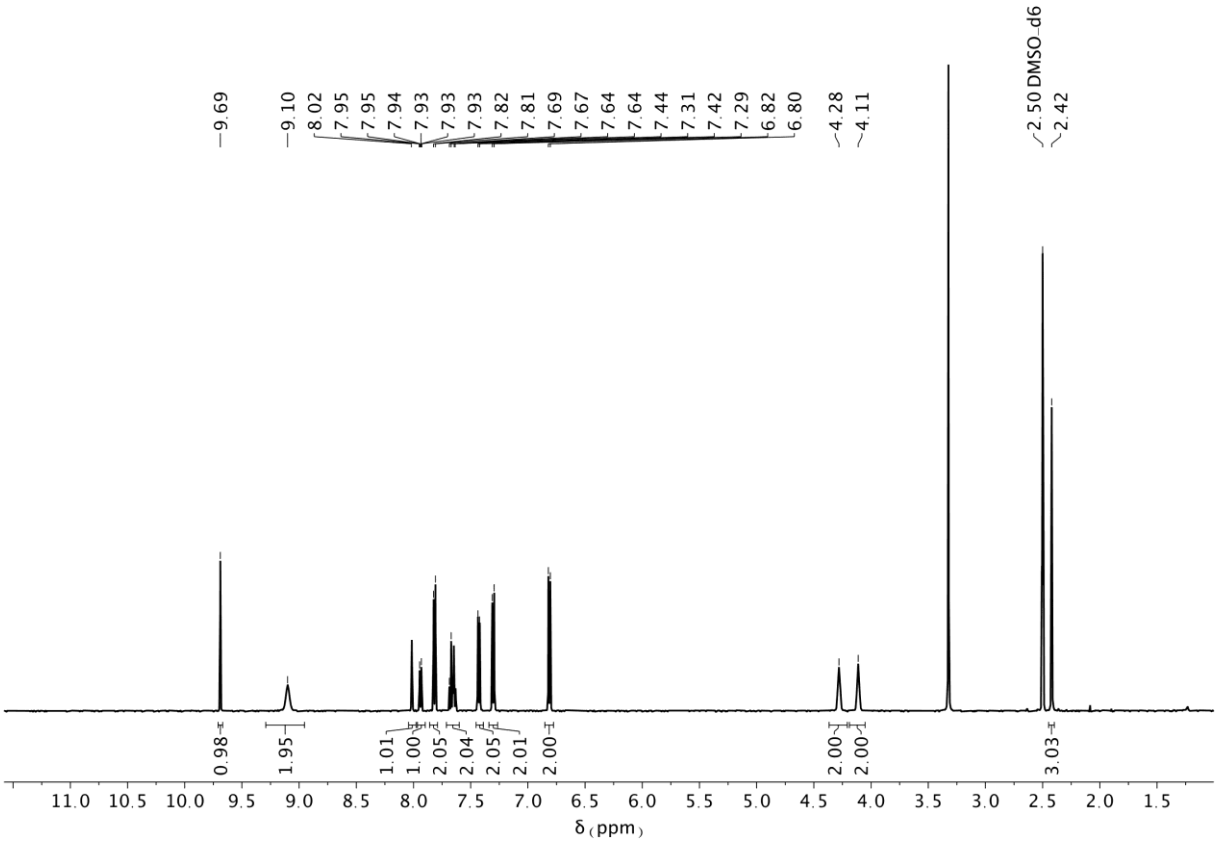

Figure S7. ^{1}H NMR spectrum of compound *E*-**3** ($(CD_3)_2SO$, 500 MHz, 298 K).

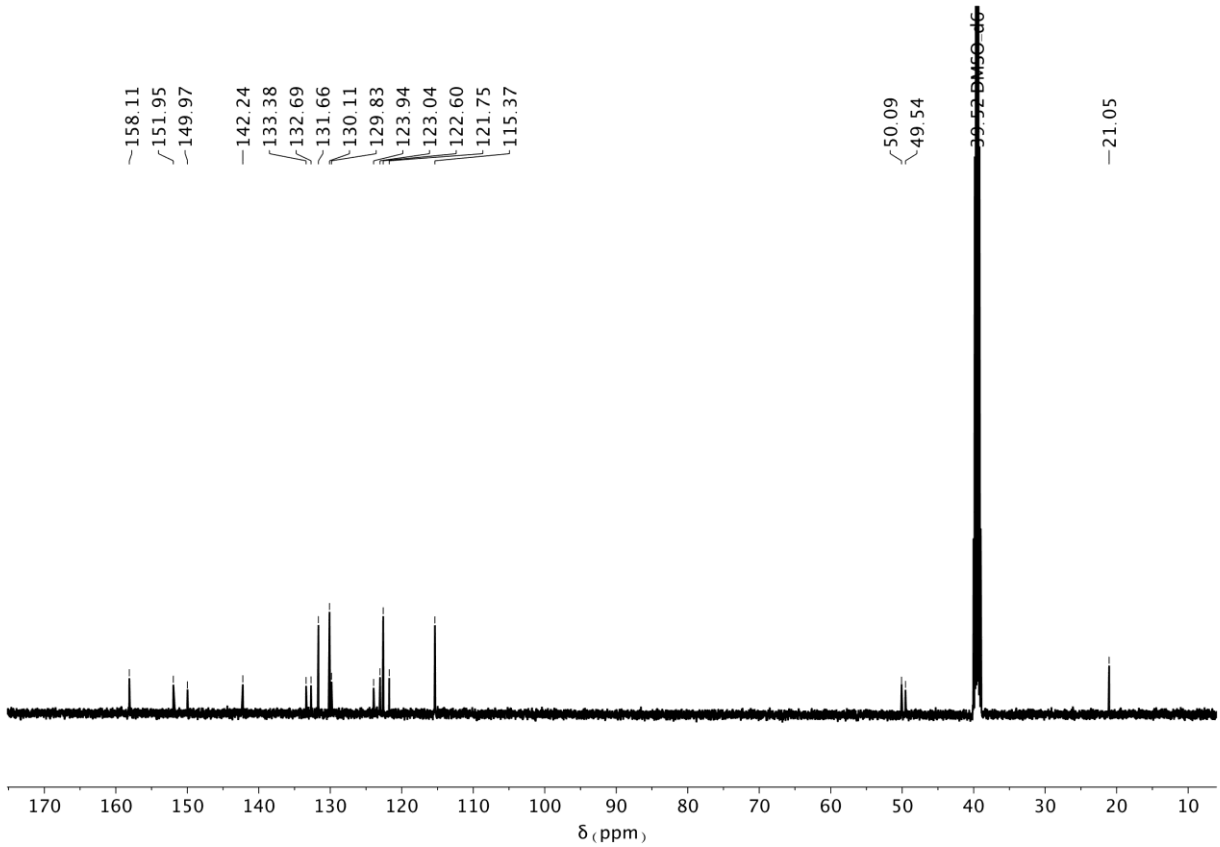

Figure S8. ^{13}C NMR spectrum of compound *E*-**3** ($(CD_3)_2SO$, 126 MHz, 298 K).

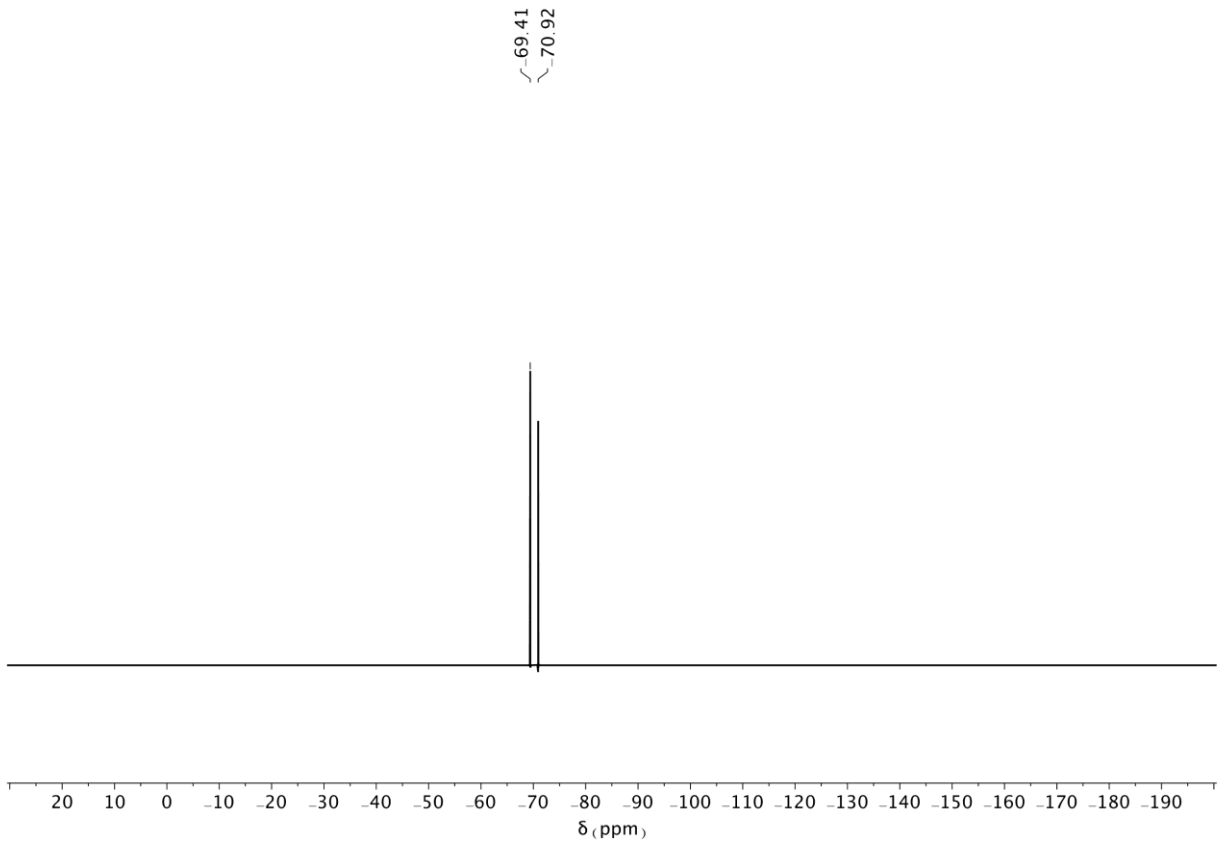

Figure S9. ^{19}F NMR spectrum of compound *E*-**3** ($(CD_3)_2SO$, 470 MHz, 298 K).

3.1.5. ^{1}H and ^{13}C NMR spectra of compound 8

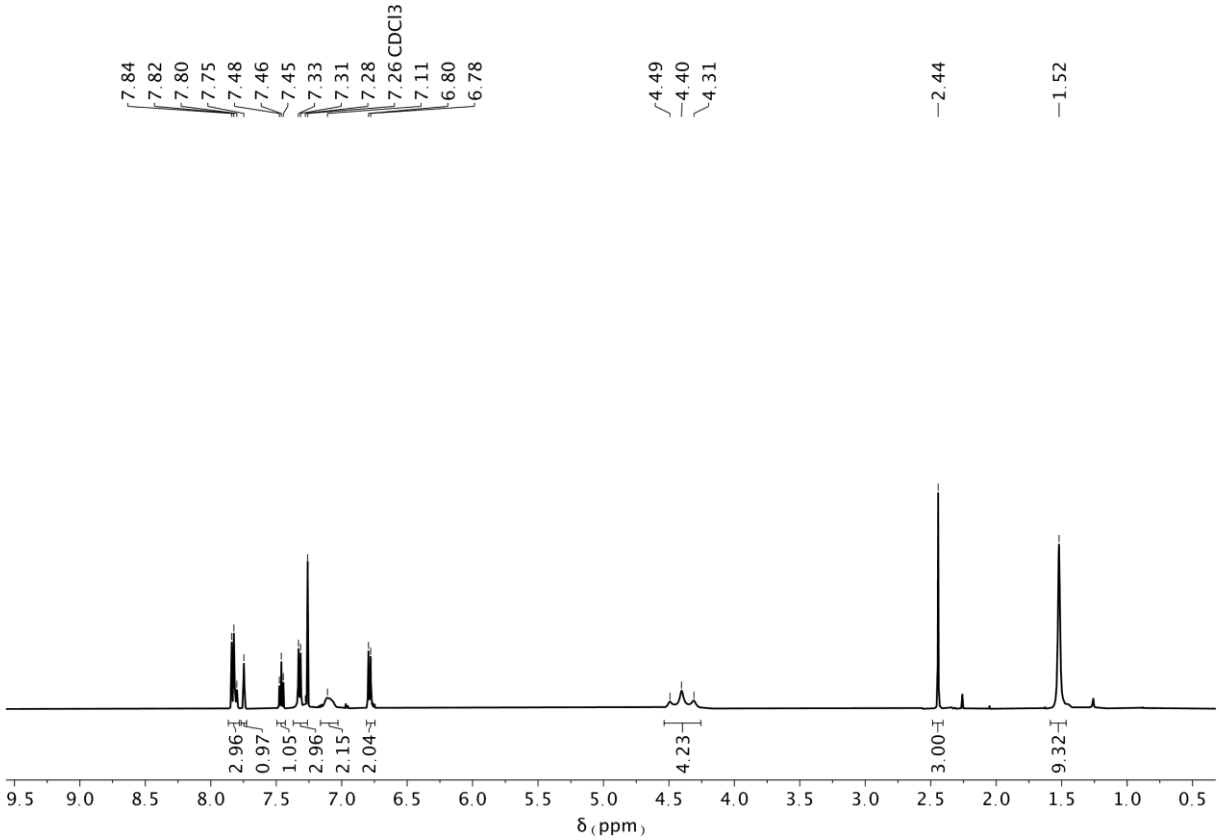

Figure S10. ^{1}H NMR spectrum of compound **8** ($CDCl_3$, 500 MHz, 298K).

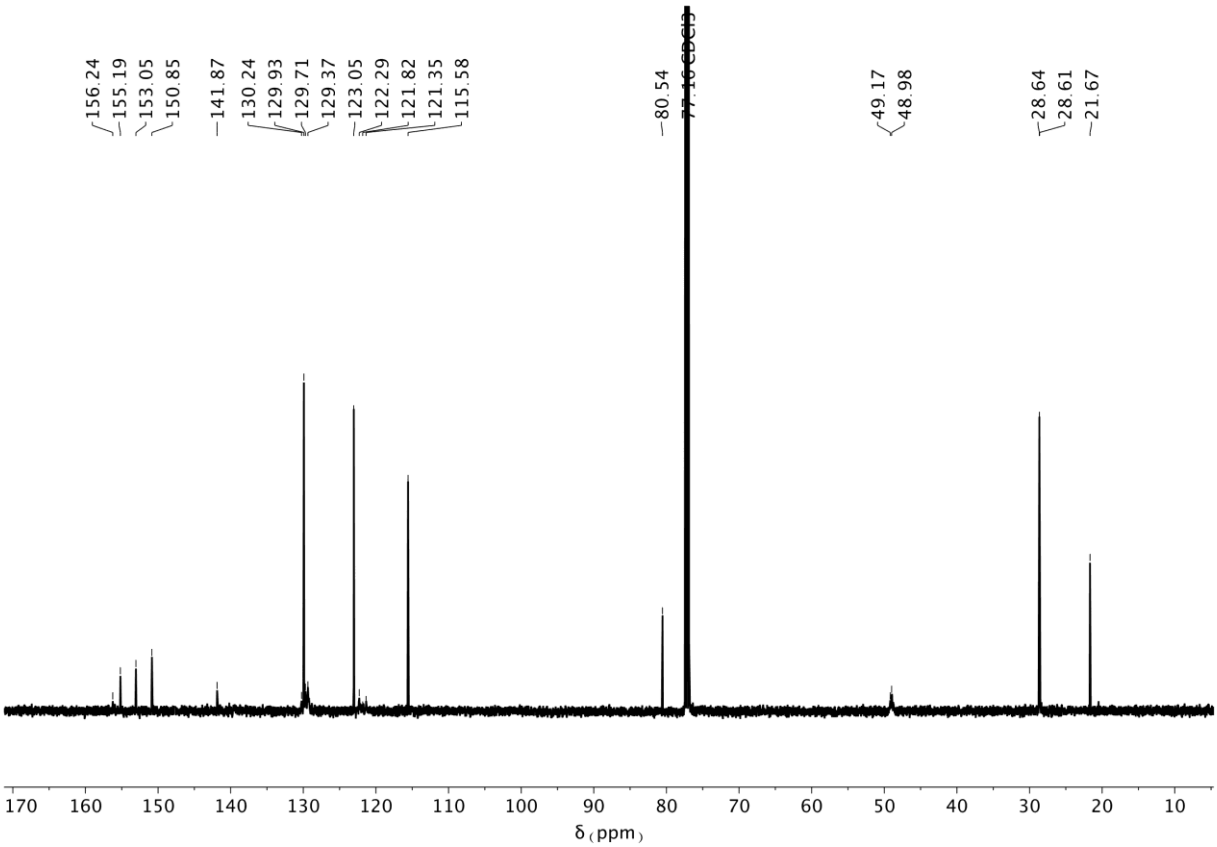

Figure S11. ^{13}C NMR spectrum of compound **8** ($CDCl_3$, 126 MHz, 298 K).

3.1.6. ^{1}H and ^{13}C NMR spectra of compound 11

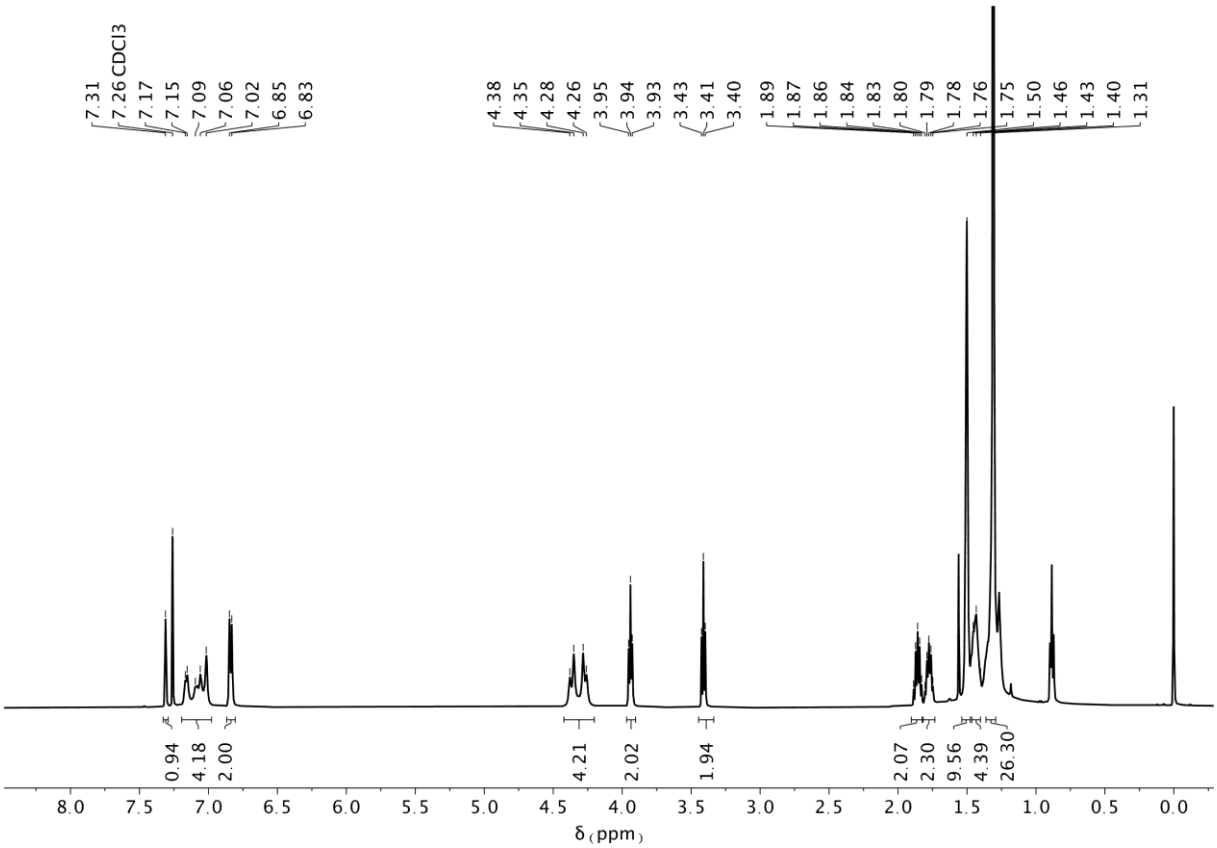

Figure S12. ^{1}H NMR spectrum of compound **11** ($CDCl_3$, 500 MHz, 298 K).

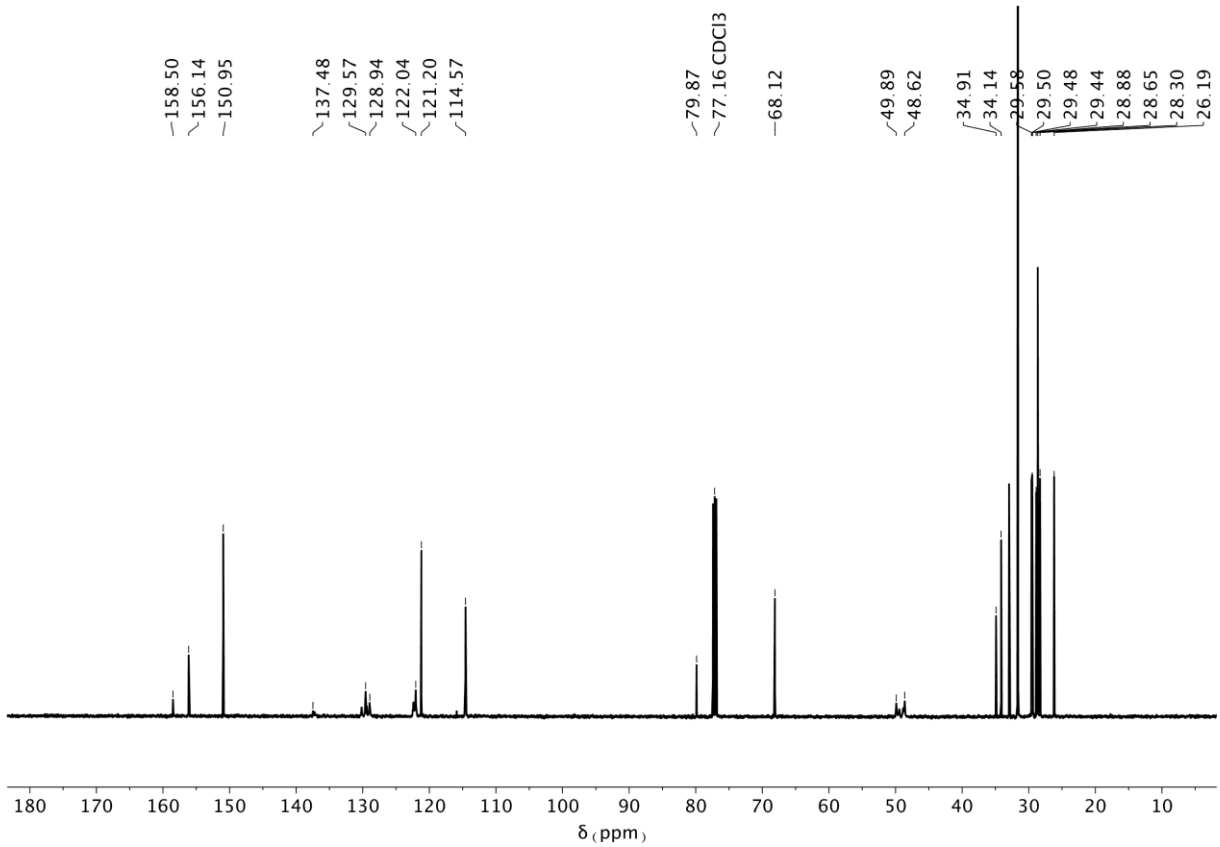

Figure S13. ^{13}C NMR spectrum of compound **11** ($CDCl_3$, 126 MHz, 298 K).

3.1.7. ^{1}H and ^{13}C NMR spectra of compound 4

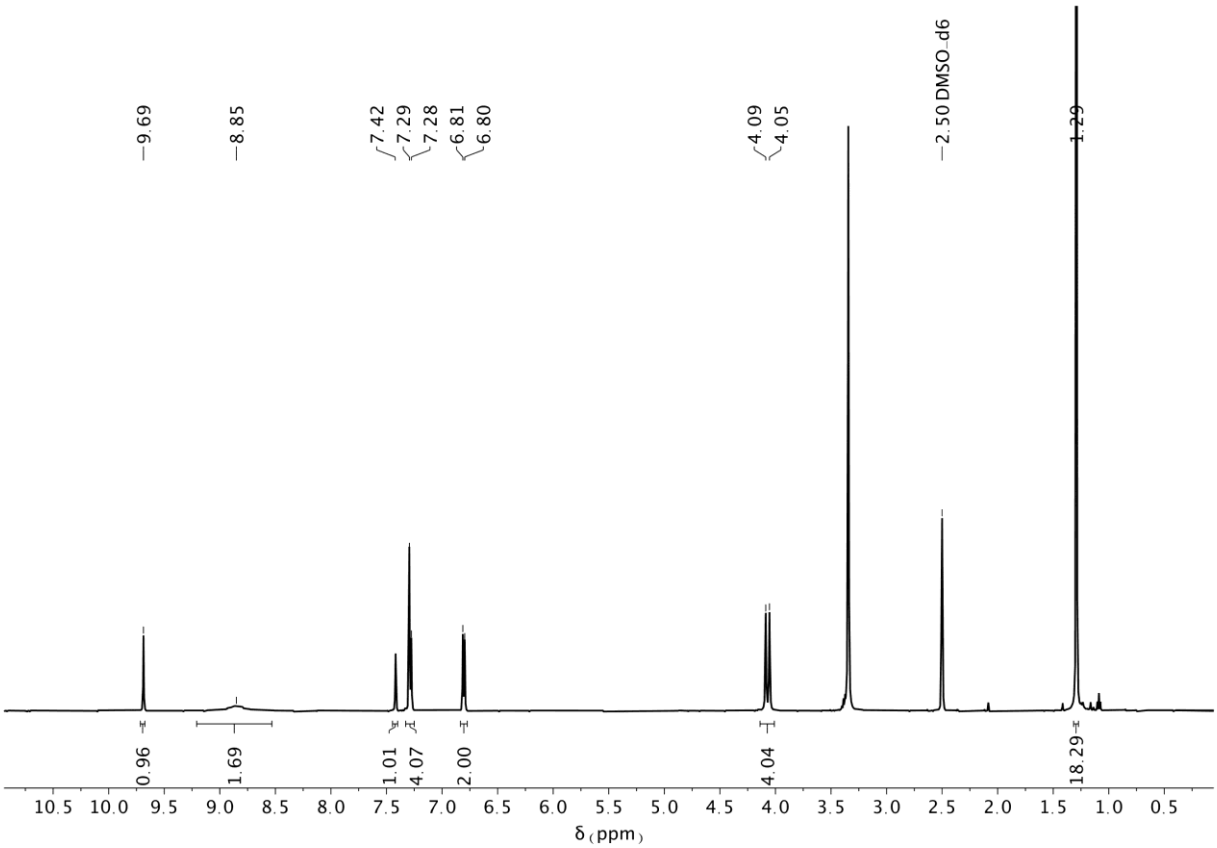

Figure S14. ^{1}H NMR spectrum of compound **4** ($(CD_3)_2SO$, 500 MHz, 298 K).

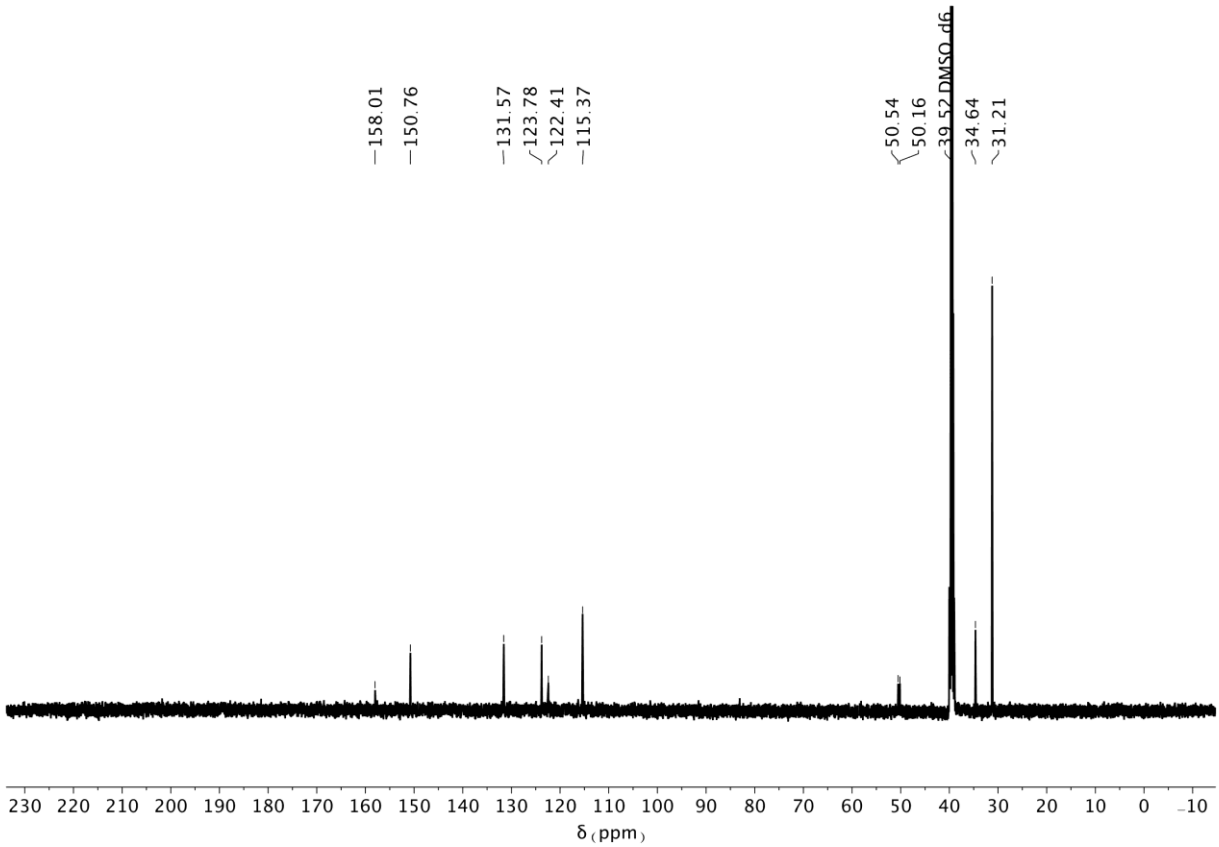

Figure S15. ^{13}C NMR spectrum of compound **4** ($(CD_3)_2SO$, 126 MHz, 298 K).

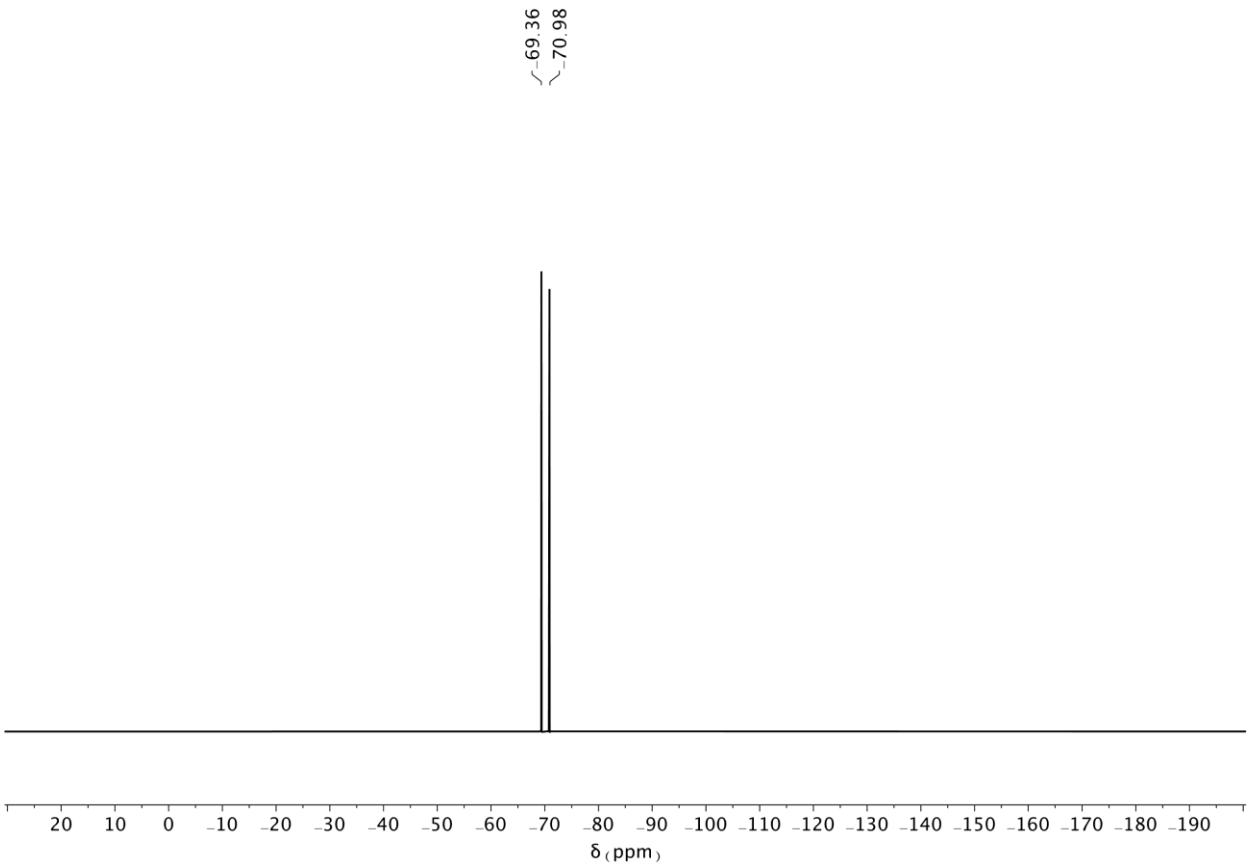

Figure S16. ^{19}F NMR spectrum of compound **4** ($(CD_3)_2SO$, 470 MHz, 298 K).

3.1.8. ^{1}H and ^{13}C NMR spectra of compound 13

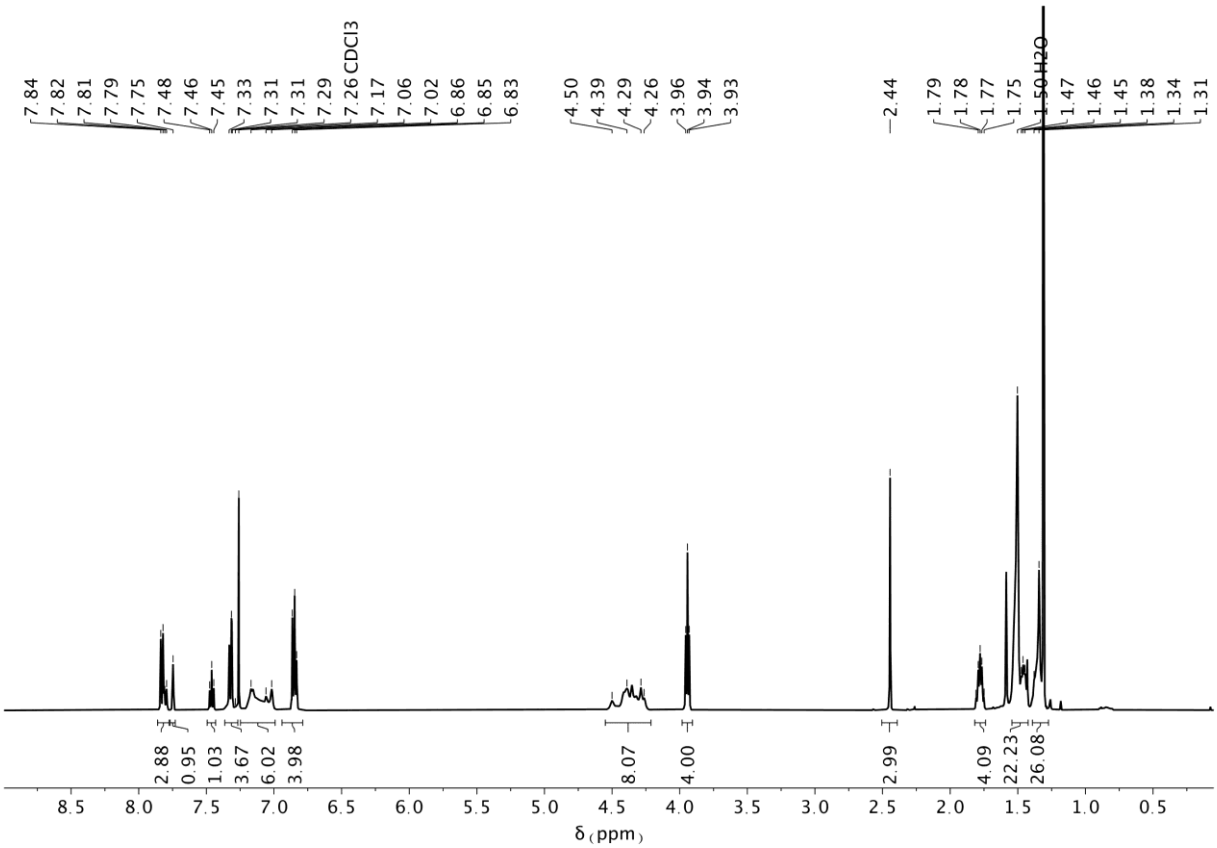

Figure S17. ^{1}H NMR spectrum of compound **13** ($CDCl_3$, 500 MHz, 298 K).

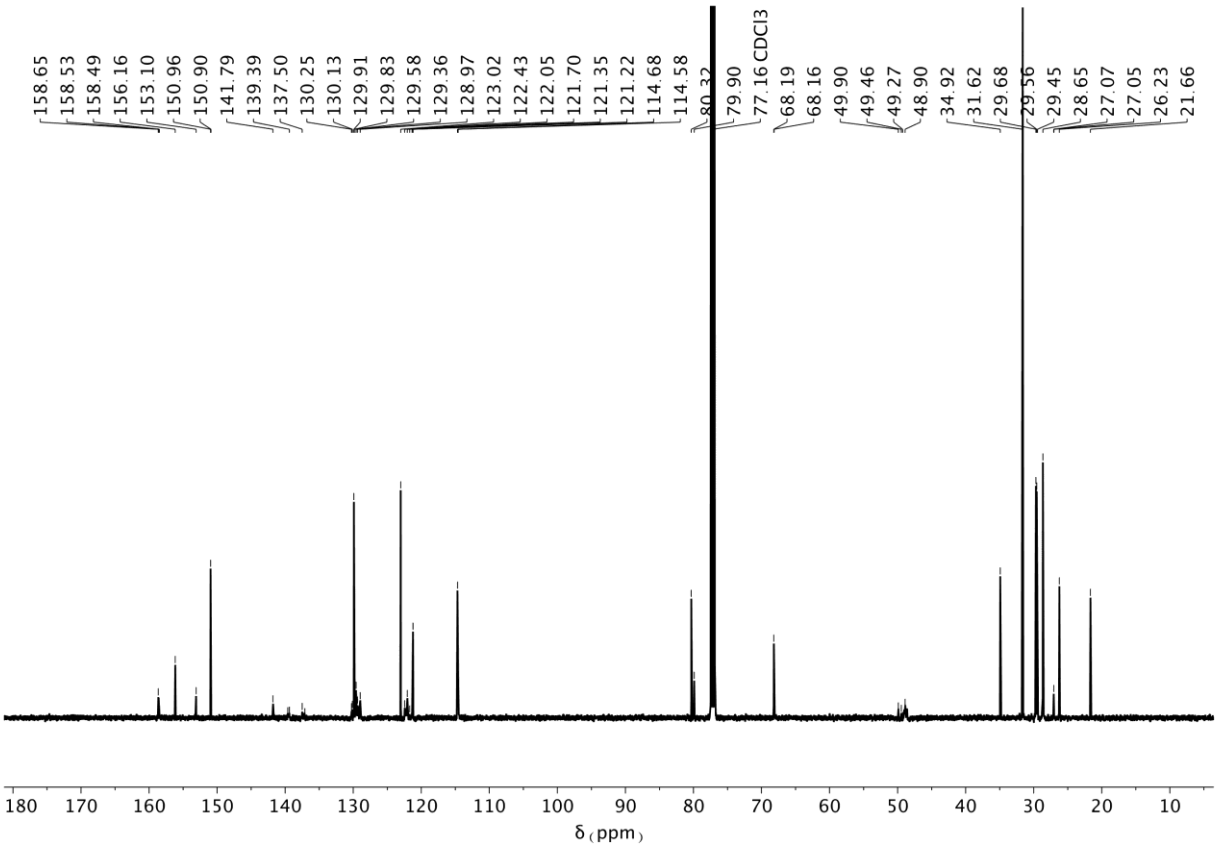

Figure S18. ^{13}C NMR spectrum of compound **13** ($CDCl_3$, 500 MHz, 126 K).

3.1.9. ^{1}H, ^{13}C and ^{19}F NMR spectra of compound *E*-1

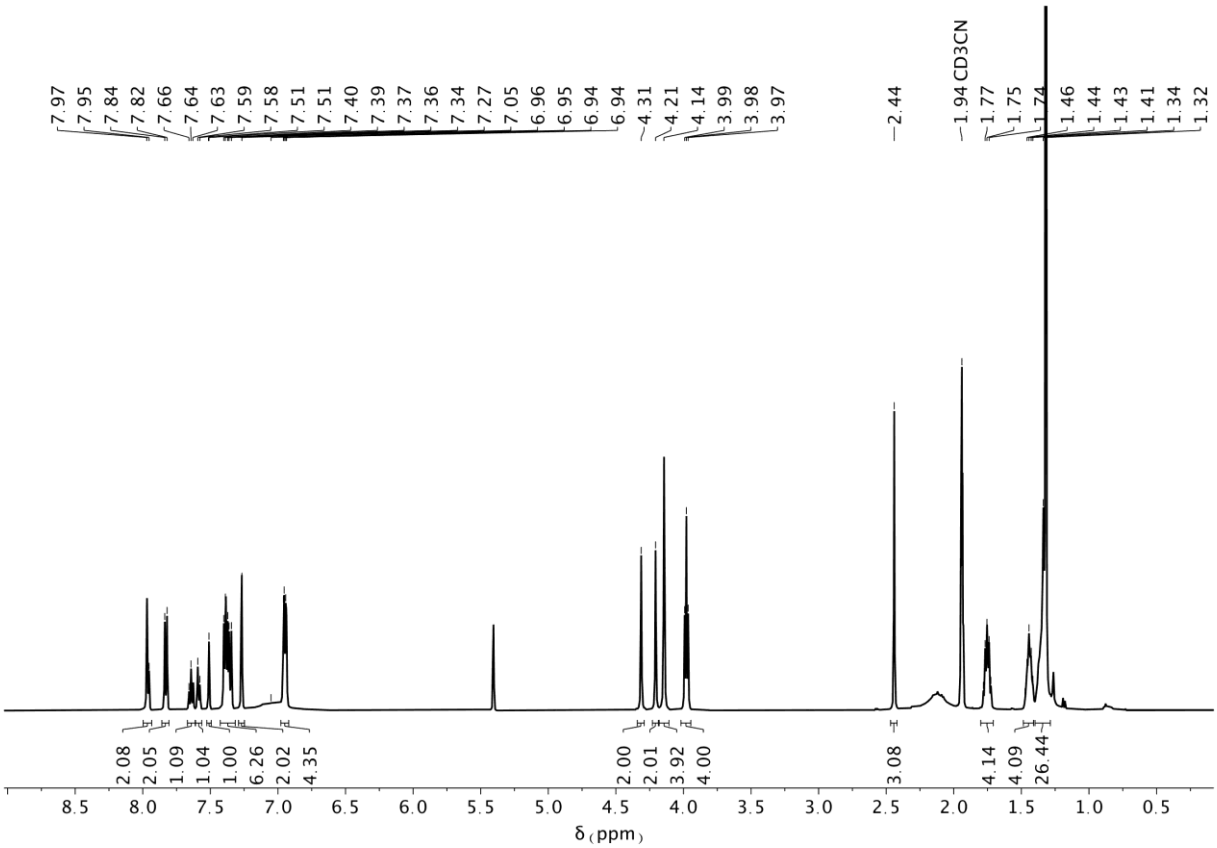

Figure S19. ^{1}H NMR spectrum of compound ***E*-1** (CD_2Cl_2/CD_3CN 3:7, 500 MHz, 298 K).

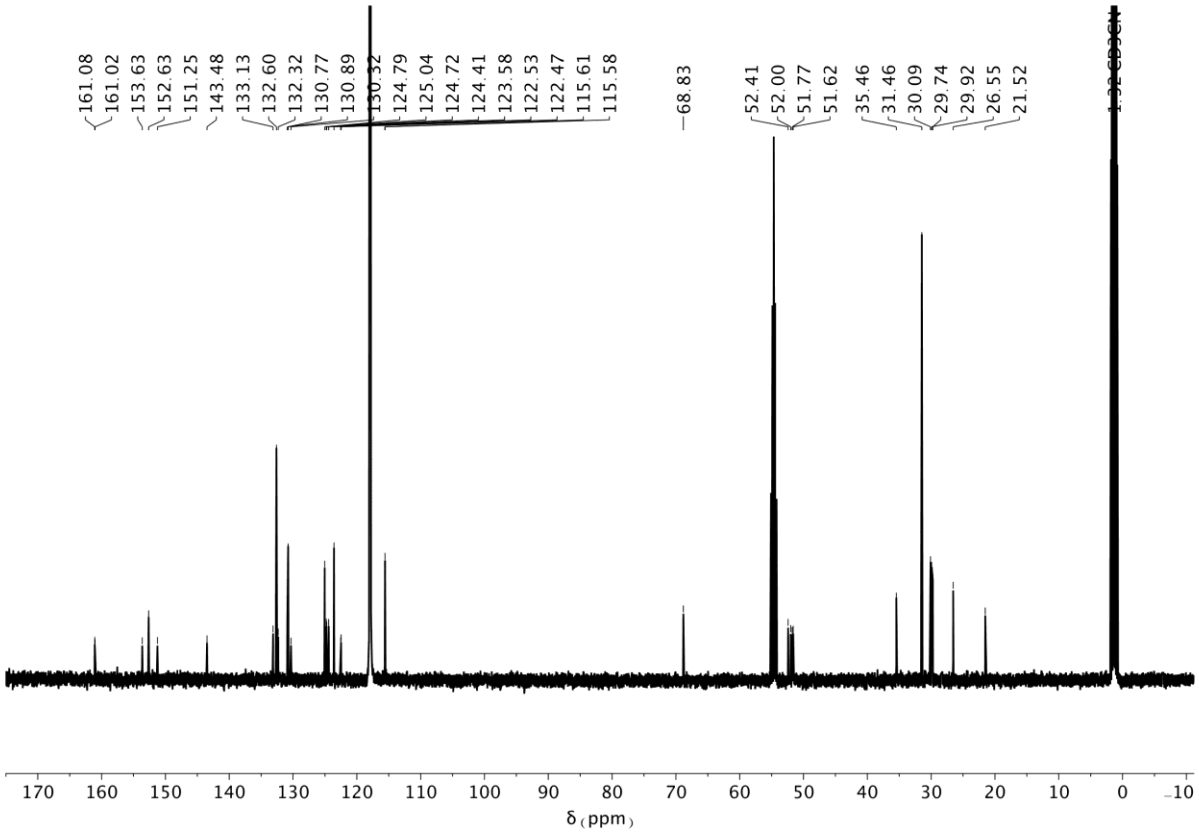

Figure S20. ^{13}C NMR spectrum of compound *E*-**1** (CD_2Cl_2/CD_3CN 3:7, 126 MHz, 298 K).

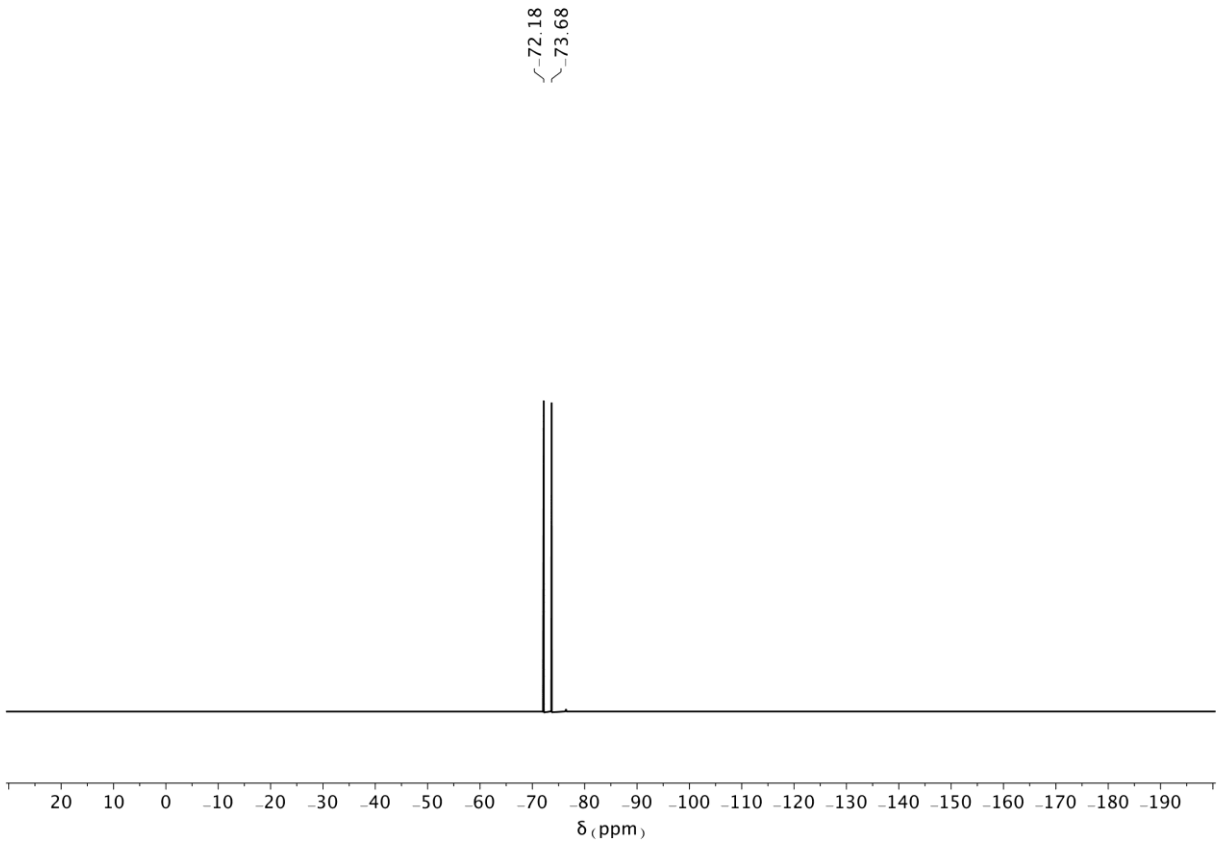

Figure S21. ^{19}F NMR spectrum of compound *E*-**1** (CD_2Cl_2/CD_3CN 3:7, 470 MHz, 298 K).

3.1.10. ^{1}H, ^{13}C and ^{19}F NMR spectra of compound 15

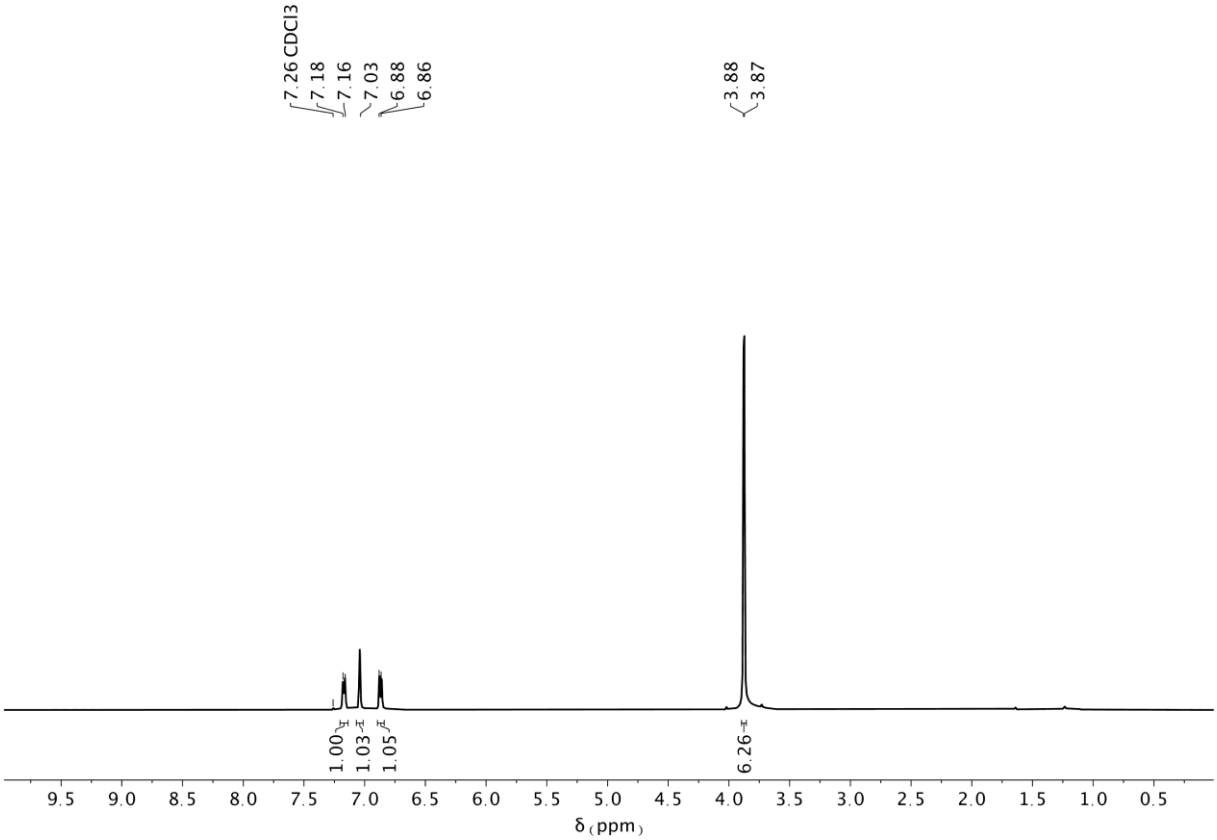

Figure S22. ^{1}H NMR spectrum of compound **15** ($CDCl_3$, 500 MHz, 298 K).

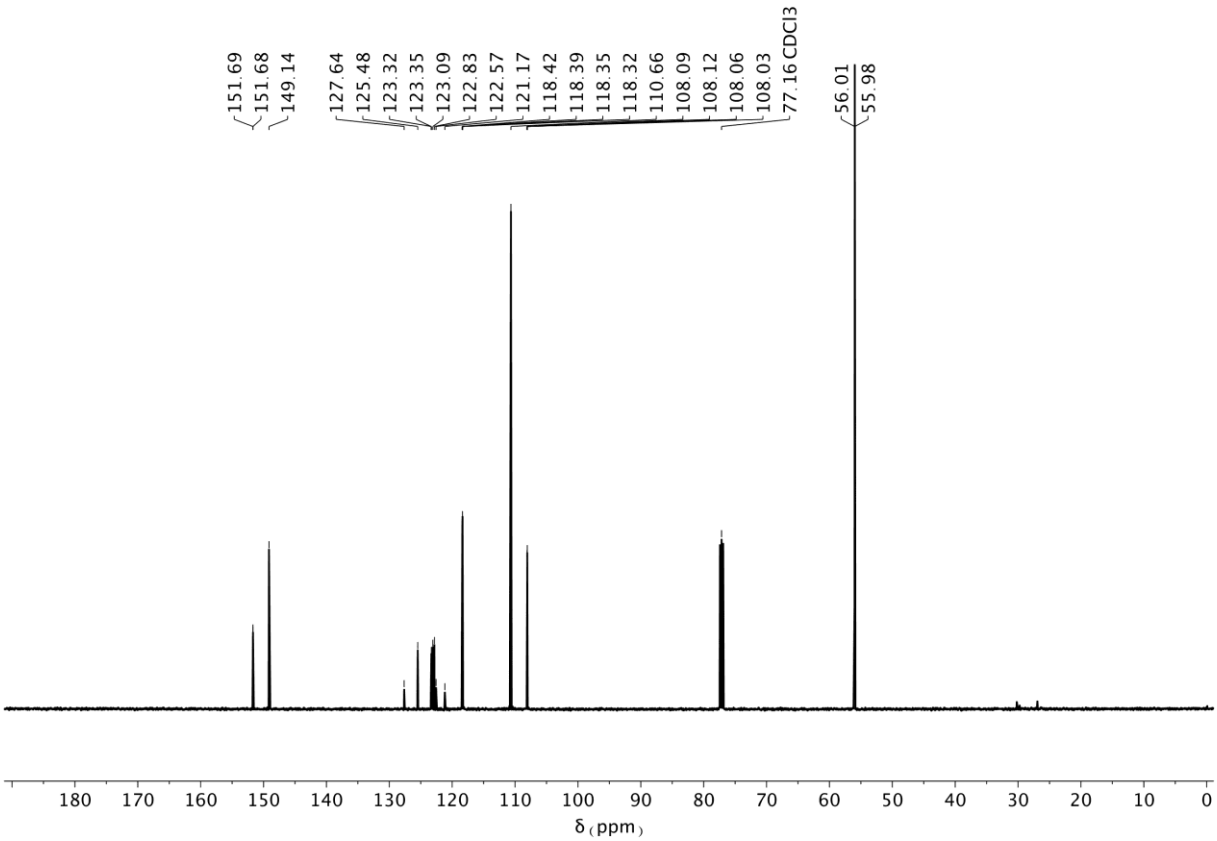

Figure S23. ^{13}C NMR spectrum of compound **15** ($CDCl_3$, 126 MHz, 298 K).

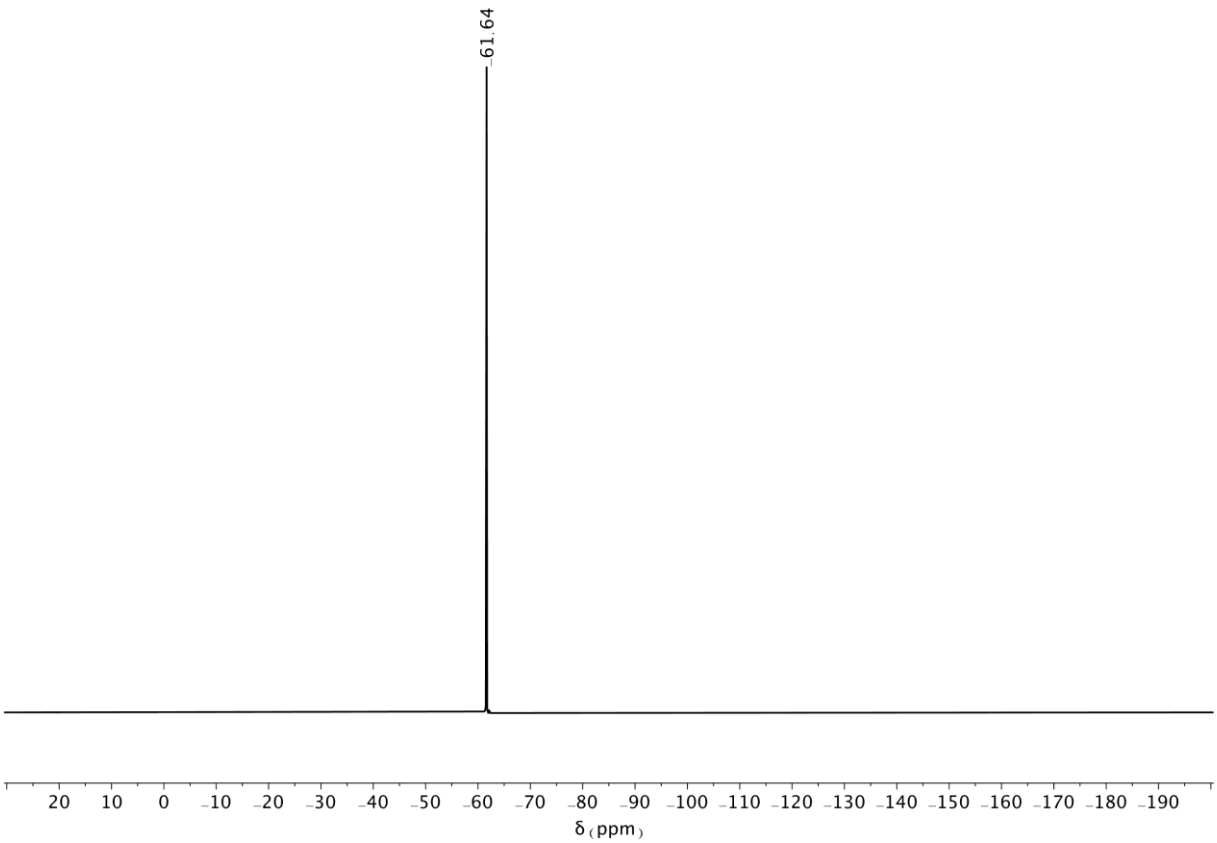

Figure S24. ^{19}F NMR spectrum of compound **15** ($CDCl_3$, 470 MHz, 298 K).

3.1.11. ^{1}H, ^{13}C and ^{19}F NMR spectra of compound 16

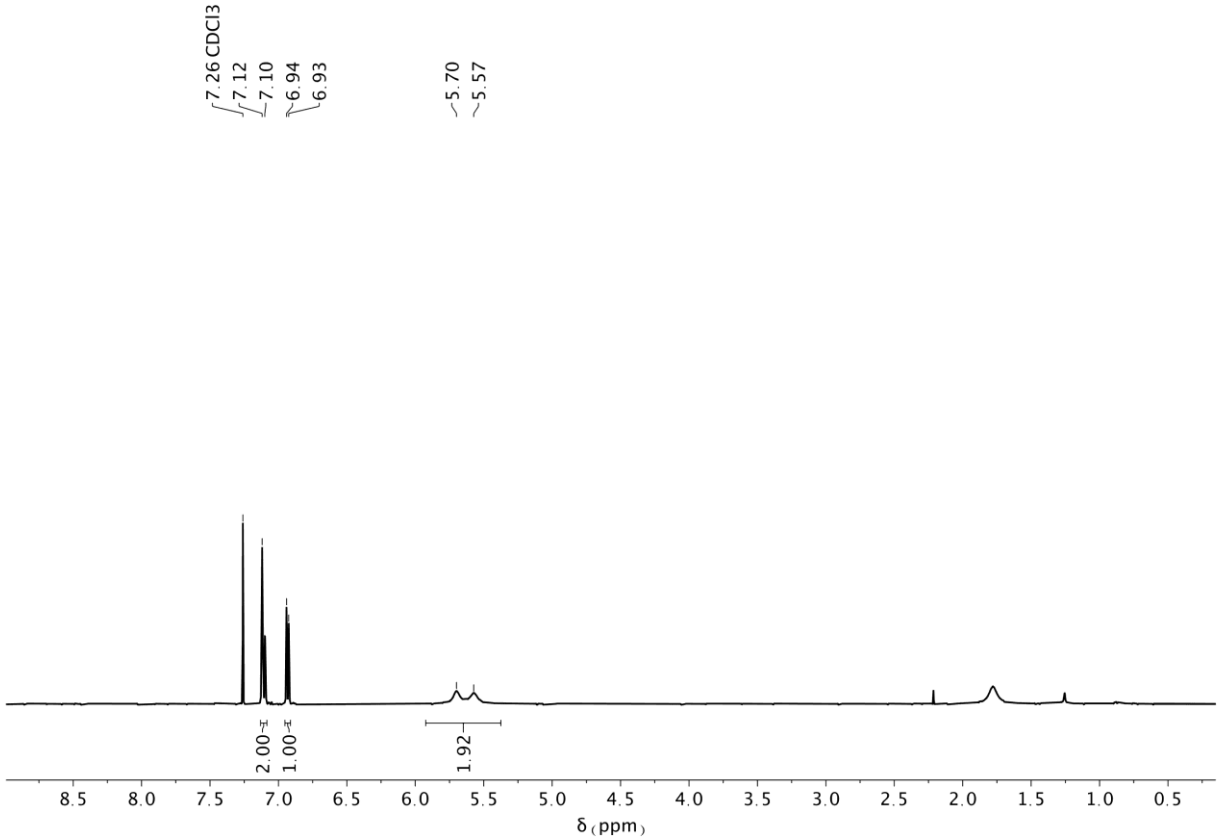

Figure S25. ^{1}H NMR spectrum of compound **16** ($CDCl_3$, 500 MHz, 298 K).

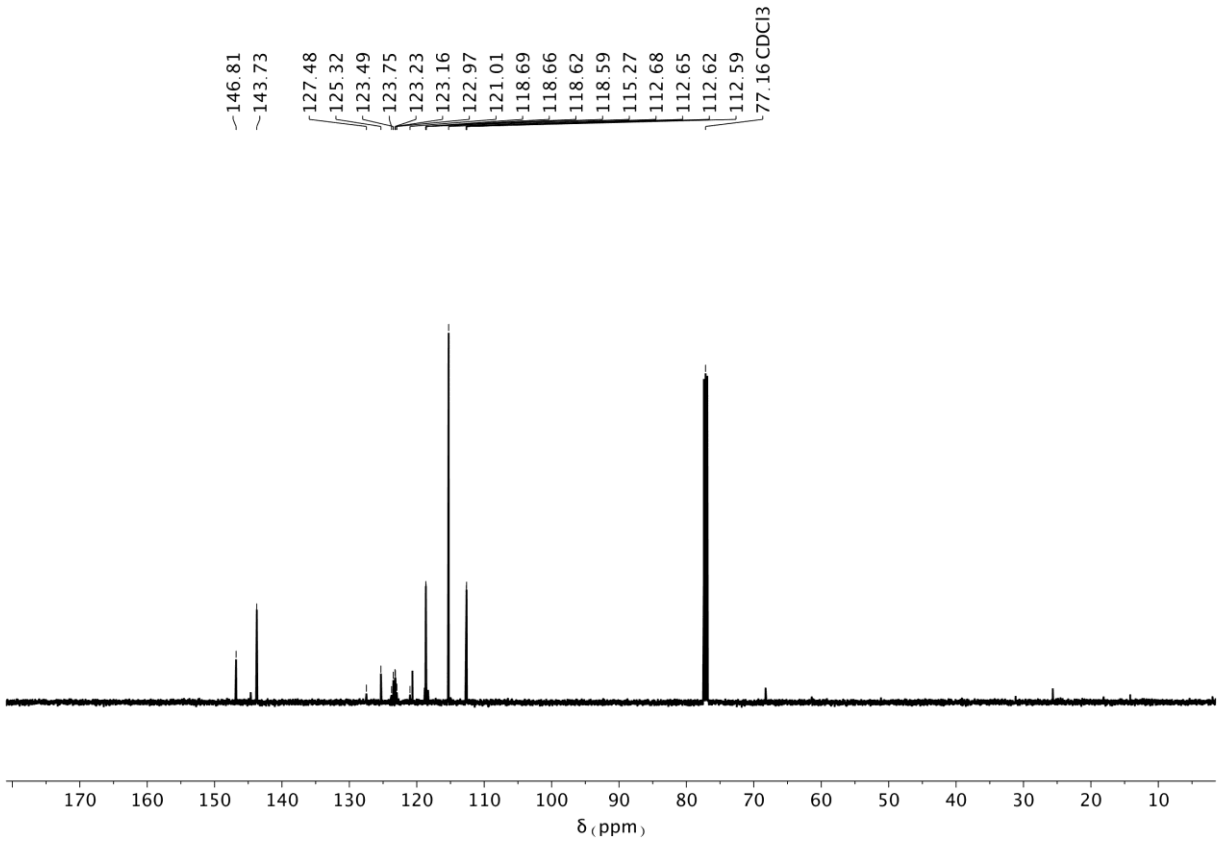

Figure S26. ^{13}C NMR spectrum of compound **16** ($CDCl_3$, 126 MHz, 298 K).

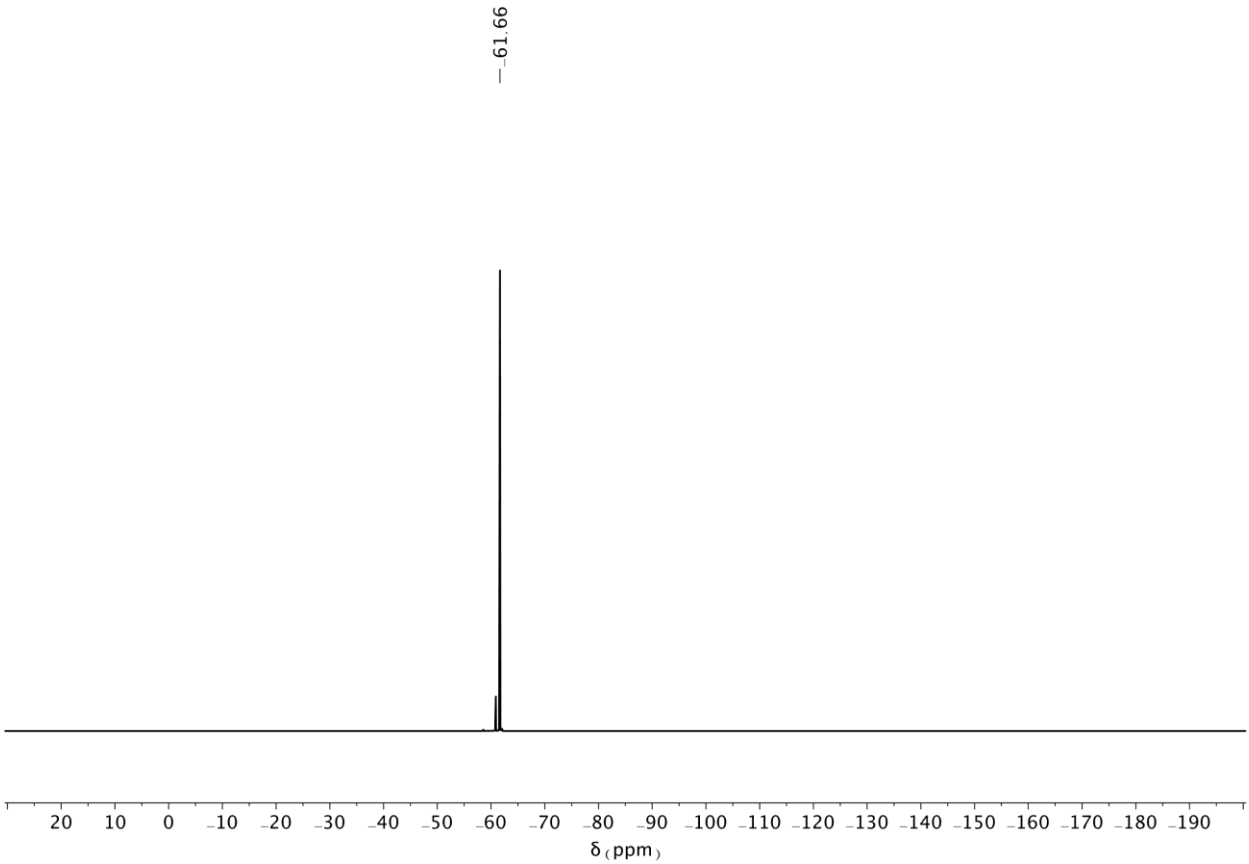

Figure S27. ^{19}F NMR spectrum of compound **16** ($CDCl_3$, 470 MHz, 298 K).

3.1.12. ^{1}H, ^{13}C and ^{19}F NMR spectra of compound 2

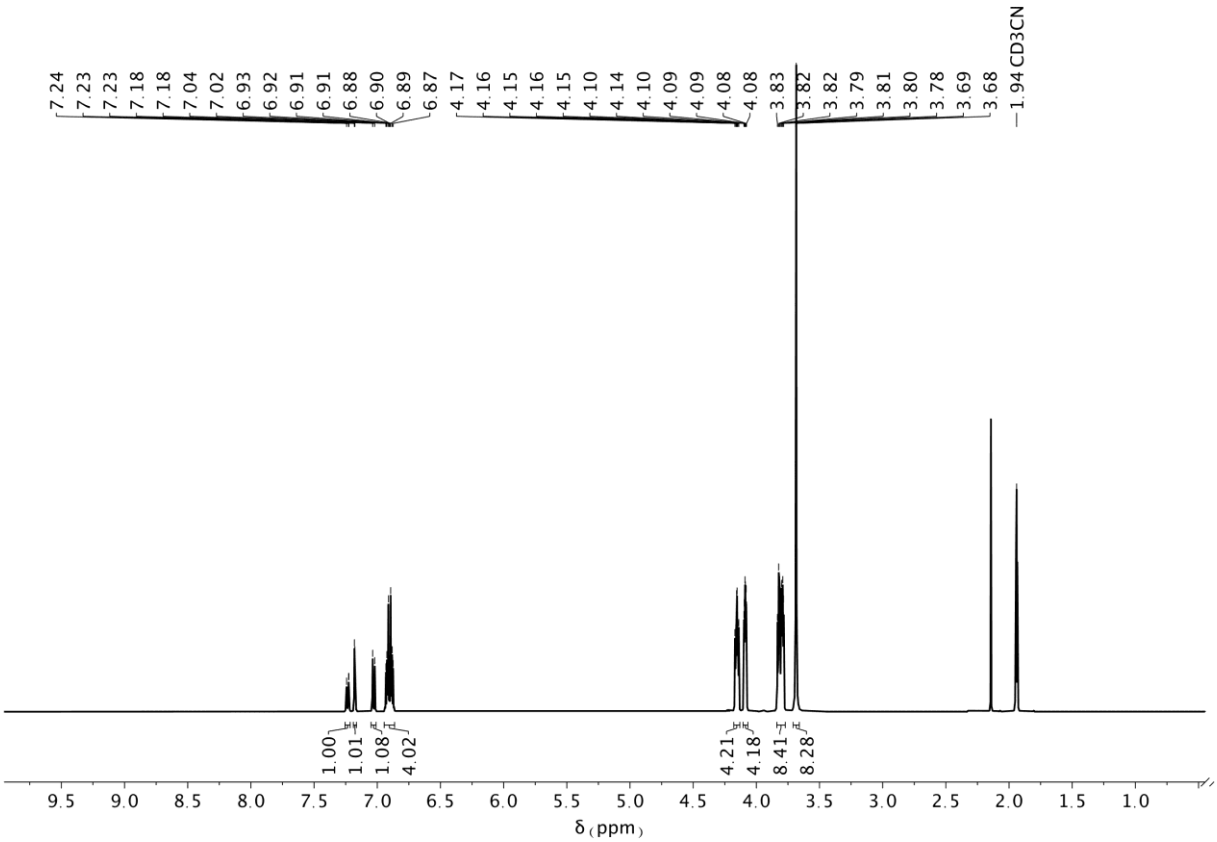

Figure S28. ^{1}H NMR spectrum of compound **2** (CD_3CN, 500 MHz, 298 K).

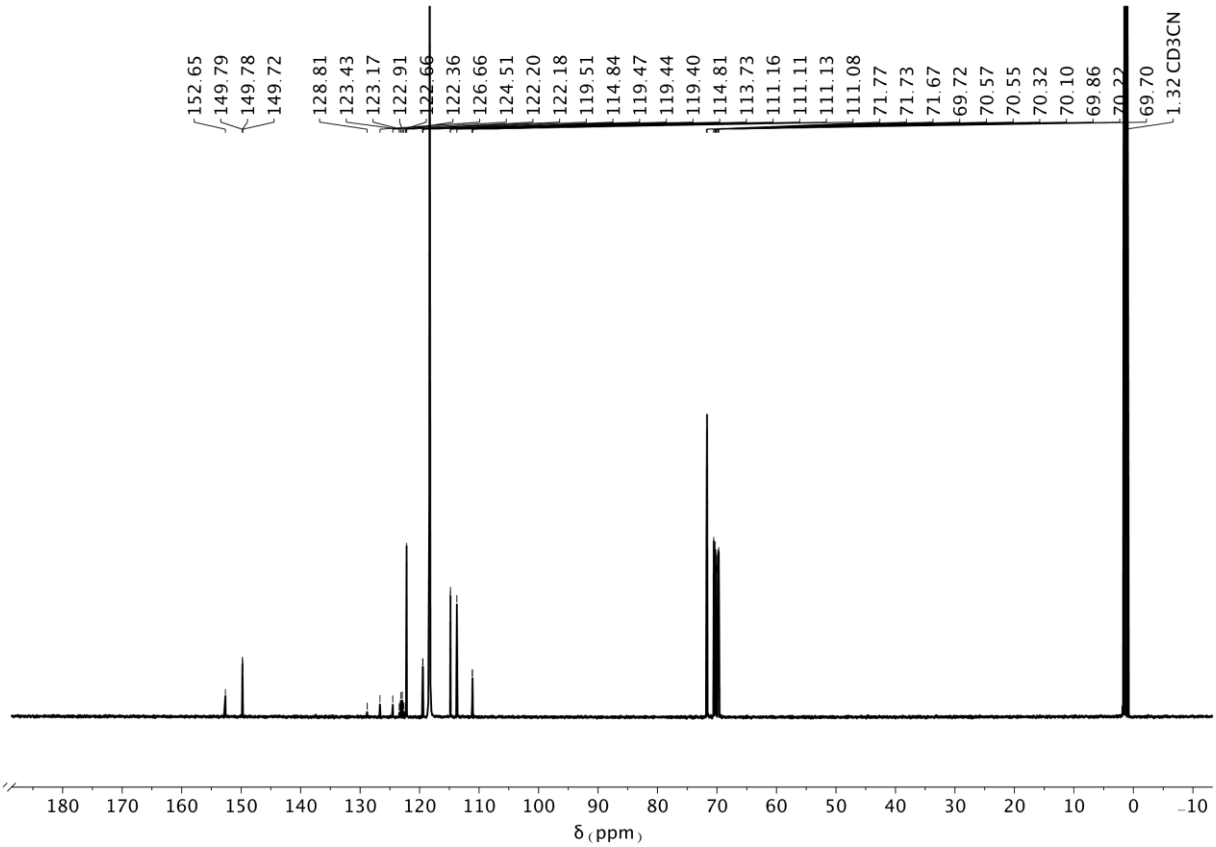

Figure S29. ^{13}C NMR spectrum of compound **2** (CD_3CN, 126 MHz, 298 K).

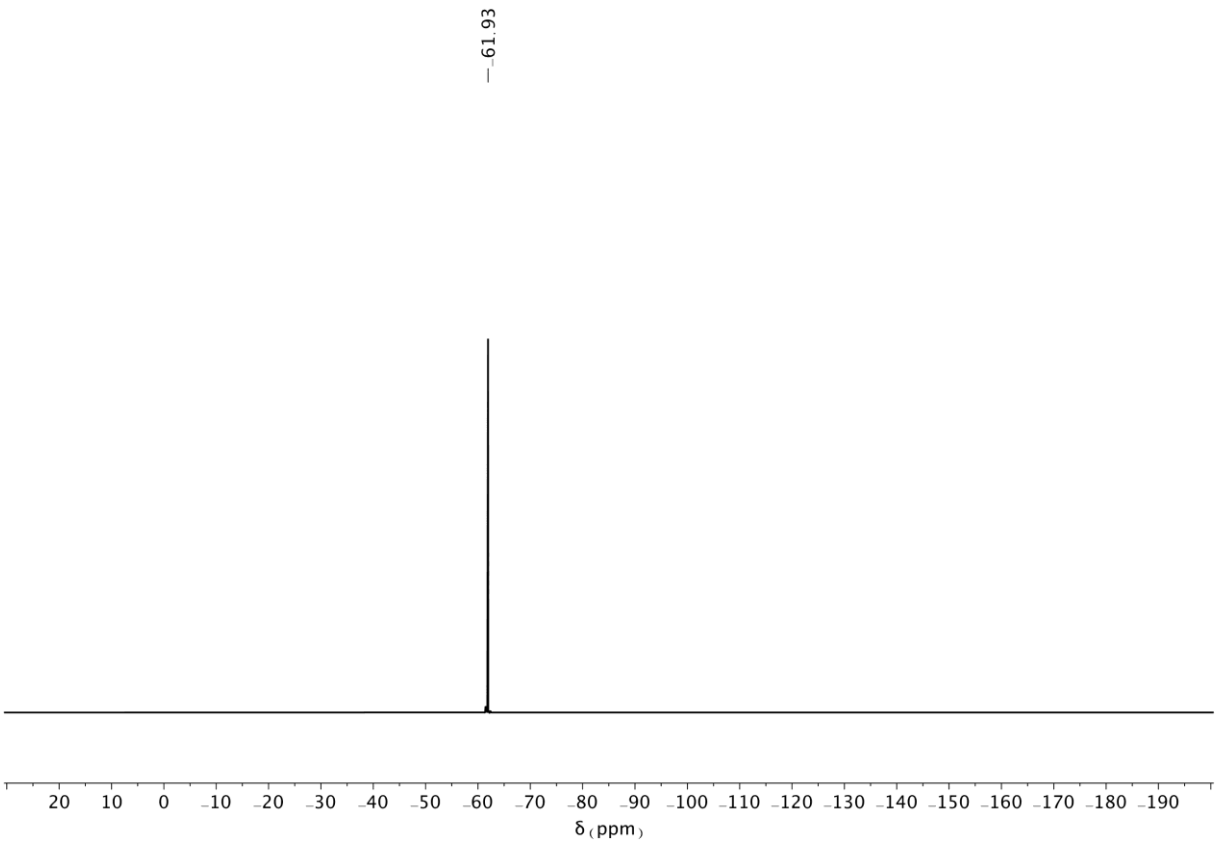

Figure S30. ^{19}F NMR spectrum of compound **2** (CD_3CN, 470 MHz, 298 K).

3.2. NMR Photoisomerization and complexation spectra

3.2.1. Isomerization and complexation of model compound *E*-3 with 2

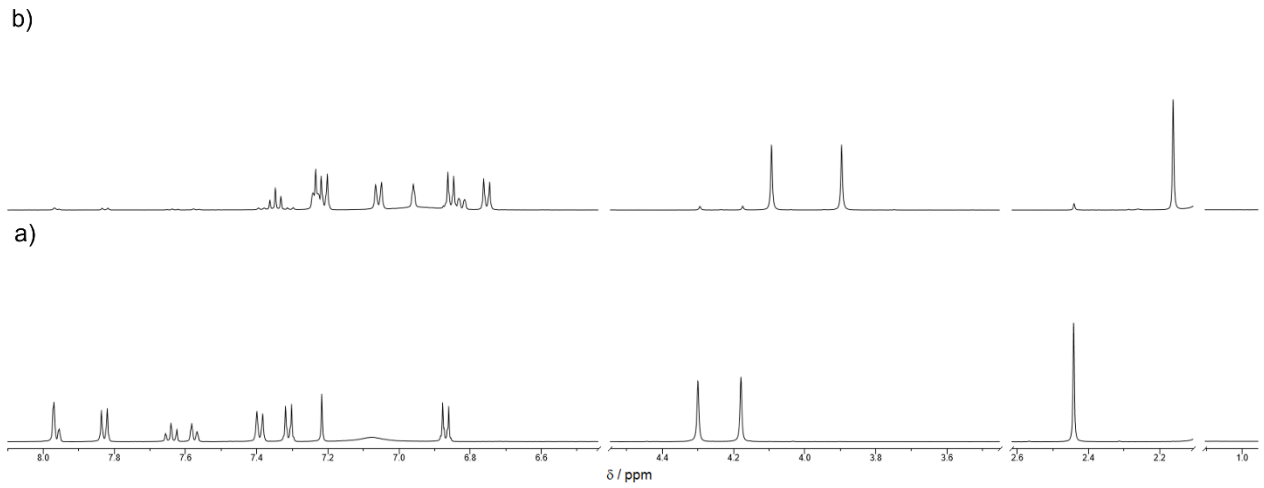

Figure S31. Partial ^{1}H NMR spectra of a) *E*-**3**; b) *E*-**3** after exhaustive irradiation at λ = 365±5 nm to obtain *Z*-**3** (5 mM, CD_2Cl_2/CD_3CN 3:7, 500 MHz, 298 K). PSS composition: *Z* : *E* = 95 : 5.

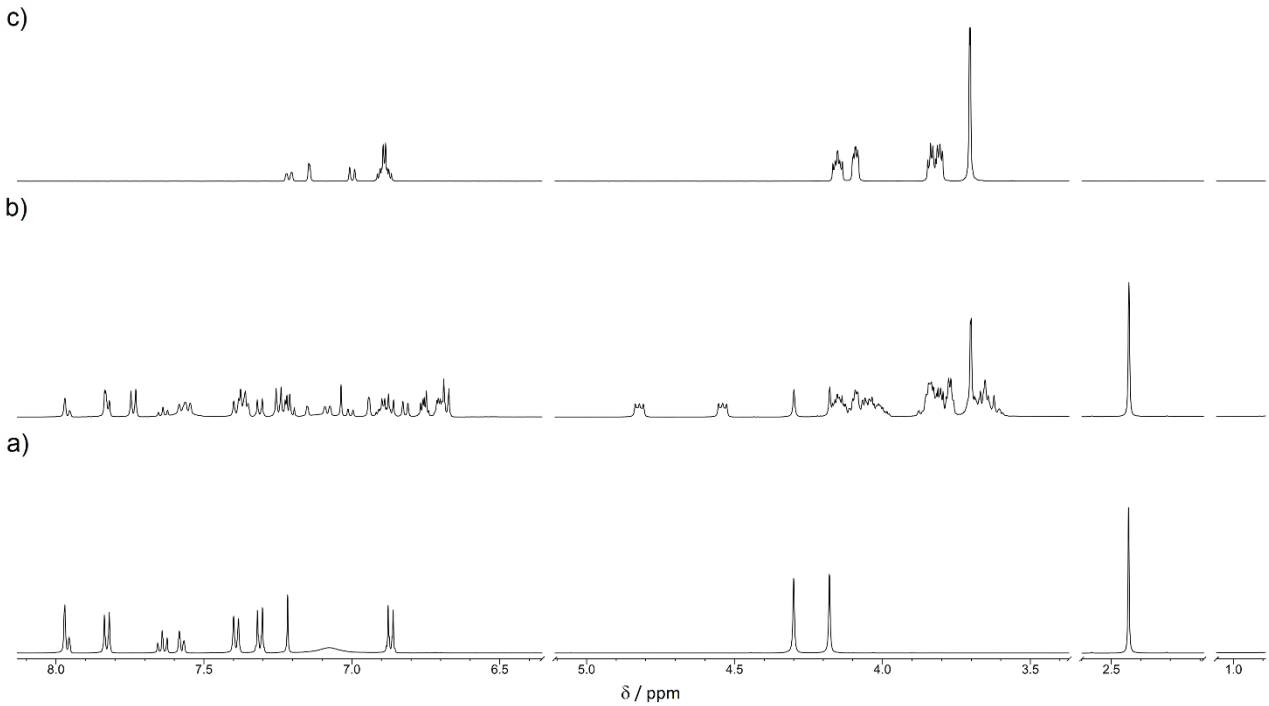

Figure S32. Partial ^{1}H NMR spectra of a) *E*-**3**; b) an equilibrated equimolar solution of *E*-**3** and **2**; c) **2**. (5 mM, CD_2Cl_2/CD_3CN 3:7, 500 MHz, 298 K). Associated fraction: 65%; calculated by integration of signals univocally assigned to complex and free axle.

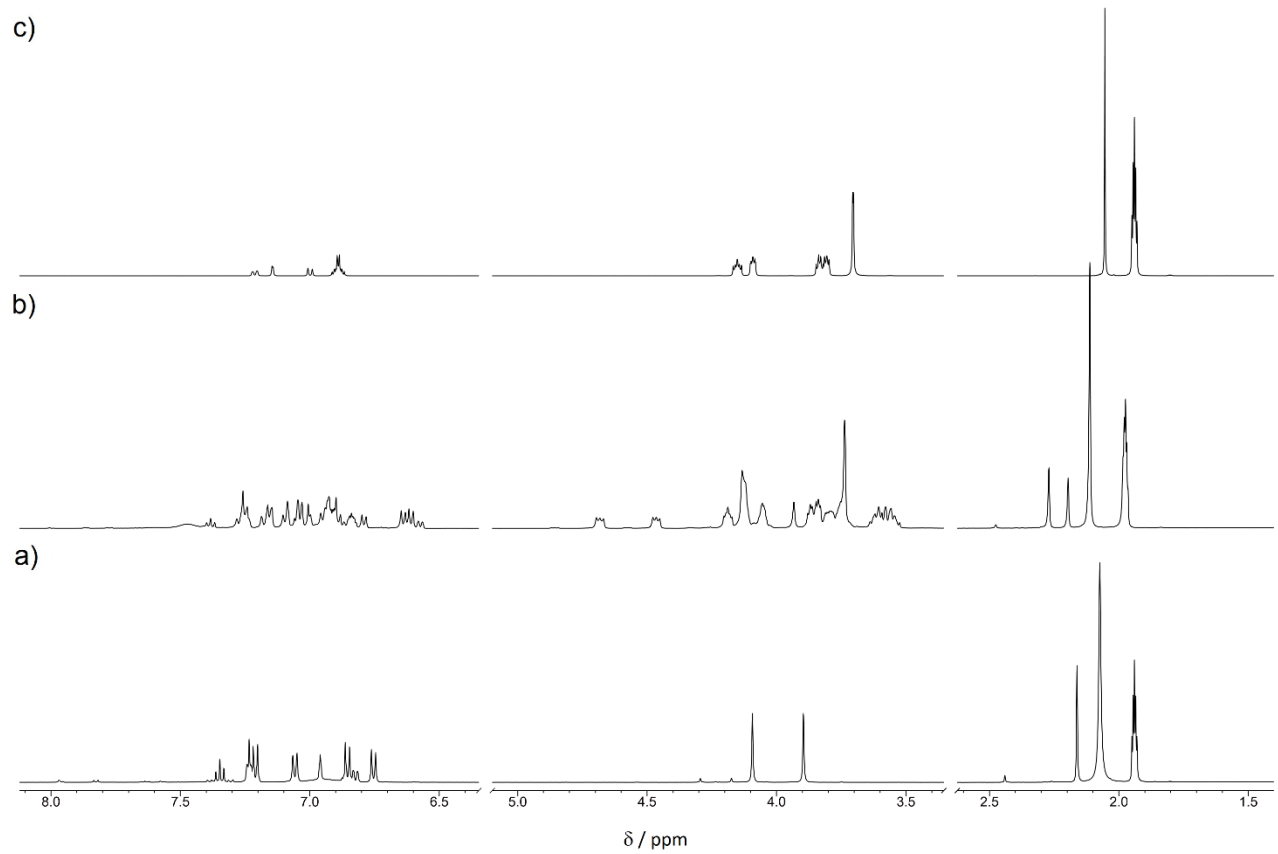

Figure S33. Partial ^{1}H NMR spectra of a) *Z*-**3**; b) an equilibrated equimolar solution of *Z*-**3** and **2**; c) **2**. (5 mM, CD_2Cl_2/CD_3CN 3:7, 500 MHz, 298 K). Associated fraction: 54%; calculated by integration of signals univocally assigned to complex and free axle.

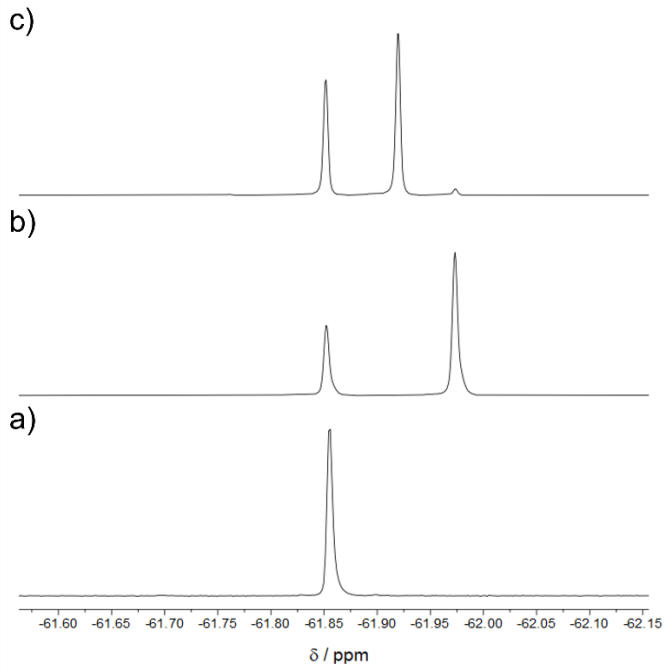

Figure S34. Partial ^{19}F NMR spectra of a) **2**; b) an equilibrated equimolar solution of *E*-**3** and **2**; c) Sample (b) after exhaustive irradiation at λ = 365 nm±5. (5 mM, CD_2Cl_2/CD_3CN 3:7, 470 MHz, 298 K).

3.2.2. Complexation of model compound 4 with 2

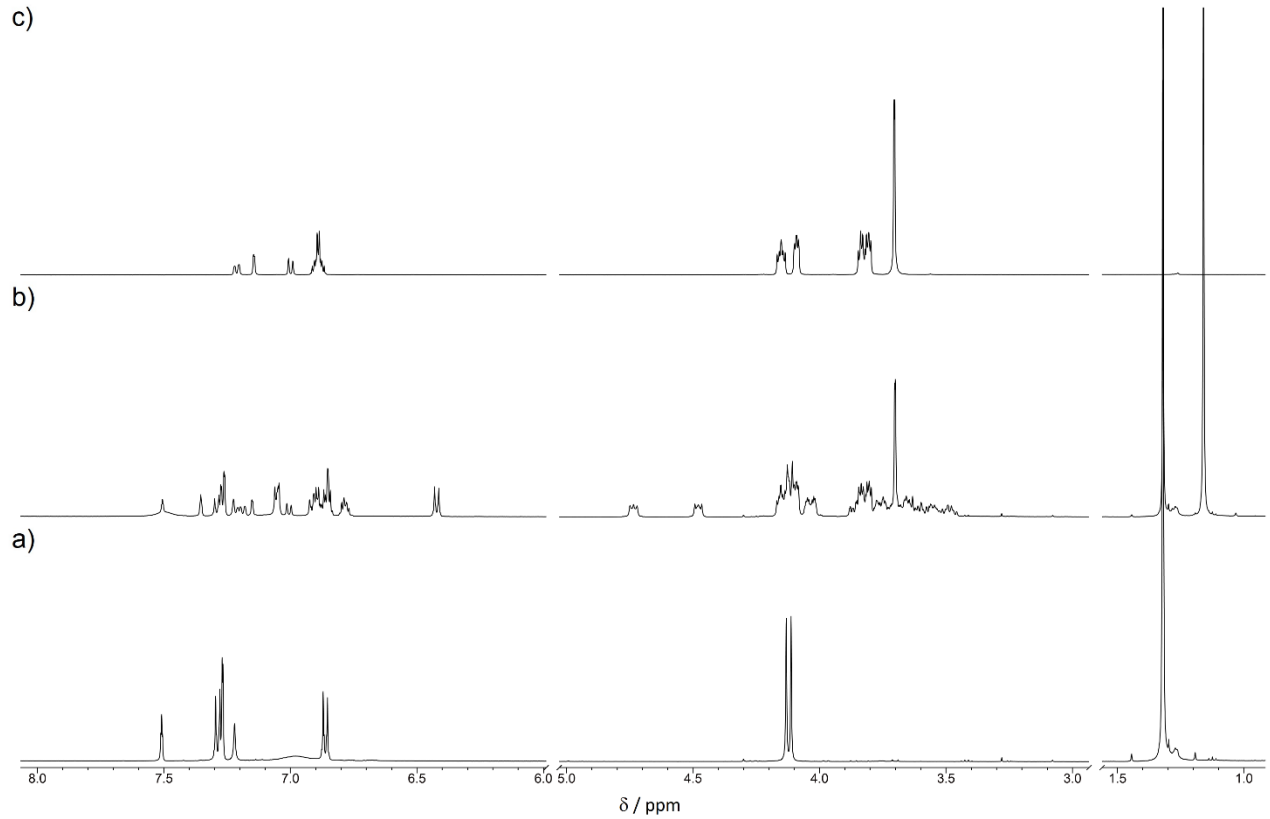

Figure S35. Partial ^{1}H NMR spectra of a) **4**; b) an equilibrated equimolar solution of **4** and **2**; c) **2**. (5 mM, CD_2Cl_2/CD_3CN 3:7, 500 MHz, 298 K). Associated fraction: 58%; calculated by integration of signals univocally assigned to complex and free axle.

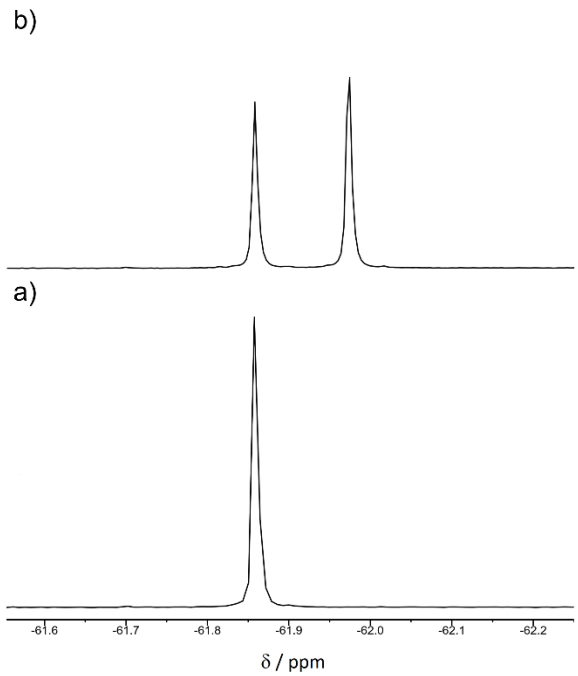

Figure S36. Partial ^{19}F NMR spectra of a) **2**; b) an equilibrated equimolar solution of **4** and **2**. (5 mM, CD_2Cl_2/CD_3CN 3:7, 470 MHz, 298 K).

3.2.3. Isomerization and complexation of compound *E*-1 with 2

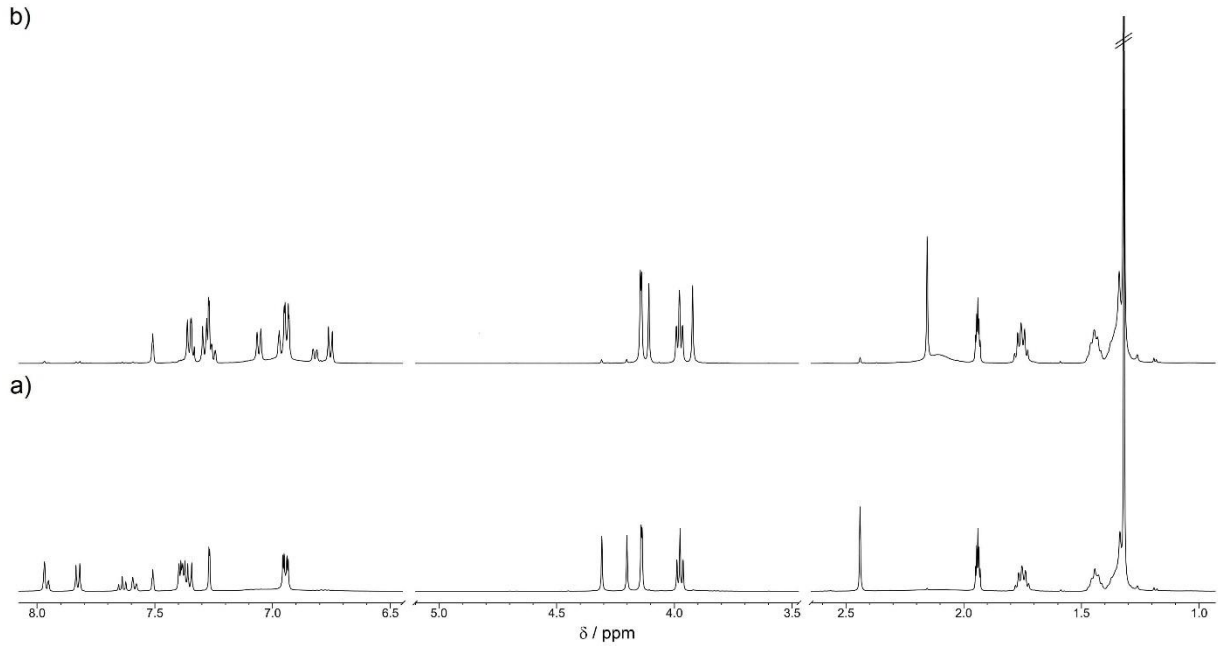

Figure S37. Partial ^{1}H NMR spectra of a) *E*-**1**; b) *E*-**1** after exhaustive irradiation at λ = 365±5 nm to obtain *Z*-**1**. (5 mM, CD_2Cl_2/CD_3CN 3:7, 500 MHz, 298 K). PSS Composition: *Z* : *E* = 95 : 5.

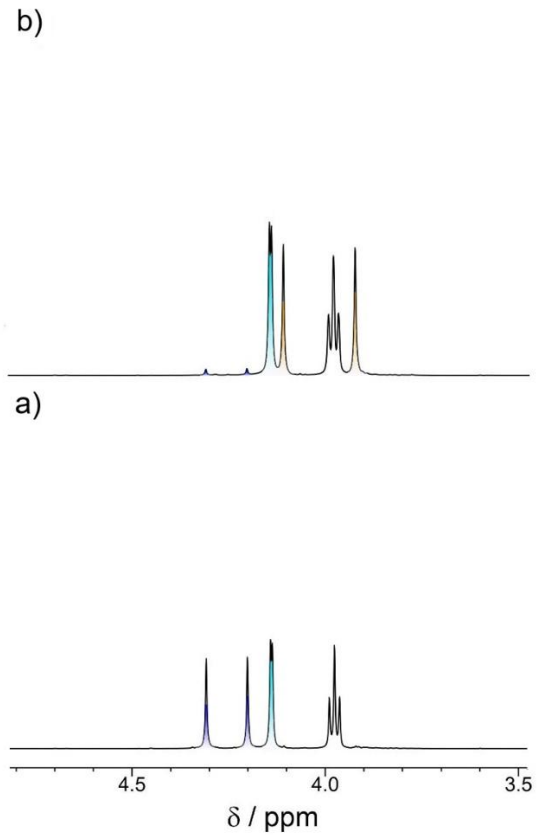

Figure S38. Partial ^{1}H NMR spectra of a) *E*-**1**; b) *E*-**1** after exhaustive irradiation at λ = 365±5 nm to obtain *Z*-**1**. (5 mM, CD_2Cl_2/CD_3CN 3:7, 500 MHz, 298 K). PSS Composition: *Z* : *E* = 95 : 5. Colored peaks highlight the signals associated with the methylene protons adjacent to the two ammonium groups: *E*-I, blue; *Z*-I, orange; II, cyan.

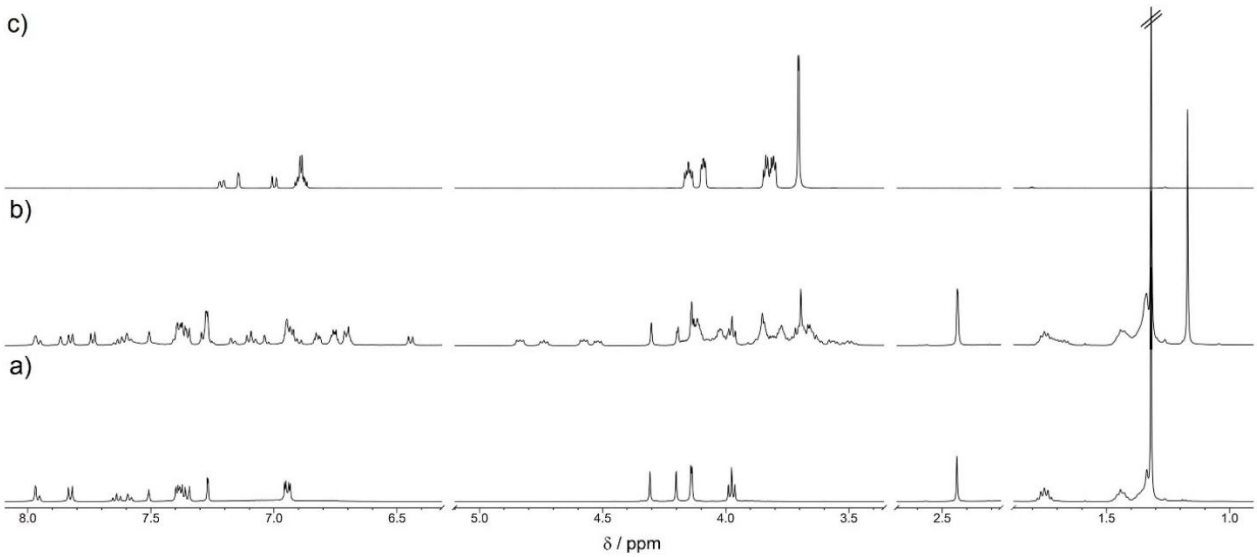

Figure S39. Partial ^{1}H NMR spectra of a) *E*-**1**; b) an equilibrated equimolar solution of *E*-**1** and **2**; c) **2**. (5 mM, CD_2Cl_2/CD_3CN 3:7, 500 MHz, 298 K). Associated fraction: I = 41 %, II = 35 %, calculated by integration of signals univocally assigned to complex and free axle.

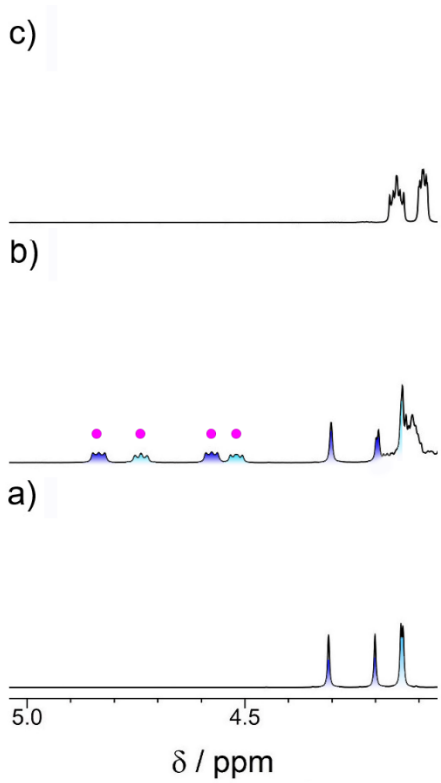

Figure S40. Partial ^{1}H NMR spectra of a) *E*-**1**; b) an equilibrated equimolar solution of *E*-**1** and **2**; c) **2**. (5 mM, CD_2Cl_2/CD_3CN 3:7, 500 MHz, 298 K). Colored peaks highlight the signals associated with the methylene protons adjacent to the two ammonium groups: *E*-I, blue; *Z*-I, orange; II, cyan. Peaks marked with the magenta dot indicate signals associated with complexed species.

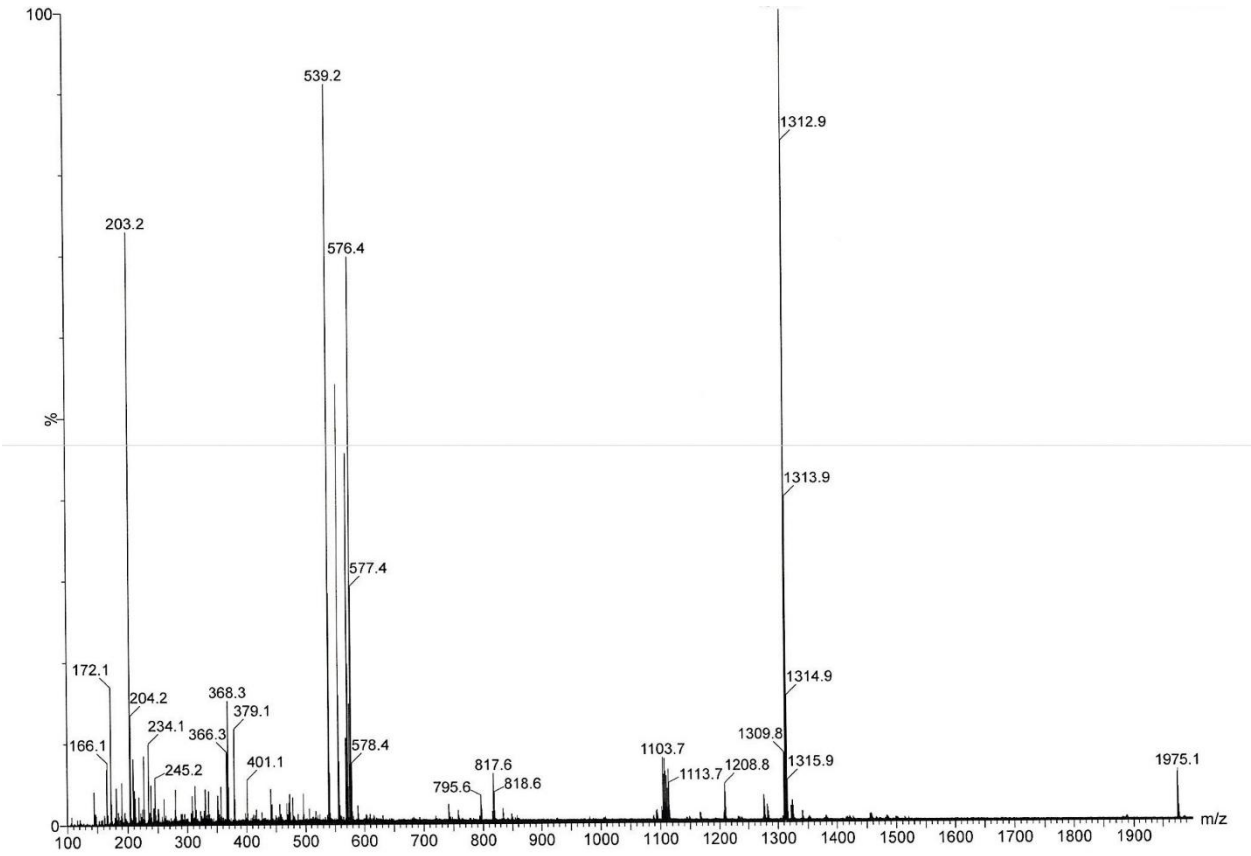

Figure S41. MALDI-TOF mass spectrum of an equilibrated equimolar solution of *E*-**1** and **2** (10 mM, CD_2Cl_2/CD_3CN 3:7) in the dark, showing the presence of both [2]pseudorotaxane and [3]pseudorotaxane species. $[\mathbf{1}+\mathbf{2}–HPF_6–PF_6^–]^+$: m/z 1311.9, $[\mathbf{1}+(\mathbf{2})_2–PF_6^–]^+$: m/z 1975.1.

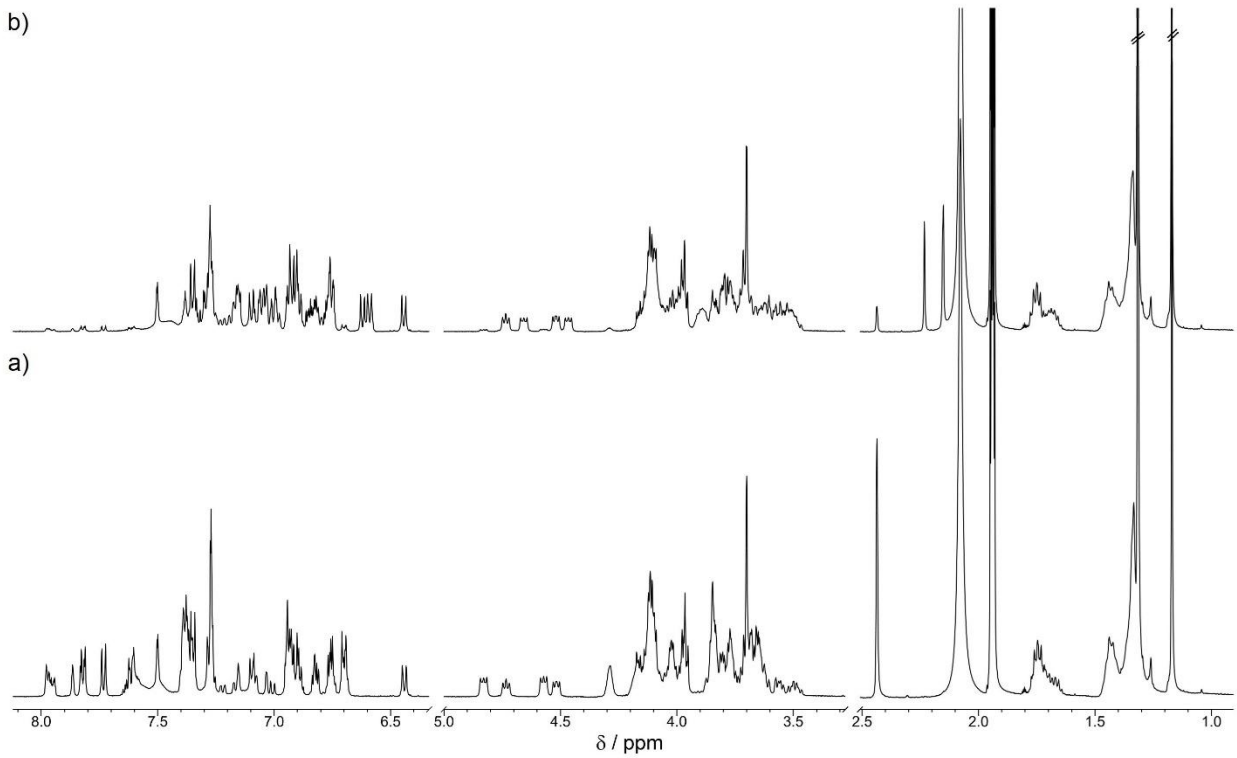

Figure S42. Partial ^{1}H NMR spectra of a) an equilibrated equimolar solution of *E*-**1** and **2**; b) an equilibrated equimolar solution of *E*-**1** and **2** after exhaustive irradiation at λ = 365±5 nm (5 mM, CD_2Cl_2/CD_3CN 3:7, 500 MHz, 298 K).

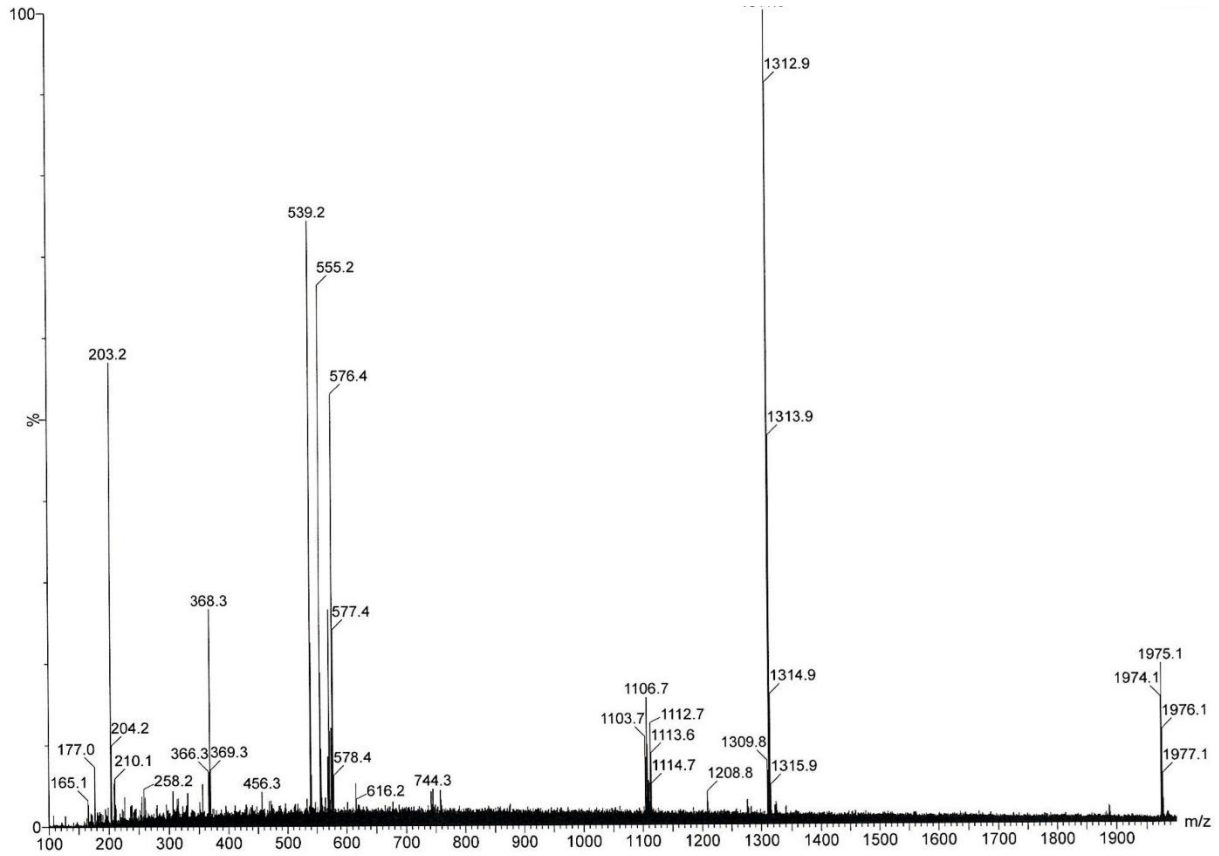

Figure S43. MS (MALDI-TOF) of an equilibrated equimolar solution of *E*-**1** and **2** (10 mM, CD_2Cl_2/CD_3CN 3:7) after irradiation at λ = 369±15 nm, showing the presence of both [2]pseudorotaxane and [3]pseudorotaxane species.
[**1**+**2**–HPF_6–PF_6^-]$^+$: m/z 1311.9, [**1**+(**2**)$_2$–PF_6^-]$^+$: m/z 1975.1.

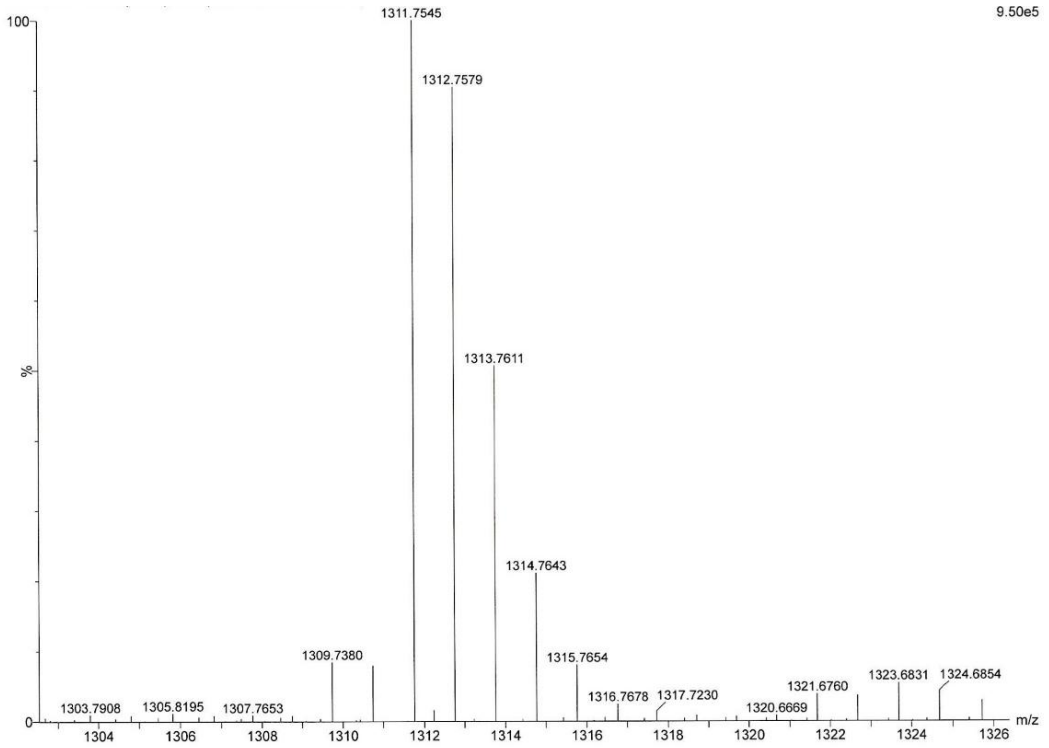

Figure S44. HRMS (MALDI-TOF) of the [2]pseudorotaxane species, measured for $[\mathbf{1}+\mathbf{2}–HPF_6–PF_6^-]^+$: m/z 1311.7545.

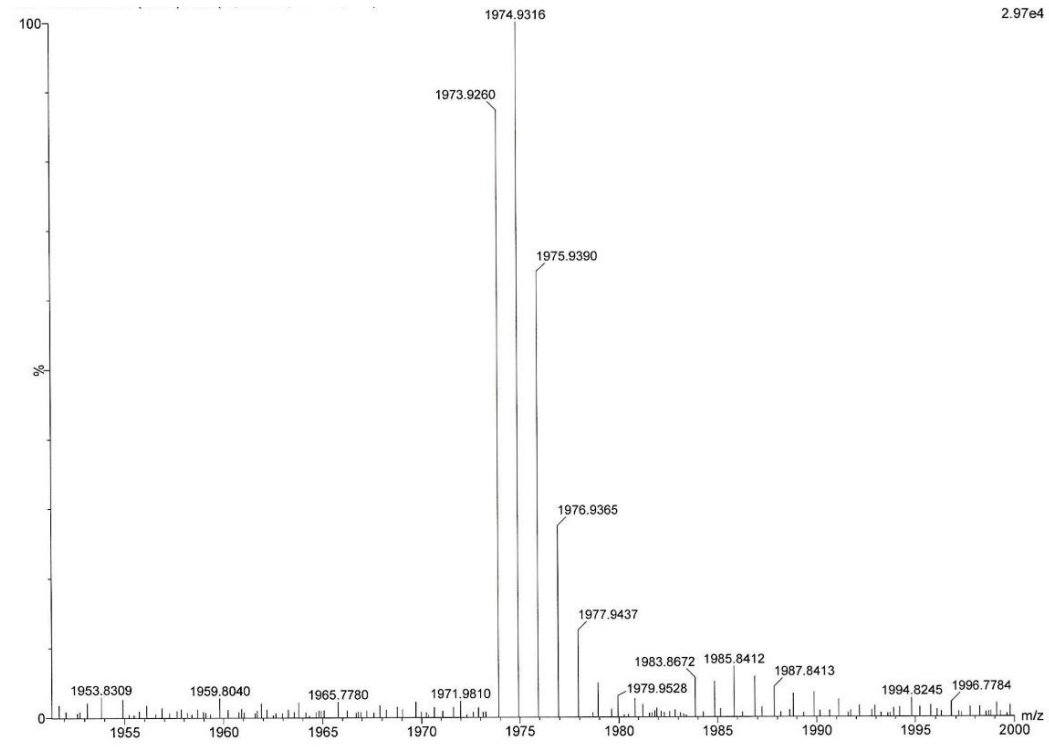

Figure S45. HRMS (MALDI-TOF) of the [3]pseudorotaxane species, measured for $[\mathbf{1}+(\mathbf{2})_2–PF_6^-]^+$: m/z 1974.9316.

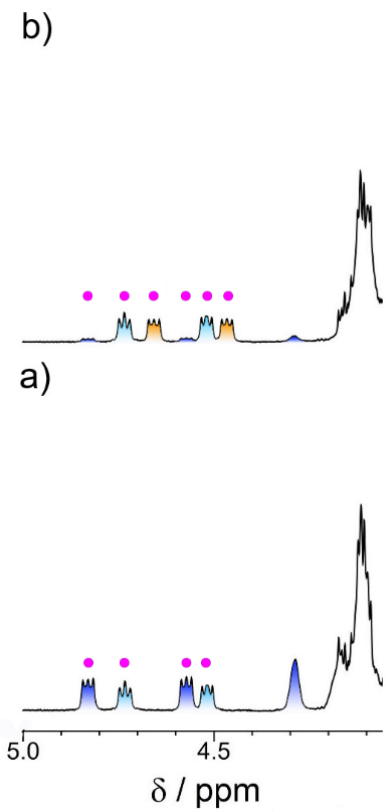

Figure S46. Partial ^{1}H NMR spectra of a) an equilibrated equimolar solution of *E*-**1** and **2**; b) an equilibrated equimolar solution of *E*-**1** and **2** after exhaustive irradiation at λ = 365±5 nm (10 mM, CD_2Cl_2/CD_3CN 3:7, 500 MHz, 298 K). Colored peaks highlight the signals associated with the methylene protons adjacent to the two ammonium groups: *E*-I, blue; *Z*-I, orange; II, cyan; peaks marked with the magenta dot indicate signals associated with complexed species.

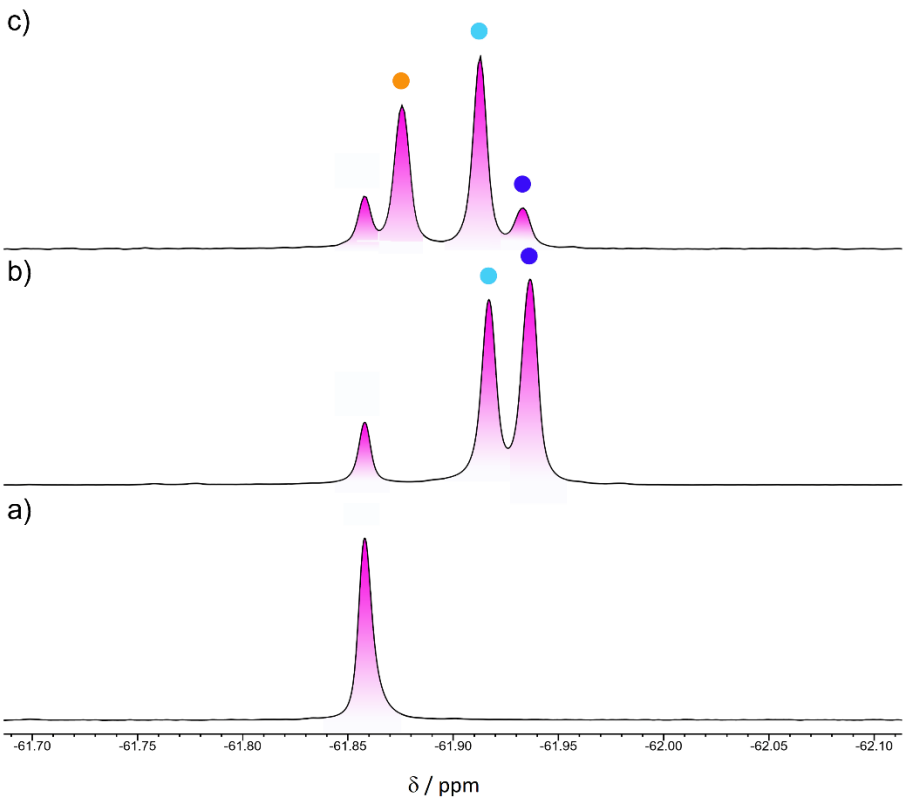

Figure S47. Partial ^{19}F NMR spectra of a) **2**; b) an equilibrated equimolar solution of *E*-**1** and **2**; c) Sample (b) after exhaustive irradiation at λ = 365±5 nm. (5 mM, CD_2Cl_2/CD_3CN 3:7, 470 MHz, 298 K). Magenta colored peaks show that the signals are associated with the trifluoromethyl group ^{19}F on **2**. Peaks marked with the colored dots indicate signals associated with complexed species: total complex on the first ammonium station *E*-I⊂**2** = *E*-**1**⊂**2**^{I}+*E*-**1**⊂(**2**)$_2$: blue; total complex on the second ammonium station II⊂**2** = *E*-**1**⊂**2**^{II}+*E*-**1**⊂(**2**)$_2$: dark blue; total free second ammonium station II = *E*-**1**+*E*-**1**⊂**2**^{I}: cyan; total complex on the first ammonium station *Z*-I⊂**2** = *Z*-**1**⊂**2**^{I}+*Z*-**1**⊂(**2**)$_2$: orange.

3.3. Determination of the association constants (*K*) from ^{1}H NMR data

Association constants were determined using the single point method from ^{1}H NMR spectra of equimolar solutions (5 mM, CD_2Cl_2/CD_3CN 3:7) of **2** with model compounds *E*-**3**, *Z*-**3** and **4**. The concentration of each component at equilibrium was calculated from the integrals of diagnostic peaks for free and complexed species, using tetrachloroethane (TCE) as an internal standard. Association constants were calculated according to the equation:

$$K = \frac{[complex]}{[free\ thread][free\ ring]} \qquad \text{(Eq. S1)}$$

The reported *K* values were calculated as the mean of the values obtained from three replicate experiments. The reported error corresponds to three times the standard deviation of the set of data for each *K* (Table S1).

Table S1. Thermodynamic data for the complexation of **2** with model compounds *E*-**3**, *Z*-**3** and **4** (5 mM, CD_2Cl_2/CD_3CN 3:7).

	K (M^{-1})	$-\Delta G°$ (kJ mol^{-1})
E-**3**⊂**2**	1030±60	17.2
Z-**3**⊂**2**	590±60	15.8
4⊂**2**	650±20	16.0

The association constant of **2** with the two ammonium stations (I and II) present in *E*-**1** is not straightforward to determine with a single point measurement. At equilibrium, before irradiation, three complexes are present, namely, *E*-**1**⊂**2**^{I}, *E*-**1**⊂**2**^{II} and *E*-**1**⊂(**2**)$_2$, and it is not possible to discriminate the NMR signals of *E*-**1**⊂(**2**)$_2$ from those of *E*-**1**⊂**2**^{I} and *E*-**1**⊂**2**^{II}. The amount of *E*-**1**⊂(**2**)$_2$ is not negligible. Treating the system as a competitive equilibrium and knowing the concentration of the species (total complex on station I, total complex on station II, total free station I, total free station II) and the associated fraction (%), the association constants at the first and second ammonium station could be respectively estimated as $K_{E\text{-I}}$ = 1050 M^{-1} and K_{II} = 650 M^{-1}. These values are consistent, within error, with those determined for model complexes *E*-**3**⊂**2** and **4**⊂**2** (Table S1). Estimating the association constant after photoisomerization becomes extremely challenging since it is not possible to determine the concentration of the species and the associated fraction: the mixture of species becomes too complex and NMR signals are largely overlapped. Considering that, for the system before irradiation, the estimated *K* values match those determined for the model complexes, it can be safely assumed that also $K_{Z\text{-I}}$ is very similar to the stability constant of model complex *Z*-**3**⊂**2**.

3.4. NMR chemical actinometry

The photon flow ($q_{n,p}$) of the optical fiber employed for NMR photochemical experiments was determined by chemical actinometry in the same experimental setup used for the characterization of the reservoir modified pump operation. The chosen chemical actinometer was dimethylazobenzene (**DMAB**).[7]

A solution of **DMAB** in CD_3CN (5 mM) was irradiated with the optical fiber within the NMR tube at λ = 365±5 nm. The *E*→*Z* conversion was monitored recording a ^{1}H NMR array acquiring spectra at 20 seconds intervals over 25 minutes. $q_{n,p}$ was determined by least-square fitting of the concentration traces of *E*-**DMAB** and *Z*-**DMAB** to the equation set associated with the photokinetic and thermal processes.

The equations related to the photoinduced *E*→*Z* and *Z*→*E* processes can be built according to the photokinetic rate law, reported as the general formula for the ith species (here i = *E*, *Z*) in Eq. S2,

$$v_i^{h\nu} = \frac{q_{n,p}b}{V}\Phi_i\varepsilon_i[i]\frac{1-10^{-A_{Tot}}}{A_{Tot}} \qquad \text{(Eq. S2)}$$

where b is the optical path (b = 0.15 cm), V is the solution volume (V = 0.5 mL), Φ and ε are respectively the photoisomerization quantum yield and the molar absorption coefficient, both at 365 nm, and A_{Tot} is the total absorbance of the mixture calculated according to Lambert-Beer's law at 365 nm (Eq. S3).

$$A_{Tot} = b\Sigma_i\varepsilon_i[i] \qquad \text{(Eq. S3)}$$

Eq. S4 describes the thermal *Z*→*E* back-isomerization reaction.

$$v_Z^{\Delta} = k_{Z\Delta}[Z] \qquad \text{(Eq. S4)}$$

Table S2. Parameters for the isomerization processes of **DMAB** in CH_3CN at λ = 365 nm and T = 298 K.[7]

ε (M^{-1} cm^{-1})		$\Phi_{E\to Z}$	$\Phi_{Z\to E}$	$k_{Z\Delta}$ (s^{-1})
E-**DMAB**	*Z*-**DMAB**			
8311	101	0.18	0.34	1.6×10^{-6}

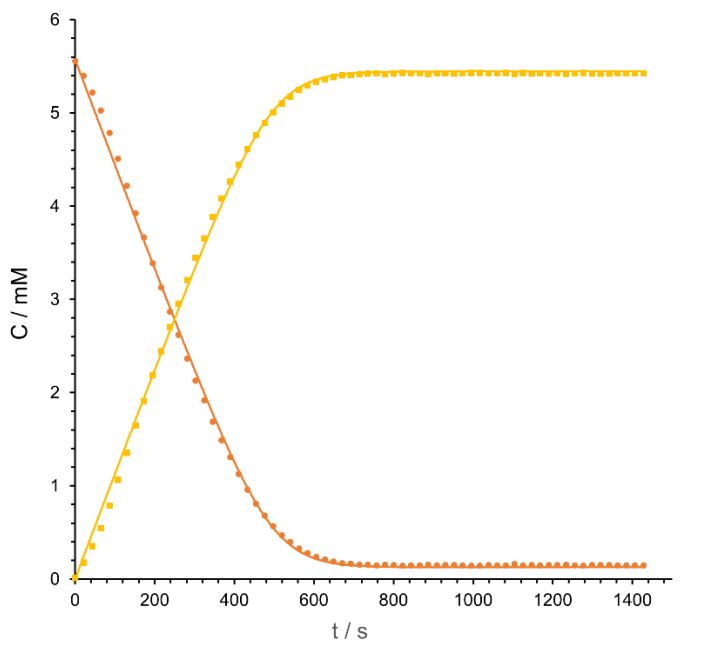

Figure S48. ^{1}H NMR kinetic traces of the photoconversion of **DMAB** (5 mM, CD_3CN, 298 K) corresponding to *E*-**DMAB** (orange) and *Z*-**DMAB** (yellow). Dotted lines correspond to the experimental data, continuous lines correspond to the fitting**.**

A photon flow of **3.1×10^{-8} Einstein s^{-1}** was calculated for irradiation performed at λ = 365±5nm, selecting the irradiation wavelength by means of a bandpass filter (OD 4.0).

The photon flow associated with the emission of the unfiltered LED source at λ_{max}= 369±15 nm was estimated considering that the λ = 365±5nm bandpass filter causes a 1.5 fold attenuation of the LED emission intensity.[8]
Hence, a photon flow of **4.65×10^{-8} Einstein s^{-1}** was calculated for irradiation performed at λ = 369±15nm.

4. UV-vis characterization

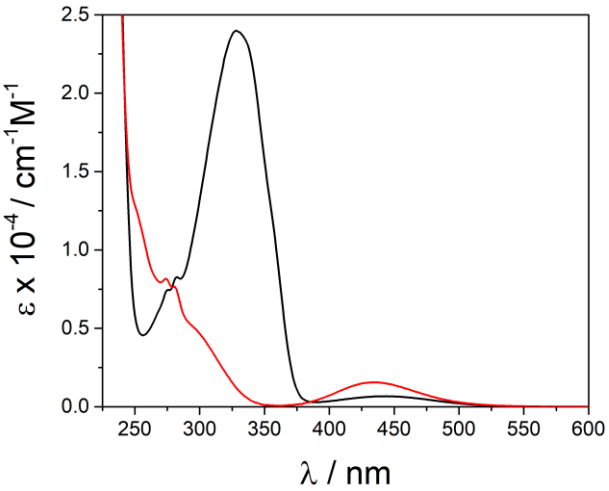

Figure S49. Absorption spectra of the *E* (black) and *Z* (red) isomers of compound **1** in CH_2Cl_2/CH_3CN 3:7.

4.1. Photoisomerization of *E*-1 and *Z*-1

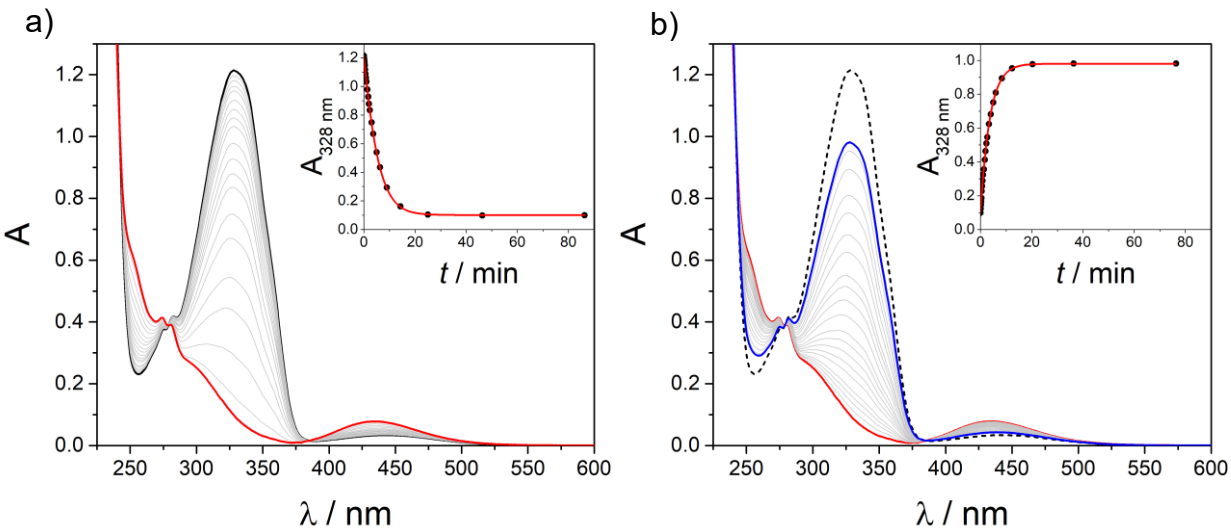

Figure S50. (a) Absorption variations of a 5.1×10^{-5} M solution of *E*-**1** in CH_2Cl_2/CH_3CN 3:7 (black line) upon irradiation at 365 nm until PSS is reached (red line); inset: absorption changes at 328 nm (black dots) together with data fitting (red line). (b) Absorption variations of a 5.1×10^{-5} M solution of *Z*-**1** in CH_2Cl_2/CH_3CN 3:7 at 365 nm PSS (red line) upon irradiation at 436 nm until PSS is reached (blue line), the dotted black line represents the original absorption trace of *E*-**1**; inset: absorption changes at 328 nm (black dots) together with data fitting (red line).

4.2. Thermal isomerization of *Z*-1

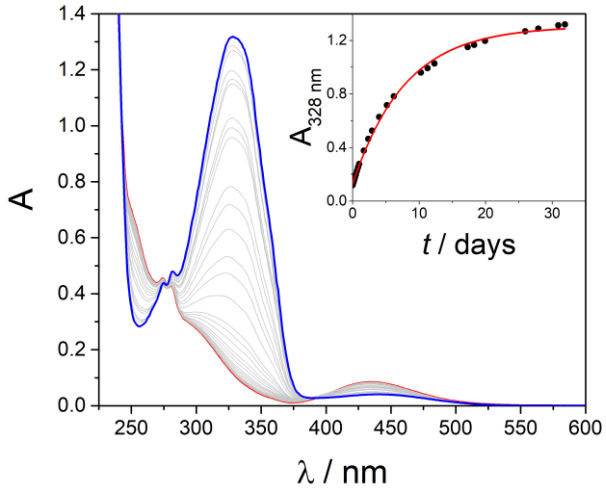

Figure S51. Thermal isomerization of a 5.1×10^{-5} M solution of *Z*-**1** in CH_2Cl_2/CH_3CN 3:7 after exhaustive irradiation at 365 nm (red line) until total recovery of the *E* isomer (blue line); inset: absorption changes at 328 nm (black dots) together with data fitting (red line).

4.3. Photoisomerization of *E*-1⊂2 and *Z*-1⊂2

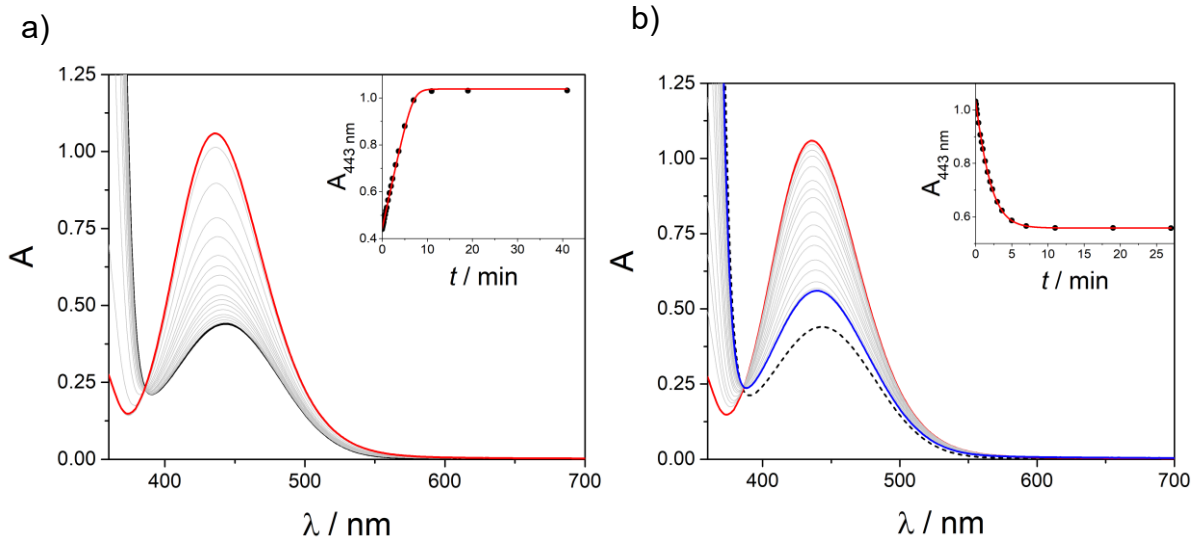

Figure S52. (a) Absorption variations of a 7.3×10^{-4} M solution of *E*-**1** in the presence of 14 equivalents of **2** in CH_2Cl_2/CH_3CN 3:7 (black line) upon irradiation at 365 nm until PSS is reached (red line); inset: absorption changes at 443 nm (black dots) together with data fitting (red line). (b) Absorption variations of a 7.3×10^{-4} M solution of *Z*-**1** in the presence of 14 equivalents of **2** in CH_2Cl_2/CH_3CN 3:7 at 365 nm PSS (red line) upon irradiation at 436 nm until PSS is reached (blue line), the dotted black line represents the original absorption trace of *E*-**1**; inset: absorption changes at 443 nm (black dots) together with data fitting (red line).

4.4. Thermal isomerization of *Z*-1⊂2

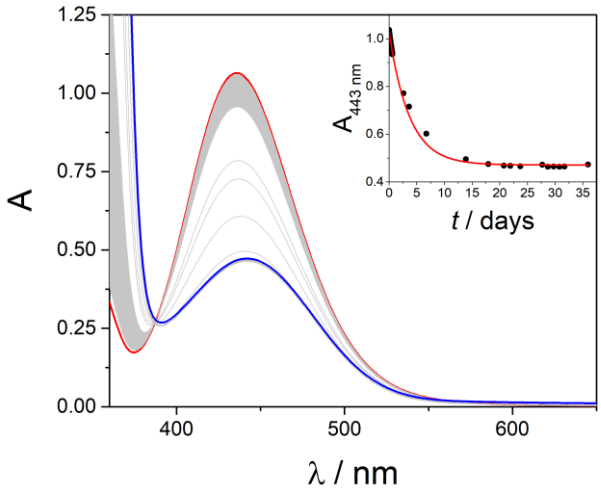

Figure S53. Thermal isomerization of a 7.3×10^{-4} M solution of *Z*-**1** in the presence of 14 equivalents of **2** in CH_2Cl_2/CH_3CN 3:7 after exhaustive irradiation at 365 nm (red line) until total recovery of the *E* isomer (blue line); inset: absorption changes at 443 nm (black dots) together with data fitting (red line).

Table S3. UV-vis photophysical and photochemical data of *E*-**1** and *E*-**1⊂2** (CH_2Cl_2/CH_3CN 3:7, 298 K).

Compound	Absorption		Isomerization				
	λ_{max} (nm)	ε (M^{-1} cm^{-1})	λ_{irr} (nm)	$\Phi_{E\rightarrow Z}$	$\Phi_{Z\rightarrow E}$	*Z* : *E* PSS, %	$k_{Z\Delta}$ (s^{-1})
E-**1**	328	24000	365	0.20	0.57	97 : 3	1.5×10^{-6}
	443	700	436	0.27	0.43	80 : 20	
E-**1⊂2**	443	600	365	0.17	0.59	95 : 5	3.1×10^{-6}
			405	0.42	0.70	80 : 20	

Table S4. Molar absorption coefficients (ε) at 365 nm (CH_2Cl_2/CH_3CN 3:7, 298 K)

Compound	Absorption	
	λ (nm)	ε (M^{-1} cm^{-1})
E-**1**	365	5700
Z-**1**	365	70
E-**1⊂2**	365	5350
Z-**1⊂2**	365	60

4.5. Threading kinetics of *E*-1

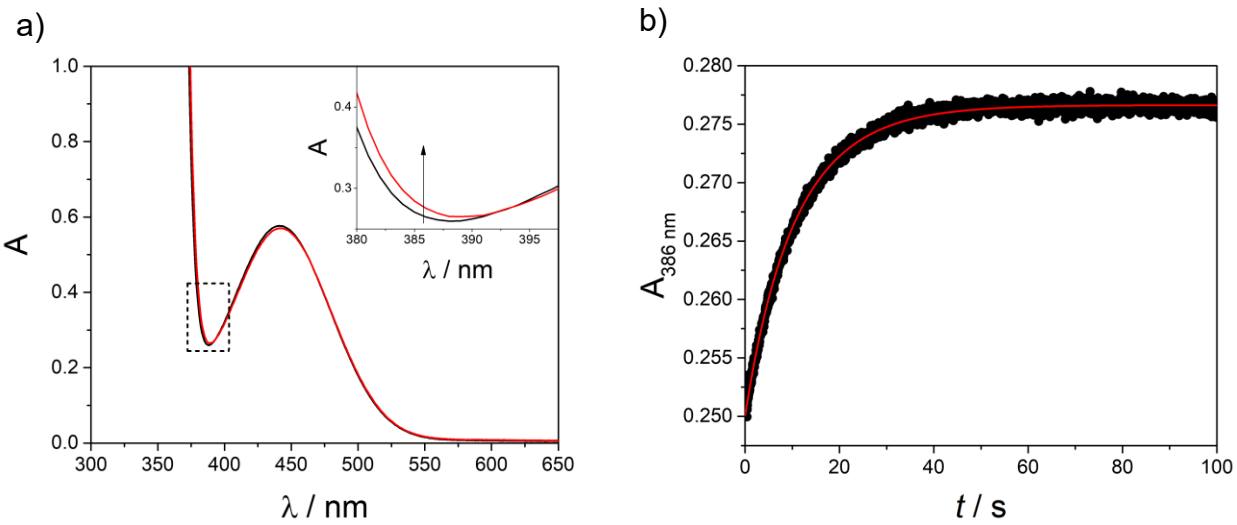

Figure S54. (a) Sum of the absorption spectra of 1.0 mM of *E*-**1** and 4.1 mM **2** (i.e., 4 equivalents) (black line), and absorption spectrum of the mixture of the two compounds in CH_2Cl_2/CH_3CN 3:7 (red line). (b) Absorption changes at 386 nm (black dots) upon rapid mixing of *E*-**1** and **2** in CH_2Cl_2/CH_3CN 3:7 monitored with a stopped flow experiment alongside the least-squares fitting (red line) according to a mixed order kinetic model, to obtain a second-order threading rate constant of 19 M^{-1} s^{-1}. Final concentrations: [*E*-**1**] = 0.5 mM, [**2**] = 2.05 mM.

5. The kinetic model

Figure S55 presents the reaction network associated with the interaction between the axle (**1**) and the macrocycle (**2**). The network consists of ten thermal reactions and four photochemical reactions, to each of which are associated rate constants (k).

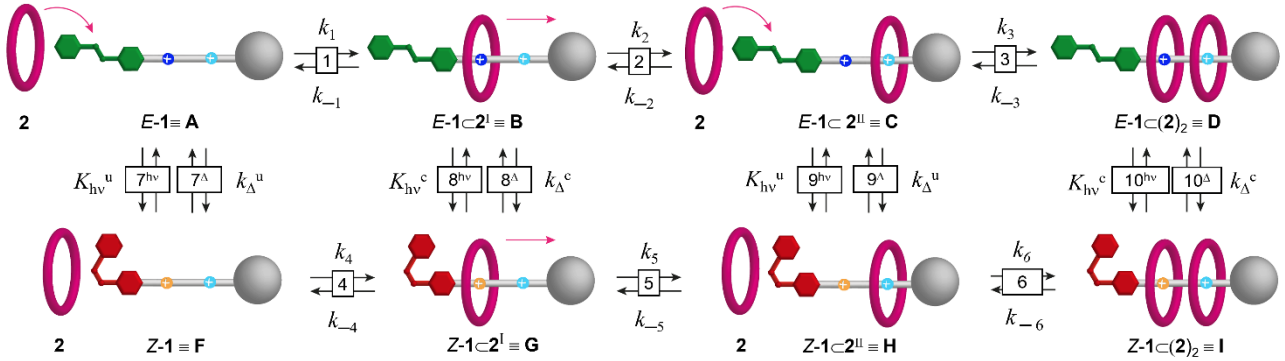

Figure S55. Network of reactions describing the operation of the reservoir modified pump. Superscripts I and II indicate the ammonium station occupied by the macrocycle in co-conformational isomers. To simplify equations, species are labelled with letters A-D for *E* isomers and F-I for *Z* isomers. The symbols 'hν' and 'Δ' are associated with the photochemical and thermal (*E*→*Z* and *Z*→*E*) isomerization processes, while the superscripts 'u' and 'c' refer to the un-complexed and complexed species respectively. Each reaction of the network is labelled according to the numbers in square boxes.

The kinetic behavior of the complete reaction network is described by a set of ten rate equations associated with the thermal reactions and eight photokinetic equations. The rate equations for thermal reactions are reported below (Eqs. S5-S14). Although formally the thermal isomerization reactions should be represented as equilibria considering both the *Z*→*E* and *E*→*Z* processes, the latter were neglected in the kinetic model, resulting in four unidirectional reactions 7^{Δ}, 8^{Δ}, 9^{Δ} and 10^{Δ} corresponding to the conversion of *Z* isomers to *E* isomers.

Reaction 1: $v_1 = k_1[\boldsymbol{A}][\boldsymbol{2}] - k_{-1}[\boldsymbol{B}]$ (Eq. S5)

Reaction 2: $v_2 = k_2[\boldsymbol{B}] - k_{-2}[\boldsymbol{C}]$ (Eq. S6)

Reaction 3: $v_3 = k_3[\boldsymbol{C}][\boldsymbol{2}] - k_{-3}[\boldsymbol{D}]$ (Eq. S7)

Reaction 4: $v_4 = k_4[\boldsymbol{AF}][\boldsymbol{2}] - k_{-4}[\boldsymbol{G}]$ (Eq. S8)

Reaction 5: $v_5 = k_5[\boldsymbol{G}] - k_{-5}[\boldsymbol{H}]$ (Eq. S9)

Reaction 6: $v_6 = k_6[\boldsymbol{H}][\boldsymbol{2}] - k_{-6}[\boldsymbol{I}]$ (Eq. S10)

Reaction 7^{Δ}: $v_{7^{\Delta}} = k_{\Delta}^{u}[\boldsymbol{F}]$ (Eq. S11)

Reaction 8^{Δ}: $v_{8^{\Delta}} = k_{\Delta}^{c}[\boldsymbol{G}]$ (Eq. S12)

Reaction 9^{Δ}: $v_{9^{\Delta}} = k_{\Delta}^{u}[\boldsymbol{H}]$ (Eq. S13)

Reaction 10^{Δ}: $v_{10^{\Delta}} = k_{\Delta}^{c}[\boldsymbol{I}]$ (Eq. S14)

The photokinetic equations for photoisomerization reactions $7^{h\nu}$, $8^{h\nu}$, $9^{h\nu}$ and $10^{h\nu}$ (*E*→*Z* and *Z*→*E* for all complexed and uncomplexed species on ammonium station I) are obtained according to the photokinetic rate law (Eq. S2).

The kinetic model thus described was used for the determination of rate constants through least-squares fitting of concentrations traces of species in ^{1}H NMR kinetic experiments (Section 6) and for the simulation of the operation of the system (Section 8).

6. Determination of kinetic constants

Kinetic constant k_1 (and k_3) = 19 M^{-1} s^{-1} was determined by fitting the absorption variation curve obtained in the UV-vis stopped-flow experiment (Section 4.5). The kinetic constant for the reverse process k_{-1} (and k_{-3}) = 1.8×10^{-2} s^{-1} was calculated as the ratio $k_1/K_{E\text{-I}}$. It is assumed that no (anti)cooperative effect is present, i.e. the interaction between **2** and the two ammonium stations in **1** is not affected by the presence of another macrocycle on the axle; hence, as explained in section 3.3., the association constants (K) values determined for model complexes *E*-**3**⊂**2**, *Z*-**3**⊂**2** and **4**⊂**2** are assumed to be representative for the association between **2** and the ammonium recognition sites (*E*-I, *Z*-I and II) in **1**. Thermal $Z\rightarrow E$ isomerization constants for complexed and uncomplexed species, k_Δ^c and k_Δ^u, were obtained by fitting of the absorption variation curves monitored by UV-vis measurements (Sections 4.2 and 4.4).

6.1. Determination of k_2 and k_{-2}

The rate constants k_2 and k_{-2} associated with the shuttling of the macrocycle in the equilibrium between the co-conformers *E*-**1**⊂**2**^{I} and *E*-**1**⊂**2**^{II} were determined by least squares fitting of the time-dependent concentration traces obtained by ^{1}H NMR monitoring of the equilibration process, considering the rate equations S5, S6, and S7 corresponding to reactions 1, 2, 3 in figure S55 respectively. The values determined for the constants were $k_2 = 3.2\times10^{-3}$ s^{-1} and $k_{-2} = 5.2\times10^{-3}$ s^{-1}.

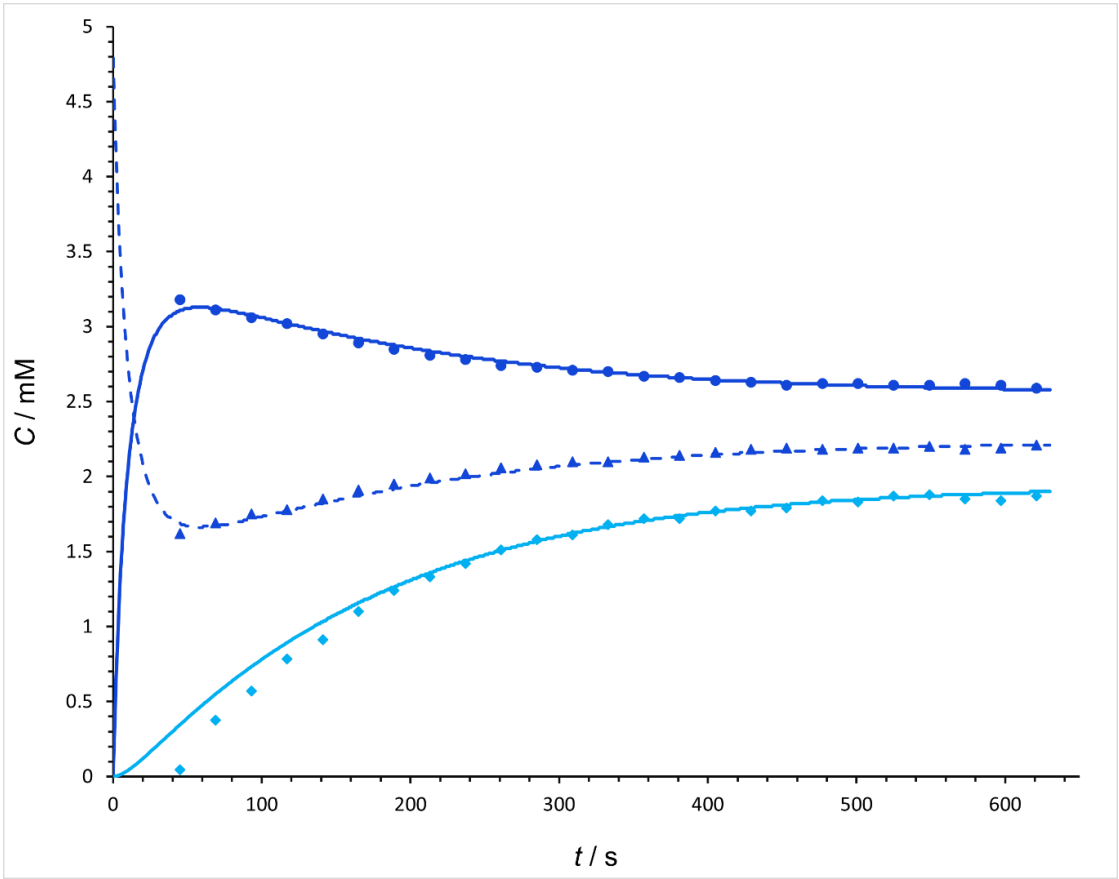

Figure S56. Time-dependent concentration traces obtained monitoring by ^{1}H NMR (500 MHz, 298 K) the equilibration process after mixing *E*-**1** (4.8 mM) and **2** (5.5 mM) in CD_2Cl_2/CD_3CN 3:7, acquiring spectra at 20 s intervals. Symbol traces represent the experimental data, while lines correspond to the fitting data. Colors and symbols are associated with the following: total complex on the first ammonium station *E*-I⊂**2** = *E*-**1**⊂**2**^{I} + *E*-**1**⊂(**2**)$_2$: blue, circles; total free first ammonium station *E*-I = *E*-**1** + *E*-**1**⊂**2**^{II}: blue, triangles; total complex on the second ammonium station II⊂**2** = *E*-**1**⊂**2**^{II} + *E*-**1**⊂(**2**)$_2$: cyan, diamonds.

6.2. Calculation of k_5 and k_{-5}

Kinetic constant k_5, associated with the shuttling of **2** from I to II in *Z*-**1**, can be calculated considering Eyring equation (Eq. S15)

$$k_5 = \frac{k_B T}{h} e^{\frac{-\Delta G_5^{\ddagger}}{RT}} \qquad \text{(Eq. S15)}$$

where k_B is the Boltzmann constant, T is the temperature, h is the Plank constant, R is the gas constant and $\Delta G^{\ddagger}_9$ is the Gibbs free energy of activation associated with the shuttling of the macrocycle from station I to station II in *Z*-**1**.
According to the scheme in figure S57, $\Delta G^{\ddagger}_5$ can be calculated considering the following equation (Eq. S16):

$$\Delta G_5^{\ddagger} = \Delta G_2^{\ddagger} - |\Delta\Delta G°| \qquad \text{(Eq. S16)}$$

Knowing kinetic constant k_2 (Section 6.1) and equilibrium association constants $K_{E\text{-I}}$ and $K_{Z\text{-I}}$ and the associated $\Delta G°$ (Section 3.3), $\Delta G^{‡}_2$ and $\Delta\Delta G°$ were determined according to equations S17 and S18, respectively:

$$\Delta G_2^{‡} = -RTln\left(k_2 \frac{h}{k_B T}\right) = 87.2\ kJmol^{-1} \qquad \text{(Eq. S17)}$$

$$\Delta\Delta G° = \Delta G^{o}_{E-I} - \Delta G^{o}_{Z-I} = -1.4\ kJmol^{-1} \qquad \text{(Eq. S18)}$$

Hence:

$$\Delta G_5^{‡} = \Delta G_2^{‡} - |\Delta\Delta G°| = 85.8\ kJmol^{-1} \qquad \text{(Eq. S16)}$$

which allowed to calculate a value for $k_9 = 5.6\times10^{-3}$ s^{-1}.

As represented in Figure S57, since azobenzene isomerization has no effect on the interaction of **2** with ammonium station II, $\Delta G^{‡}_{-5}$ should present the same value as $\Delta G^{‡}_{-2}$. Thus, rate constant k_{-5}, associated with shuttling of **2** from II to I in *Z*-**1**, was assigned the value $k_{-5} = k_{-2} = 5.2\times10^{-3}$ s^{-1}.

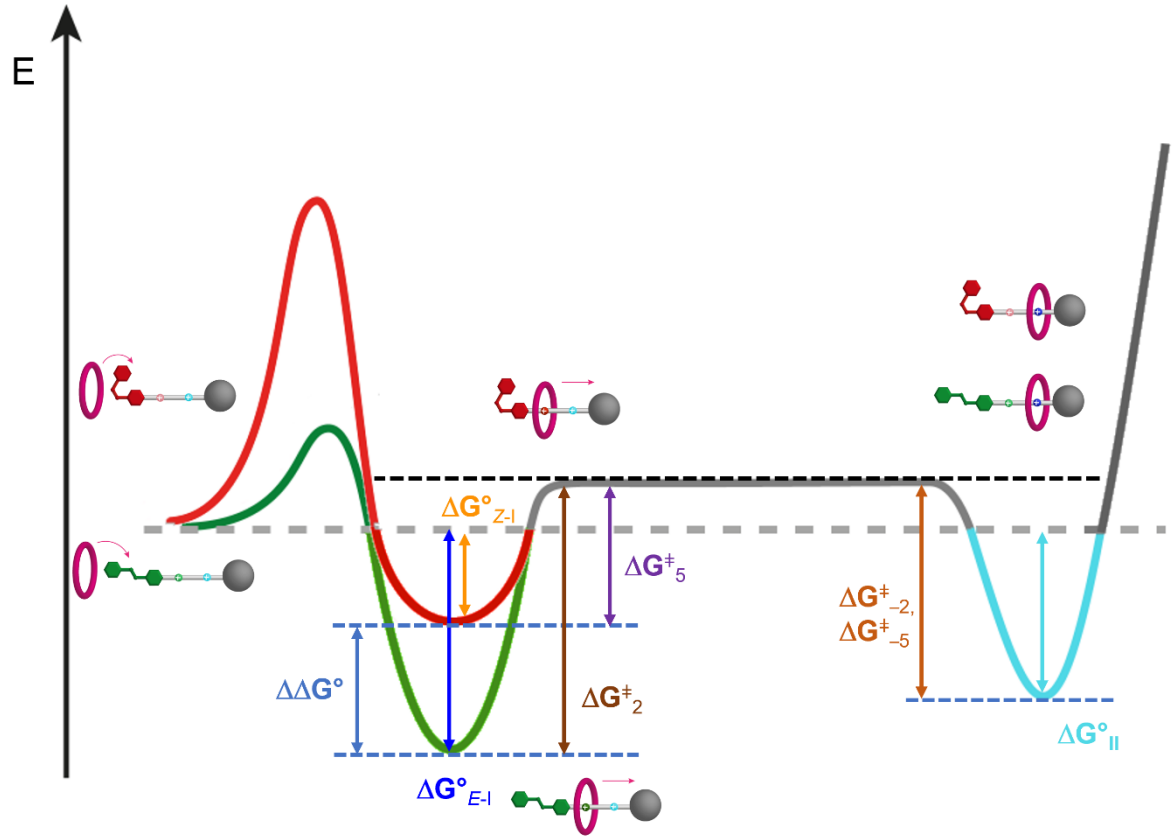

Figure S57. Schematic potential energy profile describing the threading and shuttling processes of the macrocycle **2** and either axle *E*-**1** or *Z*-**1**.

The rate constants (k_2, k_{-2} and k_5, k_{-5}) obtained reveal a quite slow shuttling process of the macrocycle along the thread which can be ascribed to the high affinity of the dibenzo-crown ether for the dibenzylammonium recognition sites, giving rise to deep wells in the potential energy profile. Moreover, it has been demonstrated in the literature that long alkyl chains can exert significant effects on the threading/dethreading kinetics pseudorotaxane formation.[9] Hence, it can be hypothesized that

the shuttling movement of DB24C8 is hindered because it requires the C10 alkyl spacer to be unfolded.

6.3. Determination of k_4 (and k_6), k_{-4} (and k_{-6})

The rate constants k_4 (and k_6) associated with the threading of **2** and *Z*-**1**, was determined by least squares fitting of the time-dependent concentration traces obtained by ^{1}H NMR monitoring of the equilibration process, considering the complete set of rate equations S5–S14 corresponding the full set of thermal reactions represented in Figure S55. The value determined for the constants was k_4 (k_6) = 1.1×10^{-3} M^{-1} s^{-1}. The kinetic constant for the de-threading process k_{-4} (and k_{-6}) was calculated as the ratio $k_4/K_{Z\text{-I}}$ to be k_{-4} (k_{-6}) = 1.8×10^{-6} s^{-1}.

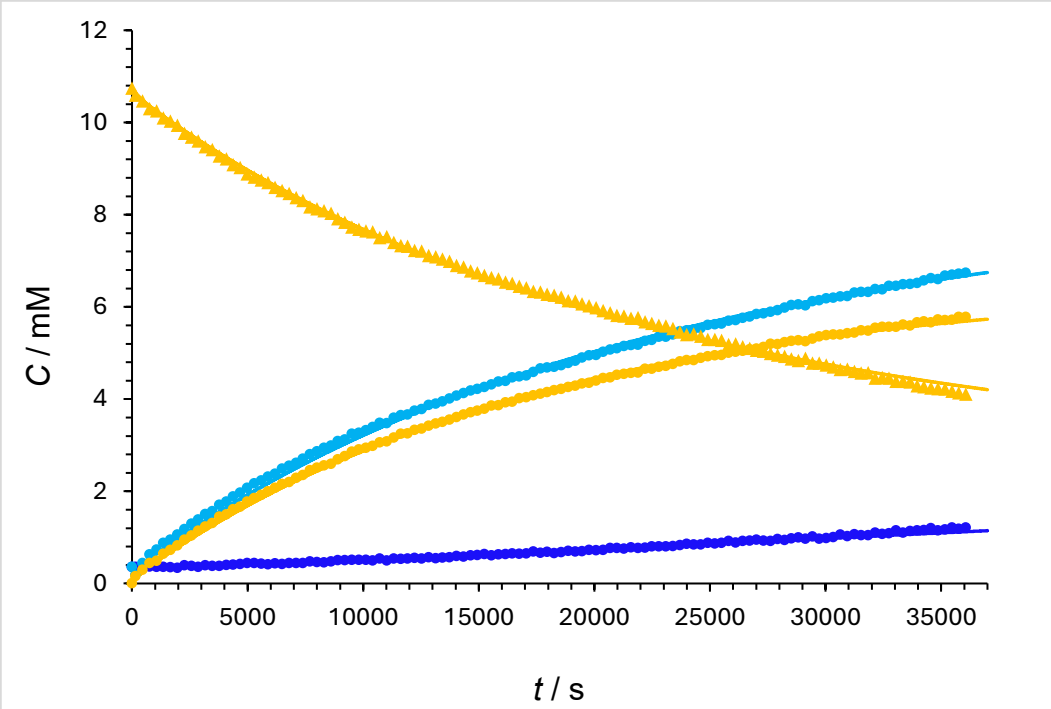

Figure S58. Time-dependent concentration traces obtained by ^{1}H NMR (500 MHz, 298 K) monitoring of the equilibration process after mixing an irradiated solution (λ = 365±5 nm) of *E*-**1** (11.0 mM) to reach PSS and **2** (67.0 mM) in CD_2Cl_2/CD_3CN 3:7, acquiring spectra at 300 s intervals. Symbol traces represent the experimental data, while lines correspond to the fitting data. Colors and symbols are associated with the following: total complex on the first ammonium station *E*-I⊂**2** = *E*-**1**⊂**2**^{I} + *E*-**1**⊂(**2**)$_2$: blue, circles; total free first ammonium station *Z*-I = *Z*-**1** + *Z*-**1**⊂**2**^{II}: orange, triangles; total complex on the first ammonium station *Z*-I⊂**2** = *Z*-**1**⊂**2**^{I} + *Z*-**1**⊂(**2**)$_2$: orange, circles; total complex on the second ammonium station II⊂**2** = *E*-**1**⊂**2**^{II} + *E*-**1**⊂(**2**)$_2$: cyan, diamonds.

7. Operation of the reservoir modified pump

The study of the operation of the system under continuous light irradiation was performed *via* NMR spectroscopy. The experimental setup involved mixing an equimolar amount of *E*-**1** and **2** (~10 mM) in a solvent mixture CD_2Cl_2/CD_3CN 3:7. The concentration and relative ratio of *E*-**1** and **2** were selected as the optimal conditions following simulation of the pump operation varying such parameters. The system was then allowed to equilibrate in the dark for 15 minutes. The solutions obtained were then irradiated within the NMR probe using the apparatus described in section 1.3; experiments were performed both with and without the 365±5 nm bandpass filter. Upon reaching a stationary composition, irradiation was stopped and the evolution of the system monitored for further time in the dark.

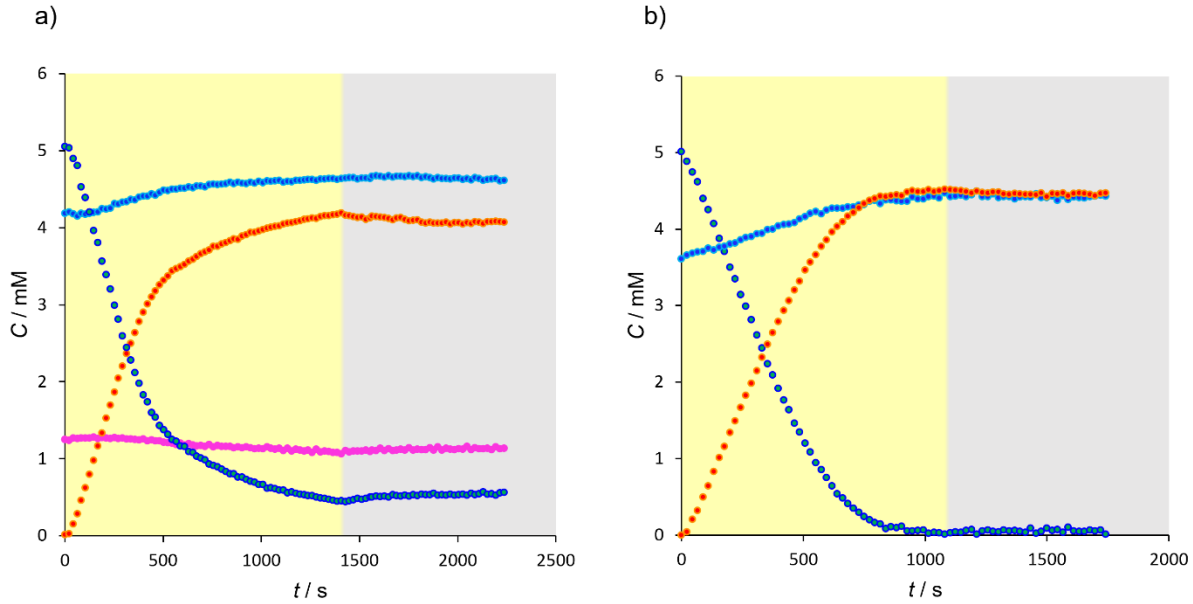

Figure S59. Time-dependent concentration traces obtained by a) ^{19}F NMR (470 MHz, 298 K) monitoring a mixture of *E*-**1** (10.2 mM) and **2** (10.6 mM) in CD_2Cl_2/CD_3CN 3:7, b) ^{1}H NMR (500 MHz, 298 K) monitoring a mixture of *E*-**1** (9.9 mM) and **2** (10.4 mM) in CD_2Cl_2/CD_3CN 3:7. In both experiments spectra were acquired at 20 s intervals. Irradiation with monochromatic light at λ = 365±5 nm was achieved using a bandpass filter. The photon flow was $q_{n,p} = 3.1\times10^{-8}$ Einstein s^{-1}. Colors are associated with the following: free **2**: magenta; total complex on the first ammonium station *E*-I⊂**2** = *E*-**1**⊂**2**^{I}+*E*-**1**⊂(**2**)$_2$: blue; total complex on the first ammonium station *Z*-I⊂**2** = *Z*-**1**⊂**2**^{I}+*Z*-1⊂(**2**)$_2$: orange; total complex on the second ammonium station II⊂**2** = *E*-1⊂**2**^{II}+*E*-**1**⊂(**2**)$_2$+*Z*-**1**⊂**2**^{II}+*Z*-**1**⊂(**2**)$_2$: cyan.

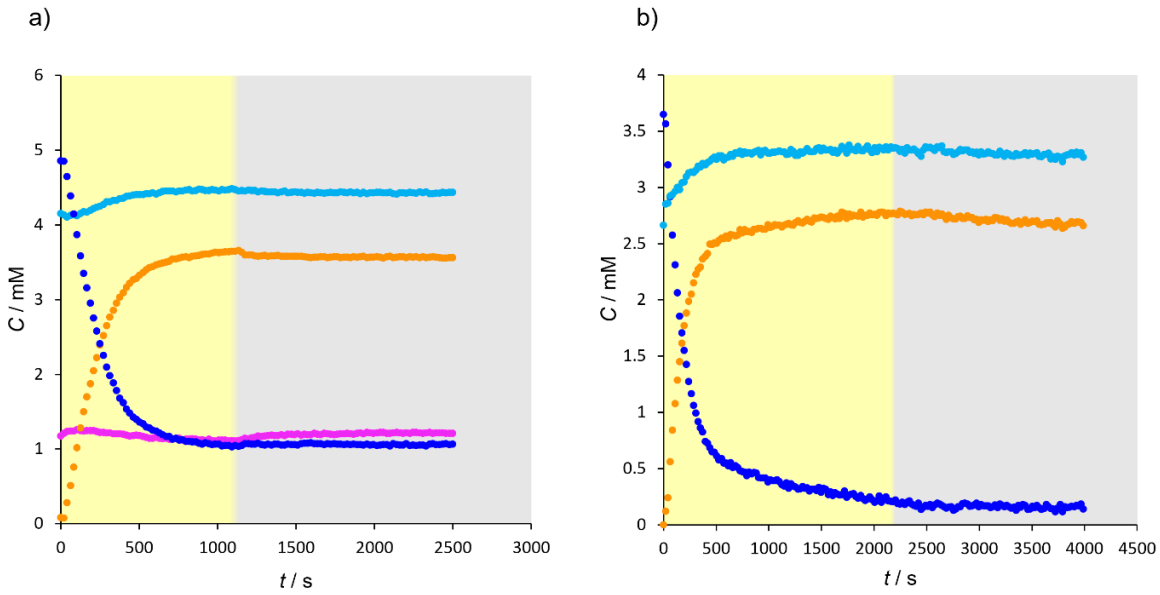

Figure S60. Time-dependent concentration traces obtained by a) ^{19}F NMR (470 MHz, 298 K) monitoring a mixture of *E*-**1** (10.1 mM) and **2** (10.2 mM) in CD_2Cl_2/CD_3CN 3:7, b) ^{1}H NMR (500 MHz, 298 K) monitoring a mixture of *E*-**1** (10.1 mM) and **2** (9.9 mM) in CD_2Cl_2/CD_3CN 3:7. In both experiments spectra were acquired at 20 s intervals. Irradiation was performed with polychromatic light at λ = 369±15 nm. The estimated photon flow was $q_{n,p}$ = 4.65×10^{-8} Einstein s^{-1}. Colors are associated with the following: free **2**: magenta; total complex on the first ammonium station *E*-I⊂**2** = *E*-**1**⊂**2**^{I}+*E*-**1**⊂(**2**)$_2$: blue; total complex on the first ammonium station *Z*-I⊂**2** = *Z*-**1**⊂**2**^{I}+*Z*-1⊂(**2**)$_2$: orange; total complex on the second ammonium station II⊂**2** = *E*-1⊂**2**^{II}+*E*-**1**⊂(**2**)$_2$+*Z*-**1**⊂**2**^{II}+*Z*-**1**⊂(**2**)$_2$: cyan.

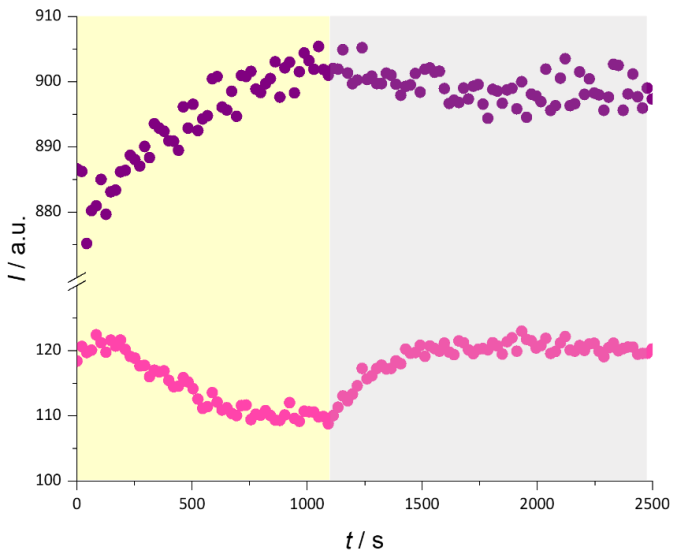

Figure S61. Time-dependent integral traces extracted from an array of ^{19}F NMR (470 MHz, 298 K) spectra monitoring a mixture of *E*-**1** (10.1 mM) and **2** (10.2 mM) in CD_2Cl_2/CD_3CN 3:7. **S**pectra were acquired at 20 s intervals. Irradiation was performed with polychromatic light at λ = 369±15 nm. The estimated photon flow was $q_{n,p}$=4.65×10^{-8} Einstein s^{-1}. Colors are associated with the following: free **2**: magenta; total complex (*E*-I⊂**2** + *Z*-I⊂**2** + II⊂**2**): purple.

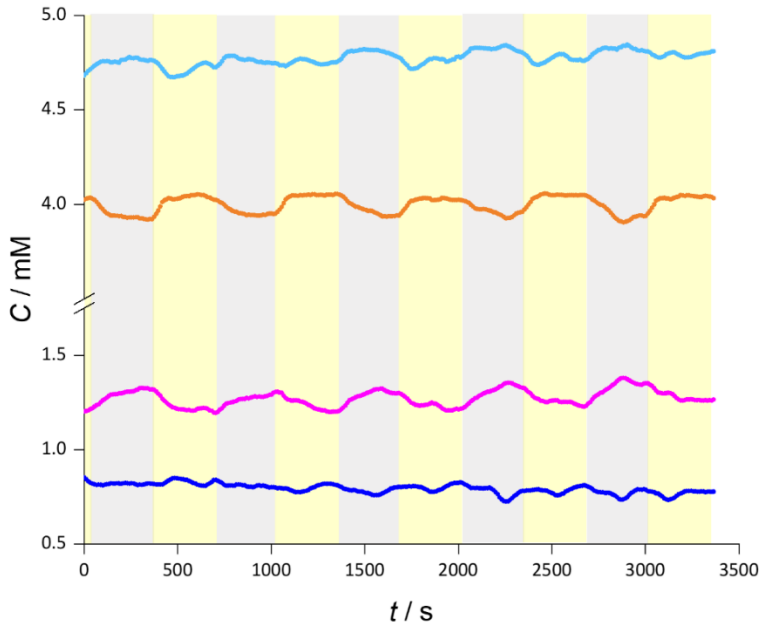

Figure S62. Time-dependent concentration traces obtained by ^{19}F NMR (470 MHz, 298 K) monitoring a mixture of *E*-**1** (9.8 mM) and **2** (11 mM) in CD_2Cl_2/CD_3CN 3:7, spectra were acquired at 10 s intervals. Irradiation was performed with polychromatic light at λ = 369±15 nm. The estimated photon flow was $q_{n,p} = 8.46\times10^{-8}$ Einstein s^{-1}. Light on/light off cycles included 300 s irradiation and 300 s dark. Colors are associated with the following: free **2**: magenta; total complex on the first ammonium station *E*-I⊂**2** = *E*-**1**⊂**2**^{I}+*E*-**1**⊂(**2**)$_2$: blue; total complex on the first ammonium station *Z*-I⊂**2** = *Z*-**1**⊂**2**^{I}+*Z*-1⊂(**2**)$_2$: orange; total complex on the second ammonium station II⊂**2** = *E*-1⊂**2**^{II}+*E*-**1**⊂(**2**)$_2$+*Z*-**1**⊂**2**^{II}+*Z*-**1**⊂(**2**)$_2$: cyan.

8. Numerical simulations

Numerical simulations of the kinetics associated with the operation of the system were performed implementing the kinetic model described in section 5 into Berkeley Madonna 10.6.1 and solving the differential equations using the fixed-stepsize integration method Runge-Kutta 4. The parameters used for simulations are reported in Table S5.
The simulation was designed to consider three steps: i) equilibration of an equimolar solution of *E*-**1** and **2** in the dark; ii) irradiation of the equilibrated mixture at the given photon flow intensity, and; iii) irradiation was then stopped by setting $q_{n,p} = 0$. Throughout the simulations it was assumed that concentration of the species was homogeneous within the irradiation volume.

Table S5. Parameters introduced in the kinetic model for the simulation of the reservoir modified pump operation**.**

Parameter	***Irradiation*** λ ***= 365±5 nm***	***Irradiation*** λ ***= 369±15 nm***
$q_{n,p}$ (Einstein s^{-1})	3.14×10^{-8}	4.65×10^{-8}
[1] (M)	10×10^{-3}	10×10^{-3}
[2] (M)	10×10^{-3}	10×10^{-3}
k_1 (M^{-1} s^{-1})	19	19
k_{-1} (s^{-1})	1.8×10^{-2}	1.8×10^{-2}
k_2 (s^{-1})	3.2×10^{-3}	3.2×10^{-3}
k_{-2} (s^{-1})	5.2×10^{-3}	5.2×10^{-3}
k_3 (M^{-1} s^{-1})	19	19
k_{-3} (s^{-1})	1.8×10^{-2}	1.8×10^{-2}
k_4 (M^{-1} s^{-1})	1.1×10^{-3}	1.1×10^{-3}
k_{-4} (s^{-1})	1.8×10^{-6}	1.8×10^{-6}
k_5 (s^{-1})	5.6×10^{-3}	5.6×10^{-3}
k_{-5} (s^{-1})	5.2×10^{-3}	5.2×10^{-3}
k_6 ($M^{-1}s^{-1}$)	1.1×10^{-3}	1.1×10^{-3}
k_{-6} (s^{-1})	1.8×10^{-6}	1.8×10^{-6}
k_Δ^u	1.5×10^{-6}	1.5×10^{-6}
k_Δ^c	3.1×10^{-6}	3.1×10^{-6}
ε_E^u	5700	650[a]
ε_E^c	5300	850[a]
ε_Z^u	70	60[a]
ε_Z^c	60	60[a]
$\Phi_{E\rightarrow Z}^u$	0.20	0.20
$\Phi_{E\rightarrow Z}^c$	0.17	0.17
$\Phi_{Z\rightarrow E}^u$	0.57	0.57
$\Phi_{Z\rightarrow E}^c$	0.59	0.59

[a]Determined by fitting of the experimental data reported in figure S60a.

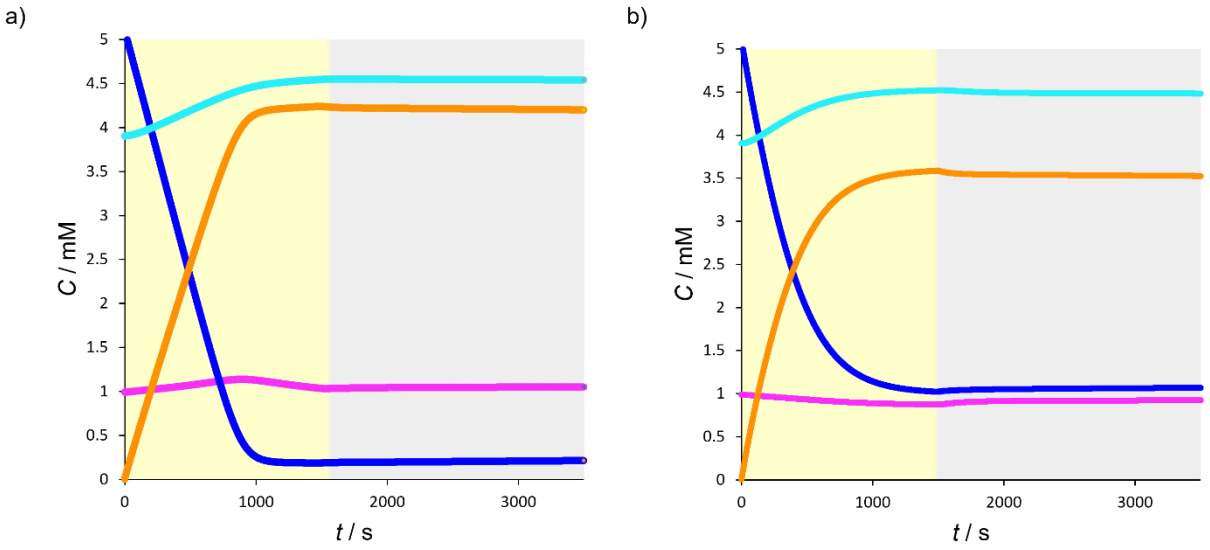

Figure S63. Time-dependent concentration traces simulated for the system, plotted starting from step ii, obtained using parameters for: a) irradiation at λ = 365±5 nm, b) irradiation at λ = 369±15 nm. Colors are associated with the following: free **2**: magenta; total complex on the first ammonium station *E*-I⊂**2** = *E*-**1**⊂**2**^{I}+*E*-**1**⊂(**2**)$_2$: blue; total complex on the first ammonium station *Z*-I⊂**2** = *Z*-**1**⊂**2**^{I}+*Z*-1⊂(**2**)$_2$: orange; total complex on the second ammonium station II⊂**2** = *E*-**1**⊂**2**^{II}+*E*-**1**⊂(**2**)$_2$+*Z*-**1**⊂**2**^{II}+*Z*-**1**⊂(**2**)$_2$: cyan.

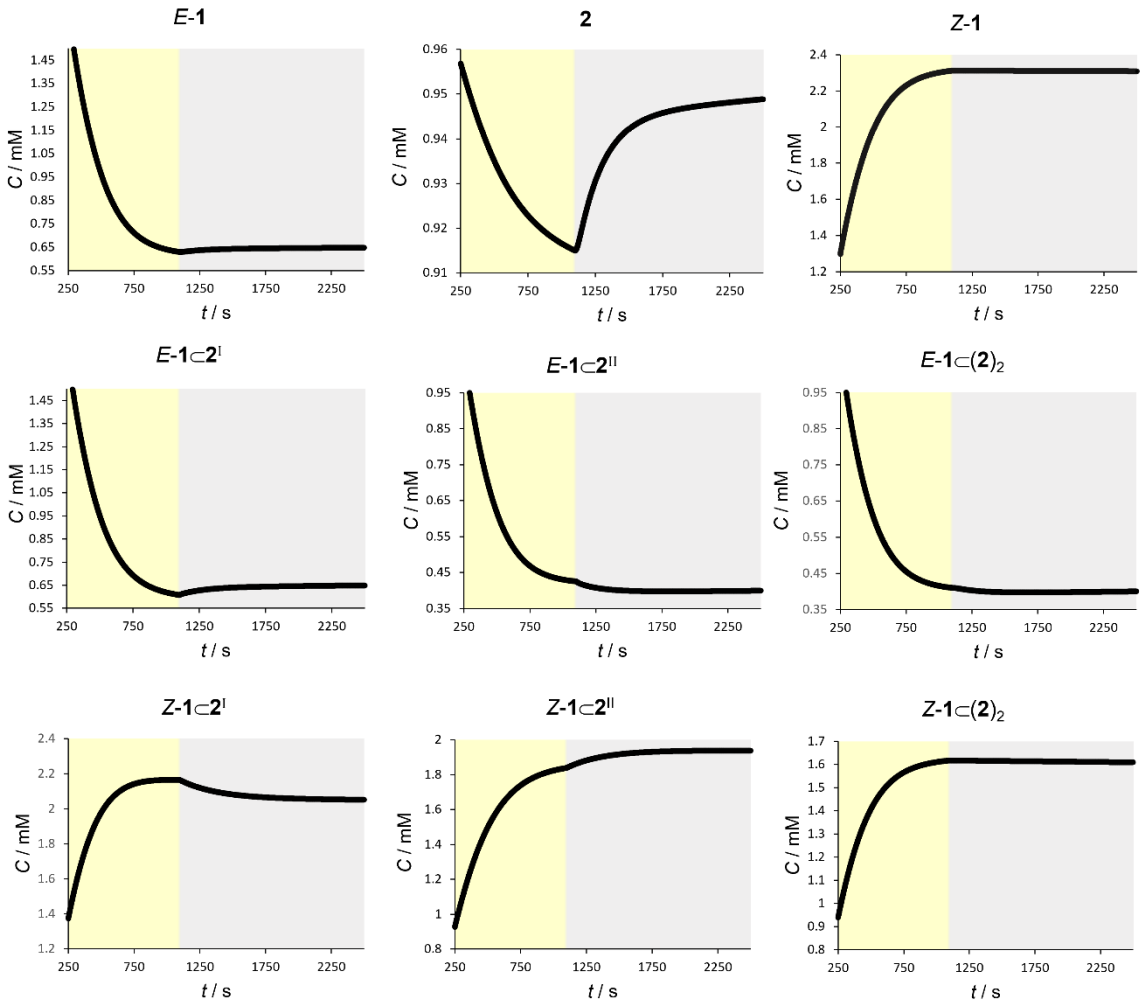

Figure S64. Partial time-dependent concentration traces simulated for each species in the reaction network, plotted starting from step ii, obtained using parameters for irradiation with polychromatic light.

The total number of moles of photons ($n_{h\nu,tot}$) provided to the irradiated solution from the light source at λ = 369±15 nm in the irradiation time can be calculated according to equation S19

$$n_{h\nu,tot} = q_{n,p}\,\Delta t = 5.1\times10^{-5}\ \text{mol} \qquad \text{(Eq. S19)}$$

The number of moles of photons ($n_{h\nu}$) absorbed by the system during irradiation time Δt was calculated using the simulation parameters for irradiation at λ = 369±15 nm according to equation S20, where A is the absorbance of the solution at the irradiation wavelength:

$$n_{h\nu} = q_{n,p}\,(1-10^{-A})\,\Delta t = 4.5\times10^{-5}\ \text{mol} \qquad \text{(Eq. S20)}$$

The number of photons $N_{h\nu}$ can be easily calculated (N_A is the Avogadro number)

$$N_{h\nu} = n_{h\nu}\,N_A = 2.7\times10^{19} \qquad \text{(Eq. S21)}$$

Considering the number of moles of **2** (n_{DBD} = 5×10^{-8} mol) pumped from solution during irradiation, the number of photons required to operate the system in order to achieve pumping of one macrocycle is 900.
The free energy change associated with out-of-equilibrium pumping can be estimated by comparing the transfer of macrocycles from solution to the axle under irradiation to the distribution of ideal gas particles in a two compartments box.[10]

$$\Delta G = N k_B T \left[x_1 ln \frac{x_1}{x_2} + (1 - x_1) ln \frac{(1-x_1)}{(1-x_2)} \right] = 6.0 \times 10^{-6} \text{ J} \qquad \text{(Eq. S22)}$$

Where N is the total number of macrocycles in the sample (3×10^{18}), x_1 = 0.11 is the molar fraction of free macrocycles at the stationary state under irradiation and x_2 = 0.12 is the molar fraction of free macrocycles at equilibrium. Considering the sample volume (V = 0.5 mL), the calculated energy density stored in the non-equilibrium steady state is ΔG = 1.2×10^{-2} J L^{-1}.

The kinetic model allowed to simulate the concentration traces of all the species in the experimental conditions (λ = 369±15 nm, $q_{n,p}$ = 4.65×10^{-8} Einstein s^{-1}, 1100 s) as well as the rates (v_{if}, v_{ir}) associated with each elementary process represented in the reaction network (Fig. S55). The simulation of such values was necessary for the estimation of the Carnot-like efficiency of the system.[8]

The global reaction rates (v_i) were calculated as:

$$v_i = v_{if} - v_{ir} \qquad \text{(Eq. S23)}$$

The affinity (A_i) of each reaction in the network at the stationary state under irradiation was determined by equation S24:

$$A_i = RT \ln \frac{v_f}{v_r} \qquad \text{(Eq. S24)}$$

The total power dissipated by the thermal steps, $T\dot{\Sigma}$, can be calculated as:

$$T\dot{\Sigma} = \sum_i A_i \, v_i = 9.4 \times 10^{-5} \text{ J s}^{-1} \qquad \text{(Eq. S25)}$$

The power absorbed by the sample at the stationary state per unit of time, $\dot{Q}_{hv}$, was calculated according to the formula:

$$\dot{Q}_{hv} = \frac{hc}{\lambda} q_{n,p} (1 - 10^{-A_{tot}}) = 9.8 \times 10^{-3} \text{ J s}^{-1} \qquad \text{(Eq. S26)}$$

Knowing the total dissipated power as well as the power absorbed by the sample, we could estimate the Carnot-like efficiency (η_c) of the system according to Eq. S27:

$$\eta_c = \frac{T\dot{\Sigma}}{\dot{Q}_{hv}} = 9.6 \times 10^{-3} \qquad \text{(Eq. S27)}$$

This figure, converted in percentage, corresponds to an efficiency of 0.9%.

9. References

[1] M. Canton, J. Groppi, L. Casimiro, S. Corra, M. Baroncini, S. Silvi, A. Credi, "Second generation light-fueled supramolecular pump" *J. Am. Chem. Soc.* **2021**, *143*, 10890.

[2] M. Curcio, F. Nicoli, E. Paltrinieri, E. Fois, G. Tabacchi, L. Cavallo, S. Silvi, M. Baroncini, A. Credi, "Chemically induced mismatch of rings and stations in [3]rotaxanes" *J. Am. Chem. Soc.* **2021**, *143*, 8046.

[3] S. J. Cantrill, G. J. Youn, J. F. Stoddart, D. J. Williams, "Supramolecular daisy chains" *J. Org. Chem.* **2001**, *66*, 6857.

[4] F. V. Marcoline, J. Furth, S. Nayak, M. Grabe, R. I. Macey, "Berkeley Madonna Version 10-A simulation package for solving mathematical models" *CPT: PSP* **2022**, *11*, 290.

[5] M. Montalti, A. Credi, L. Prodi, M. T. Gandolfi, *Handbook of Photochemistry, 3rd Ed.* CRC Press, Boca Raton, **2006**.

[6] E. Fischer, "The calculation of photostationary states in systems A⇆B when only A is known" *J. Phys. Chem.* **1967**, *71*, 3704.

[7] L. Casimiro, L. Andreoni, J. Groppi, A. Credi, R. Métivier, S. Silvi, "4,4′- Dimethylazobenzene as a chemical actinometer" *Photochem. Photobiol. Sci.* **2022**, 21, 825.

[8] S. Corra, M. Tranfić Bakić, J. Groppi, M. Baroncini, S. Silvi, E. Penocchio, M. Esposito, A. Credi, "Kinetic and energetic insights into the dissipative non-equilibrium operation of an autonomous light-powered supramolecular pump" *Nat. Nanotechnol.* **2022**, *17*, 746.

[9] A. Arduini, R. Bussolati, A. Credi, A. Secchi, S. Silvi, M. Semeraro, M. Venturi, "Toward directionally controlled molecular motions and kinetic intra- and intermolecular self-sorting: threading processes of nonsymmetric wheel and axle components" *J. Am. Chem. Soc.* **2013**, *135*, 9924.

[10] V. Serreli, C.-F. Lee, E. R. Kay, D. A. Leigh, "A molecular information ratchet" *Nature* **2007**, *445*, 523